NASA Contractor Report 3763

A Wing Concept for Supersonic Maneuvering

William H. Mason

CONTRACT NAS1-15357
DECEMBER 1983

25th Anniversary
1958-1983

NASA

NASA Contractor Report 3763

A Wing Concept for Supersonic Maneuvering

William H. Mason
Grumman Aerospace Corporation
Bethpage, New York

Prepared for
Langley Research Center
under Contract NAS1-15357

National Aeronautics
and Space Administration

**Scientific and Technical
Information Branch**

1983

ACKNOWLEDGEMENT

The development project described in this report was carried out as a team effort by NASA Langley Research Center and Grumman Aerospace Corporation personnel. Micro Craft, Inc. also participated in some of the model fabrication work. In particular, the ideas that form the basis of this work are due to R. Meyer and the development plan was conceived by G. DaForno, both of the Grumman Aerospace Corporation. David S. Miller made significant contributions as the technical monitor for NASA. Numerous key people from the Grumman Aerodynamics and Aerodynamic Test sections, the R&D Center, and the NASA Langley Research Center Supersonic Aerodynamics Branch also made important contributions to the effort, and their work is gratefully acknowledged.

CONTENTS

A WING CONCEPT FOR SUPERSONIC MANEUVERING

William H. Mason
Grumman Aerospace Corporation

SUMMARY

This report describes a theoretical and experimental program in which a wing concept for supersonic maneuvering was developed and then demonstrated experimentally in a series of wind tunnel tests. For the typical advanced fighter wing, the problem of obtaining efficient attached flow lift at maneuvering C_L's occurs due to development of a strong crossflow shock and boundary layer separation. A natural means of achieving efficient supersonic maneuvering is based on controlling the nonlinear inviscid crossflow on the wing in a manner analogous to the attached flow supercritical aerodynamic design methods developed for transonic speeds. The application of supercritical aerodynamics to supersonic speeds is carried out using supercritical conical camber (SC^3). The substantial experimental data base is described in three separate wind tunnel reports; two of the computer programs used in the work are also described in a separate report. This report provides an overview of the effort, together with a discussion of the relationship of nonlinear aerodynamic design to current practice. Based on the development program, it appears that a controlled supercritical crossflow can be reliably obtained on fighter-type wing planforms, with an associated drag-due-to-lift reduction of about 20% projected using this concept.

INTRODUCTION

The possibility of developing a new fighter aircraft with vastly improved supersonic persistence has been studied extensively in recent years. Two major conferences (ref. 1 and 2) have been devoted in large part to this topic, and improved aerodynamic performance is one of several essential elements necessary

for obtaining this goal. Insight into the technology requirements and their integration can be obtained from a recent U.S. Air Force study (ref. 3).

Experience has demonstrated that tactical aircraft will be required to maneuver efficiently at speeds around the cruise condition, and this is evidenced in emerging supersonic maneuver point performance requirements for advanced fighters. Thus, it can be anticipated that a fighter cruising at supersonic speeds will also be required to maneuver at supersonic speeds; this is the problem addressed in the present report.

Supersonic wing design methodology presently in use in this country was developed for designing supersonic transports and is based on linear aerodynamic theory (ref. 4). Fighter aircraft have wings with less sweep and round leading edges when compared with an SST. The cruise lift coefficient will also be higher than that for transport designs, with sustained maneuvering C_L's about twice the cruise values. These conditions constitute an aerodynamic design problem that is more severe than linear theory can treat. Figure 1 shows the severity of the maneuver wing design problem. The maneuver lift coefficient is typically twice the maximum value for which linear theory methods are considered applicable. Beyond the upper bound, figure 2 shows how these linear theory wings fail to achieve the predicted drag-due-to-lift. The

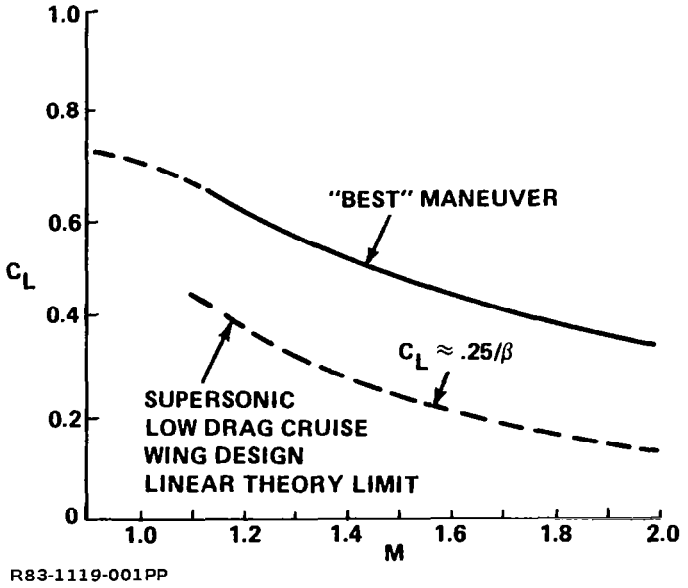

Figure 1. - Maneuvering flight lift requirements.

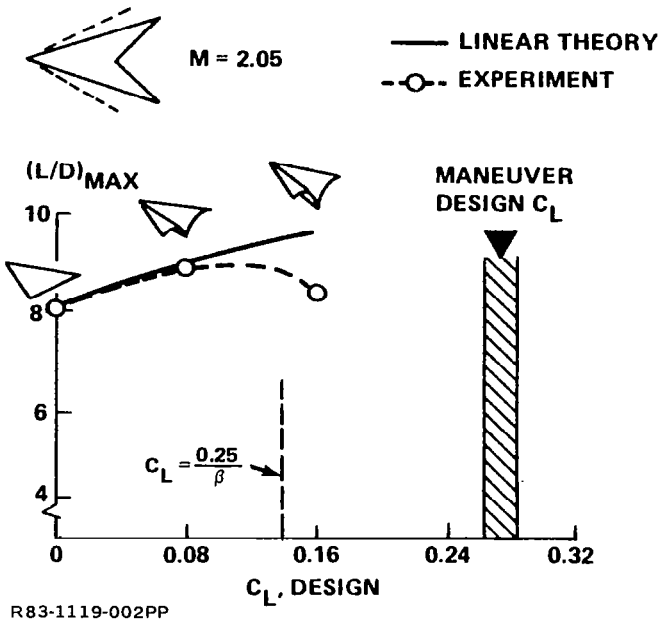

Figure 2. - Representative L/D loss with increasing design lift using linear theory.

potential drag improvement that could be realized by obtaining the predicted linear theory minimum drag performance at maneuver C_L's is illustrated in figure 3. The higher drag level corresponds to the $1/C_{L_\alpha}$ value, while the lower level represents the linear theory minimum drag value.

Perhaps the first analysis of the difficulties that arise using linear theory wing design methodology under these circumstances was given by Brown, et al (ref. 5). That paper identified the key contributor to linear theory breakdown as being related to crossflow velocities above the sonic value - supercritical crossflow. A detailed discussion of the relationship between linear theory breakdown and supercritical crossflow was given in the introduction of a recent paper by Mason and Miller (ref. 6). Figure 4 shows the nature of the problem. Figure 4A illustrates a conical wing for which the pressure distribution in the spanwise direction is presented. The crossflow starts at the stagnation point, expands around the leading edge to supercritical velocities, and is terminated by a crossflow shockwave. Because the crossflow plays the dominant role in establishing the upper surface flowfield, the pressure distributions will be studied as spanwise distributions in this report. The inviscid

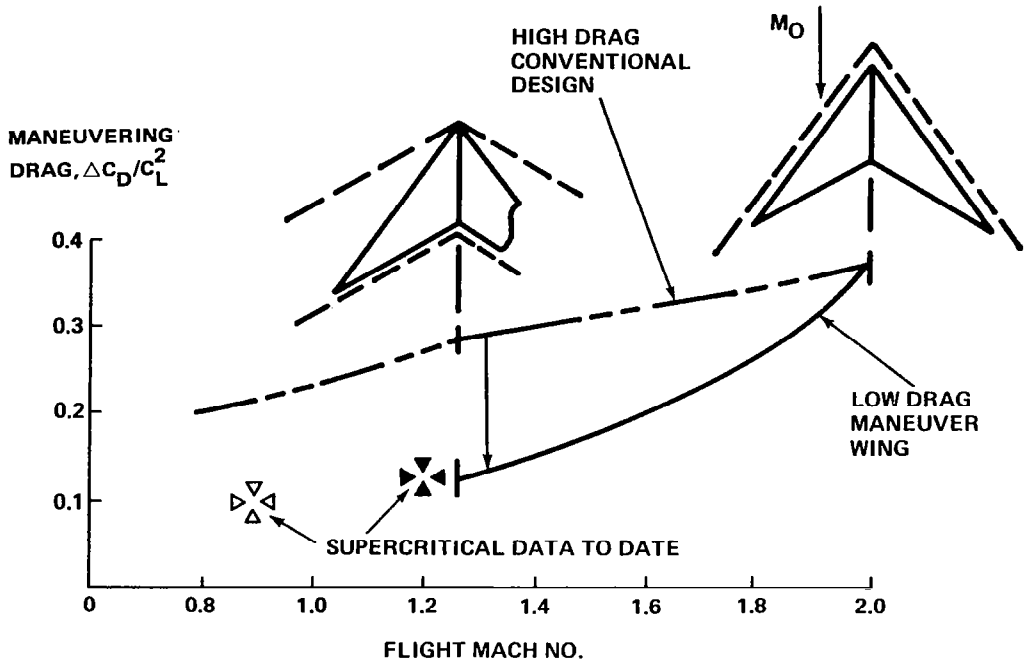

R83-1119-003PP

Figure 3. - Potential drag reduction available at supersonic maneuver conditions.

surface pressure predictions for an uncambered delta wing are shown in figure 4B, which illustrates the differences between linear and nonlinear theoretical spanwise pressure distributions due to the presence of supercritical crossflow. Two adverse features of the pressure distribution - the recompression after the leading edge spike and the crossflow shock - can cause boundary layer separation. The two main areas where linear theory is inadequate can easily be identified. First, note that the linear theory contains a singularity at the leading edge, preventing the possibility of describing the nature and extent of the leading edge expansion. Secondly, linear theory cannot predict crossflow development once the crossflow becomes supercritical. Inboard of the crossflow shock wave, linear theory is again accurate. Minor differences between linear and nonlinear flow predictions occur uniformly on the lower surface. Note that nonlinear effects do not necessarily degrade wing performance and, in fact, a number of examples have been given recently (ref. 7) wherein the nonlinear effects were shown to lead to improved performance.

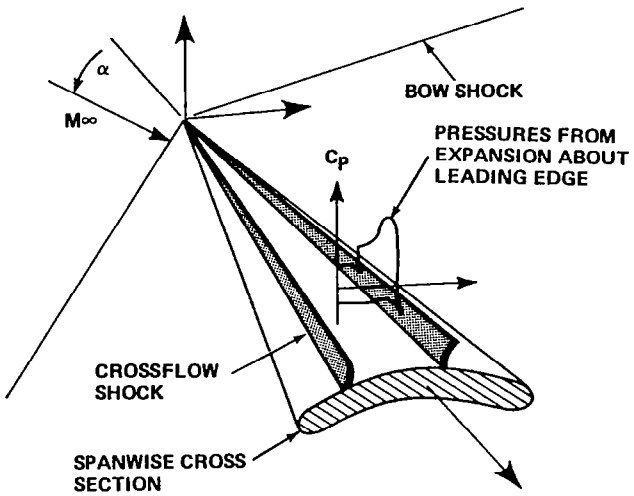

A. TYPICAL FLOW IN CROSSFLOW PLANE

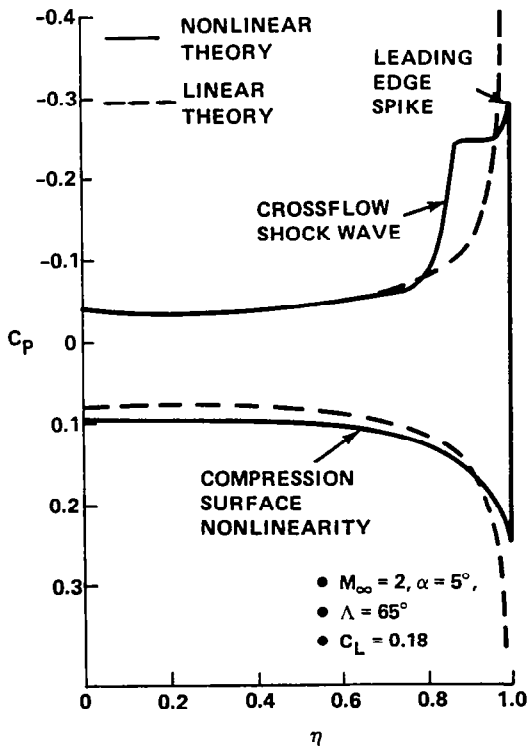

B. UNCAMBERED DELTA WING WITH ELLIPTIC THICKNESS DISTRIBUTION

R83-1119-004PP

Figure 4. - Crossflow velocity effects in supersonic flow.

The growing awareness of the importance of accounting for nonlinear effects in supersonic wing design led to two new approaches to the design problem. The first approach, which is directed toward cruise wing design, is based on modifications and extensions of the linear theory methodology and is being actively developed by Carlson and co-workers (ref. 8 and 9). The second approach is directed toward tactical aircraft applications, in particular supersonic maneuvering, and is described herein. In this method, the wing design is developed using the solution of the complete nonlinear potential flow equations and the exact boundary conditions. Use of the complete flow equations and boundary conditions allows for an explicit evaluation of the leading edge flowfield and the nonlinear supercritical crossflow. Initially, the required computational methodology was developed using the natural geometry for highly swept wings - conical camber.

The use of conical flow models for developing wing shapes received extensive attention in the 1950's. In the U.S., the conical camber wing concept was developed by Hall and co-workers at the NACA Ames Aeronautical Laboratory (ref. 10 and 11). The wing shape was developed using a combination of constant pressure loading shapes developed by R.T. Jones for linear supersonic conical flows (ref. 12). In particular, the loadings were combined in such a manner that the centerline camber slope singularity was eliminated and the spanload was nearly elliptical. After some modifications which simplified the geometry, an NACA conical camber shape was established and a modified form of the NACA conical camber shape was used on the F-102A and F-106 (ref. 13) fighter aircraft. The resulting wing camber used in these designs appears to be extreme, and is readily apparent when viewing these aircraft. It is interesting to note that, although the camber shape was developed based on supersonic flow theory, the main benefits of conical camber for drag reduction occurred at subsonic speeds. More recently, NACA conical camber was used in the F-15 wing design (ref. 14).

Conical camber was also explored in several experimental programs in the United Kingdom during the mid 1950's (described by Squire, ref. 15). In those efforts a family of geometric shapes was specified, and the minimum drag combination of shapes was found. The work was based on slender wing theory, and thus was even less accurate than the linear theory results used for the NACA conical camber shape. In addition, it was difficult to control the adverse

pressure gradient at the leading edge with those theories and, once again, no significant reductions in drag-due-to-lift were found in experiments. Outside of the Government laboratories, S.H. Tsien used linear theory to find the minimum drag conical wing (ref. 16). His work, compared to modern computational aerodynamics results which do not include the conical flow restriction, showed that there is little, if any, performance penalty associated with the conical flow assumption.

THE SC^3 CONCEPT

Based on the markedly improved understanding of wing design that resulted from the transonic supercritical aerodynamic development work in the late 1960's and 1970's, a new concept for supersonic wing design emerged. The SC^3 wing concept provides a means of achieving attached flow high lift efficiently at supersonic speeds. The idea was originated in 1976 at Grumman by R. Meyer and is illustrated schematically in figure 5. The sketch on the left indicates the key feature - a conical panel supporting a controlled supercritical (super-

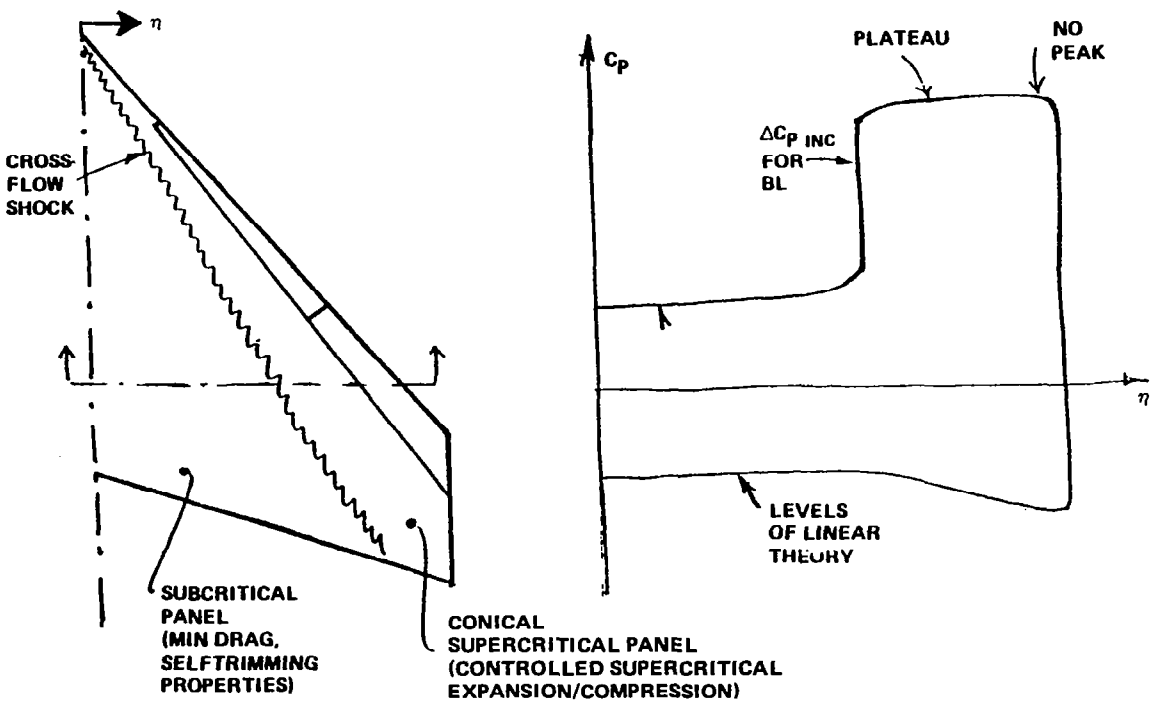

Figure 5. - The supercritical conical camber wing concept-SC^3.

critical conical camber; SC^3) crossflow expansion and recompression. By controlling the expansion and subsequent recompression, the lift available on the upper surface is obtained without producing an adverse pressure gradient or crossflow shock wave sufficiently strong to separate the boundary layer. The concept in effect extends the attached flow transonic supercritical aerodynamics to supersonic speeds by recognizing that the Mach number normal to the leading edge on the typical supersonic cruise fighter wing would be transonic at supersonic speeds. A key ingredient of the idea is to exploit the nonlinear portions of the flowfield to obtain a well-behaved and attached upper surface flow at high lift coefficients. The concept is implemented by carefully tailoring the upper surface geometry to achieve the desired controlled supercritical expansion and recompression.

APPLICATION OF SC^3 TO SUPERSONIC MANEUVERING

The use of subcritical crossflow as a criterion for determining the limits for linear theory leads to rather stringent limitations on wing sweep and C_L. A simple analysis given by Brown et al (ref. 5), and found by more exact numerical calculations to be accurate, is given in figure 6. For a 60° swept wing, the figure provides an estimate of the C_L limit for linear theory applications. For the subsonic leading edge cases, the SC^3 concept would be required for any design conditions above the critical C_L. Typical maneuver design points exceed this limit by a factor of two.

The explicit treatment of the nonlinear inviscid flow required in executing the SC^3 concept depends on the availability of reliable calculation methods that can treat the mixed flow nature of the problem. Remarkable progress has been made in developing this methodology. The initial breakthrough was made by Grossman (ref. 17) using the conical flow approximation and the ideas developed in computational aerodynamics for 2D transonic computations (ref. 18). The resulting code was called COREL (conical relaxation). The version of the COREL code that evolved during the present study is described in detail in a companion report (ref. 19). A discussion of the related computational methodology issues that arise in implementing the SC^3 concept is provided in Appendix A. In addition to COREL, two other computer codes were used during this work. A

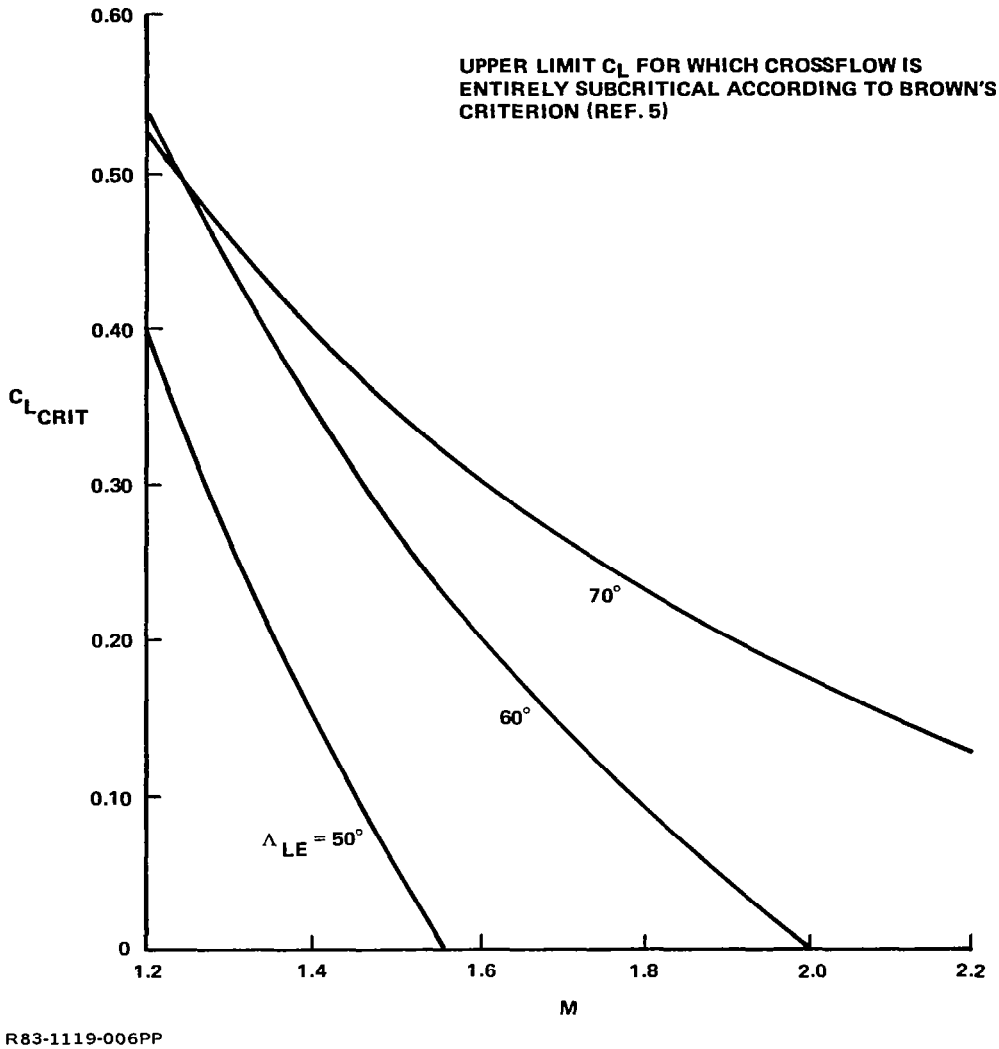

Figure 6. - Typical C_L limits for maintaining subcritical crossflow.

linear theory panel method code (also described in ref. 19) that combines attractive features of a number of other linear theory methods was developed for this work and is known as W12SC3; W12 indicates a combination of the so-called Woodward I (ref. 20) and Woodward II (ref. 21) methods, with modifications for the SC^3 concept leading to the W12SC3 designation. Finally, the COREL methodology was extended to treat non-conical geometries by M. Siclari of the Grumman R&D Center and that code was designated NCOREL (non-conical relaxation). These three codes were used to perform all of the detailed calculations.

The expectations in drag-due-to-lift performance and range of application can be further illustrated in figure 7. This figure shows, for a delta wing, how the flat wing theory with and without leading edge suction compares to the linear theory minimum drag and Jones lower bound predictions. The Jones lower bound prediction is useful in identifying the induced drag due to the wake and the wave drag-due-to-lift components. Note that the flat plate 100% leading edge suction and minimum drag predictions are nearly the same. The figure shows that the minimum drag should be obtained for values of $\beta \cot \Lambda$ of about 0.75, although the minimum is very flat and insensitive to $\beta \cot \Lambda$ over a 0.6 to 0.9 range. Based on a survey of supersonic wing design performance and the extensive experimental evaluation of linear theory derived wings by Mack (ref. 22), it appears that linear theory has provided good results up to $\beta \cot \Lambda$ = 0.75, while advanced fighter aircraft will typically cruise with supersonic leading edges (ref. 23) and maneuver supersonically over a range including the upper range of $\beta \cot \Lambda$ (0.8 to 0.9). This is the range for which the Mach

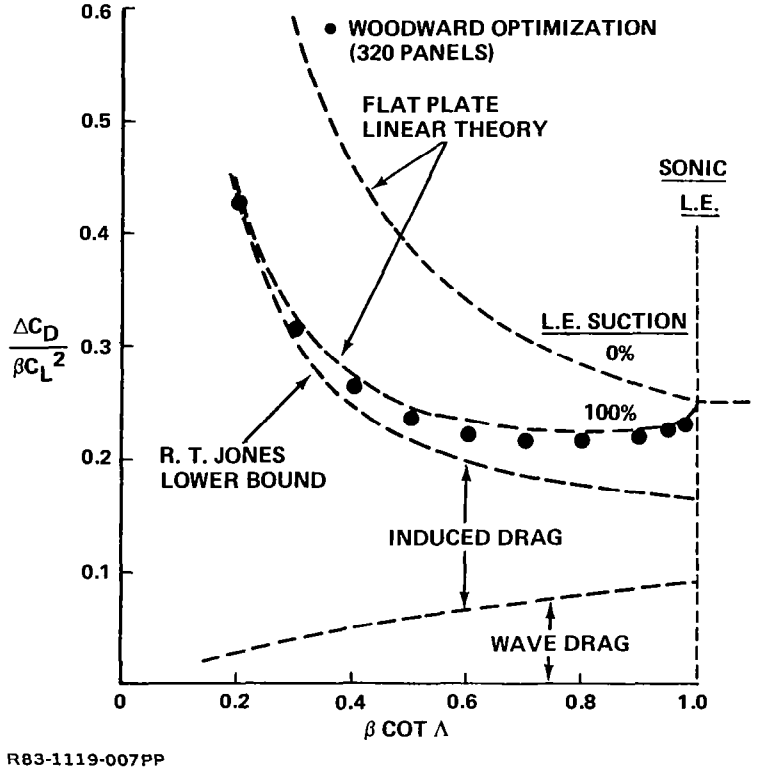

R83-1119-007PP

Figure 7. - Comparison of drag-due-to-lift performance levels from various theories for a delta wing.

numbers normal to the leading edge are transonic and SC^3 is required to design the wing. Thus, in addition to the C_L criterion, the SC^3 concept can be categorized as providing improved wings for design conditions above the linear theory $\beta \cot \Lambda$ "limit" of 0.75 for most C_L's.

A key assumption inherent in this discussion is that the linear theory drag minimum should be achievable even if the local flowfield contains nonlinearities. A theoretical basis for this assumption is not available. However previous work by the author (ref. 7) has shown that, for a number of supersonic flow model problems, the inclusion of nonlinear flowfield effects leads to performance values that actually exceed the linear theory level.

Some insight into the magnitude of the potential drag reduction can be obtained by looking at the results of the arrow wing model problem. Figure 8 shows the difference between 0% and 100% leading edge suction, where the 100%

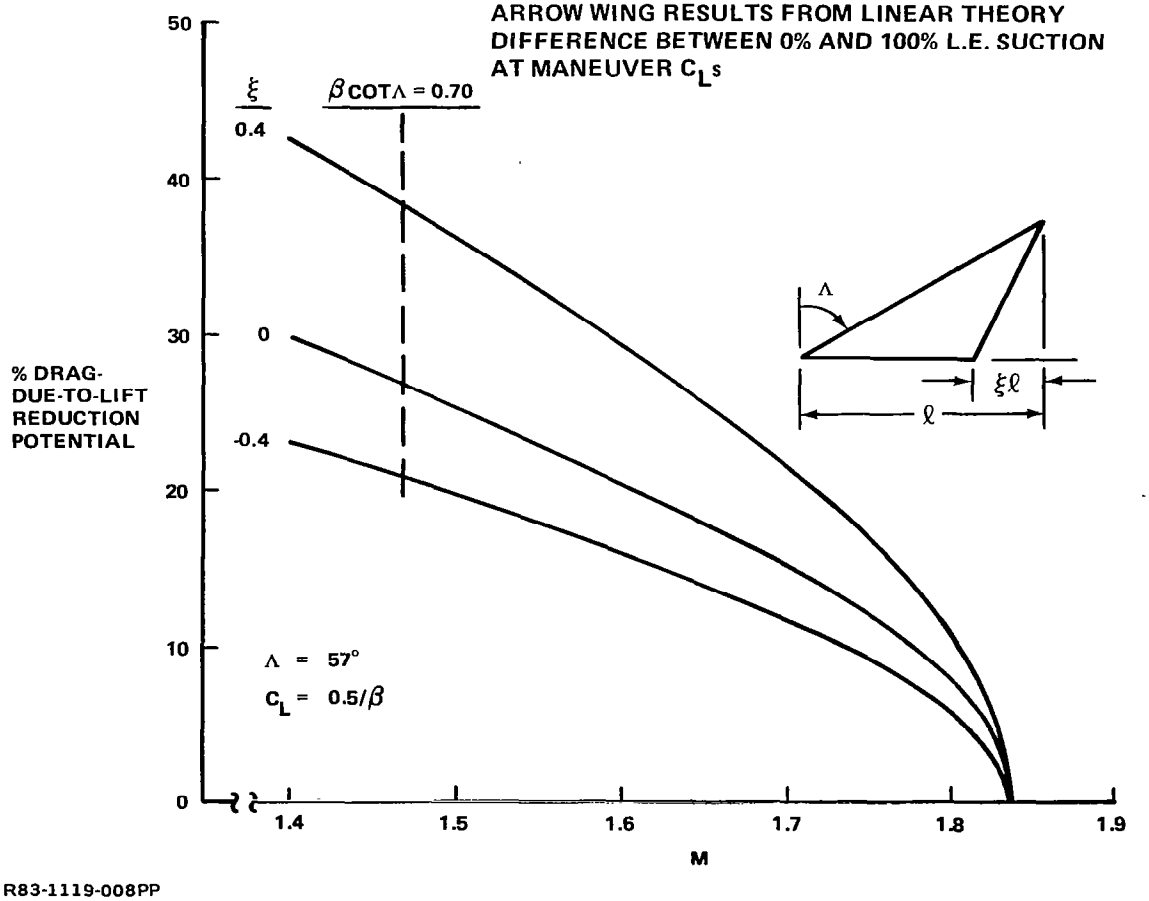

R83-1119-008PP

Figure 8. - An example of the drag reduction potential of the SC^3 concept.

suction flat wing result was shown in figure 7 to provide a useful estimate of the linear theory minimum drag using wing camber and assuming that no suction will be available. Clearly, the potential benefits increase rapidly with decreasing Mach number and increasing notch ratio. The lower Mach number limit for the applicability of SC^3 has not been established, but if $\beta \cot \Lambda = 0.70$ ($M_n = 0.80$) is arbitrarily selected as a lower bound on the transonic normal Mach number, M = 1.47 is a possible value for the lower limit of SC^3 in the 57-degree wing sweep case.

SPANWISE SECTION EFFECTS ON SUPERCRITICAL CROSSFLOW DEVELOPMENT

The implementation of an SC^3-type pressure distribution requires the generation of a wing shape that supports the SC^3-type pressures. This is achieved by considering the spanwise section in a manner analogous to the design of traditional airfoil shapes, and this was done using the conical flow approximation, which with a minor additional correction (ref. 19) has been found to be surprisingly accurate for general wing geometry. Since no inverse method exists (Appendix A), the development process consists of analyzing families of geometric shapes and selecting those that appear useful for further development, based primarily on the pressure distribution results. This section describes a few of the most useful cases considered during the study.

Consider first an uncambered wing with the spanwise section consisting of a super-elliptic thickness distribution. A previous paper (ref. 6) has shown that the basic super-elliptic thickness distribution leads to a well-behaved expansion at the leading edge. Figure 9 shows the pressure distribution development with increasing angle-of-attack. The strong cross-flow shock is clearly undesirable. The corresponding COREL drag predictions are shown as a percentage of the linear theory leading edge suction values in figure 10. For an uncambered delta wing of the type analyzed, linear theory predicts that the leading edge suction is independent of the lift coefficient. However, the COREL predictions vary rapidly when presented in this form. The prediction is in excess of 100% for the very low lift cases. With increasing lift, the crossflow quickly becomes supercritical and effective leading edge suction decreases rapidly with increasing lift until the predictions fall below the 0%

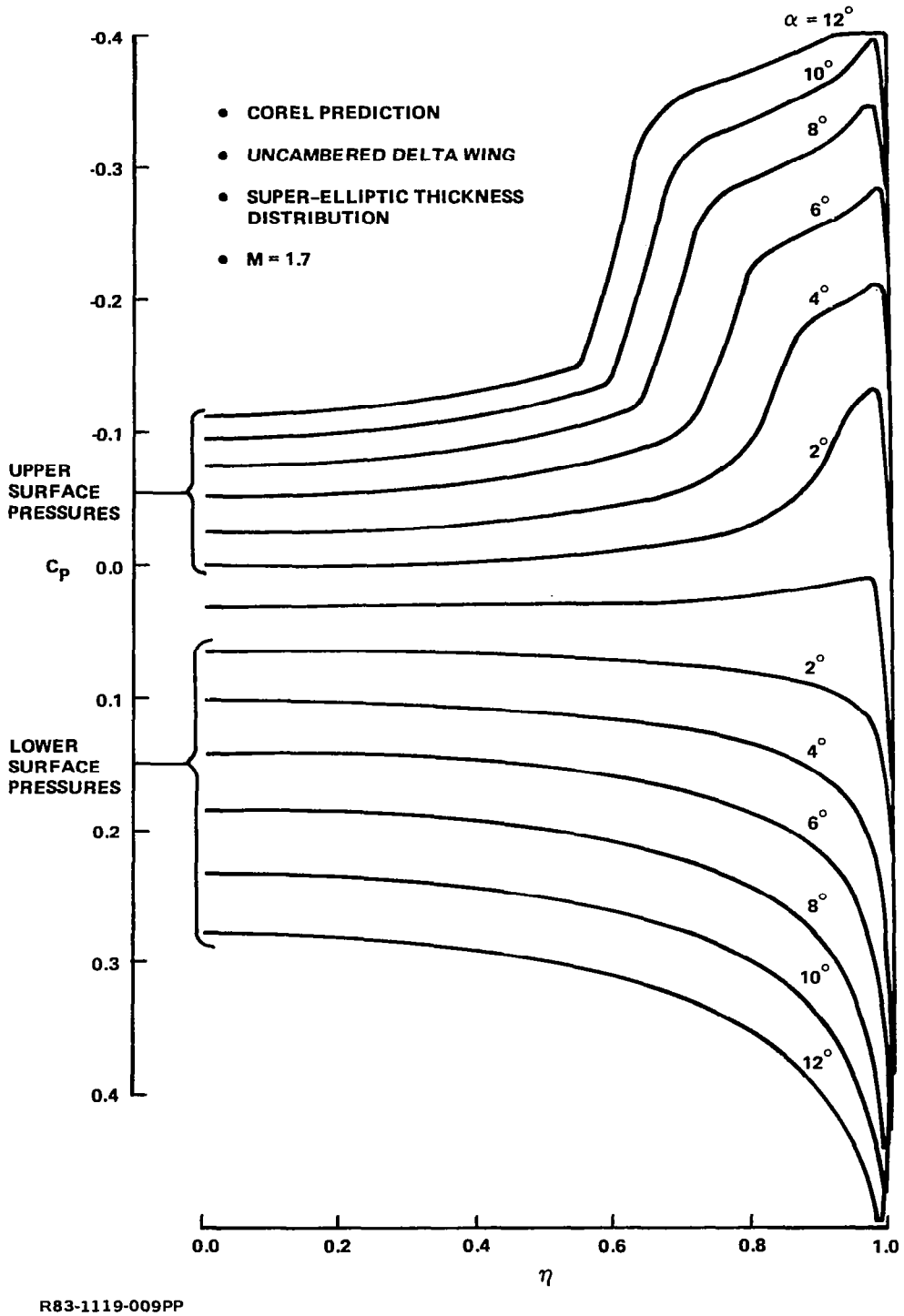

Figure 9. - Typical inviscid pressure distribution development with increasing angle-of-attack.

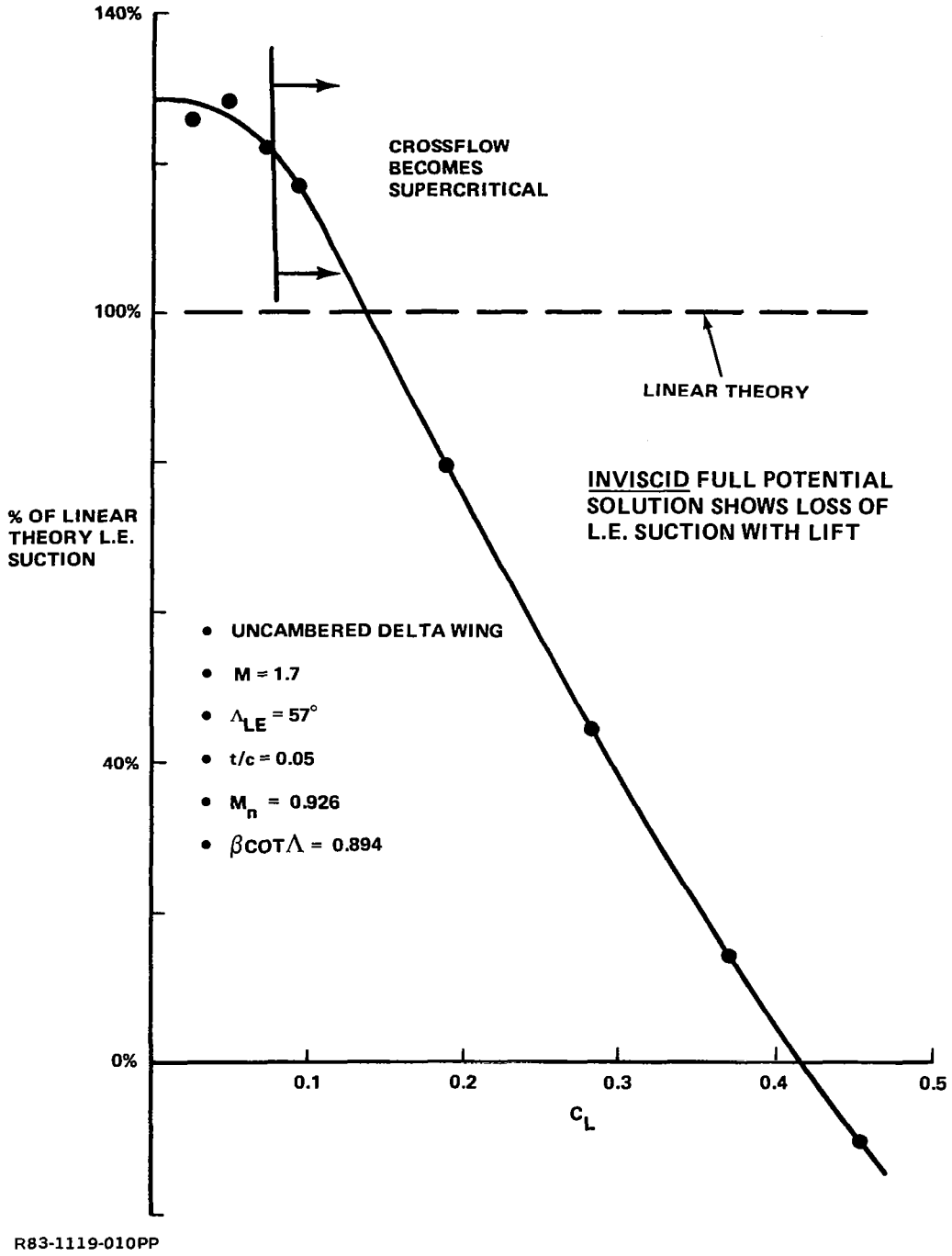

Figure 10. - Inviscid change with lift of the linear theory drag-due-to-lift parameter.

leading edge suction level. Traditional analysis has interpreted similar experimental trends as being due to boundary layer effects caused by the leading edge expansion and rapid recompression. However, this figure shows

that the effective leading edge suction performance of a wing computed using a nonlinear analysis does change and, in fact, decreases rapidly with increasing lift coefficient.

Camber effects can be illustrated using a simple spanwise circular arc camber distribution. A number of different simple geometric shapes were studied; the circular arc camber distribution, together with the super-elliptic thickness envelope, appeared to come closest to producing a pressure distribution similar to the desired SC^3 type shown in Figure 5. Figure 11 shows the pressure distribution and crossflow Mach numbers for several camber deflection angles, δ_f. The C_L was held constant and the angle-of-attack increased to account for the changes in lift with camber. A relatively flat rooftop occurs for a deflection of 15°. The related drag performance is shown in figure 12. In figure 12A, the minimum drag occurs for deflections of about 20°. Figure 12B shows the variation with lift for four of the camber shapes. At the higher

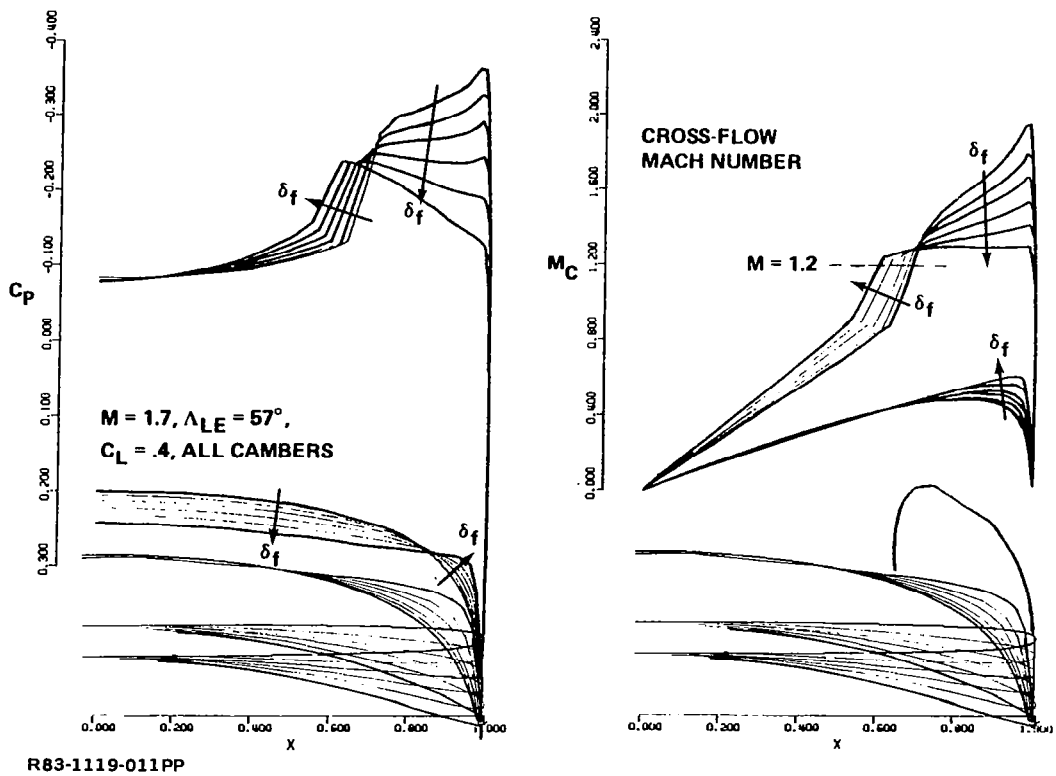

Figure 11. - Concial camber design using COREL - effect of circular arc camber on pressure and Mach number distributions.

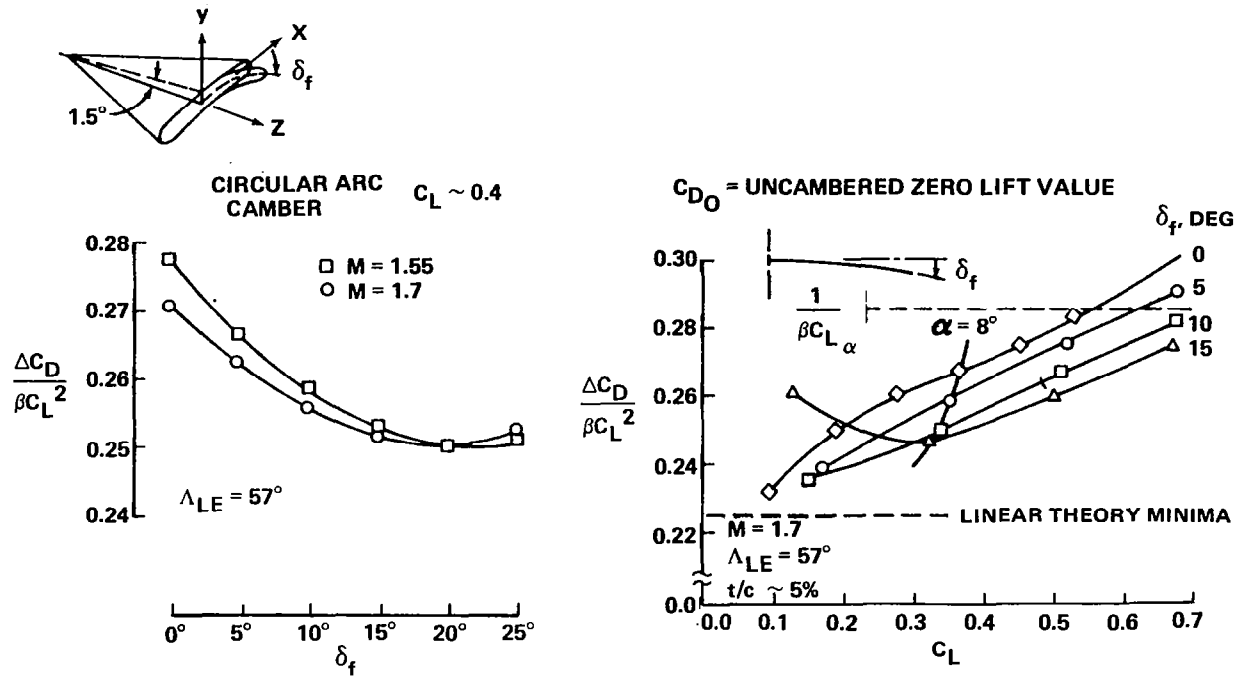

R83-1119-012PP

Figure 12. - Conical camber design using COREL: effect of circular arc camber on drag-due-to-lift.

lift coefficients ($C_L \simeq 0.4$) the drag is predicted to be reduced to a value about halfway between the $1/C_{L_\alpha}$ value and the linear theory minima.

The dihedral angle, Γ, provides an additional degree of freedom in that linear theory predicts no dihedral effect on the pressure distribution. Dihedral was studied using COREL, and the results showed that the plateau pressure shape can be adjusted using dihedral without making significant changes to the subcritical pressures. An example of this is given in figure 13.

The results for the various spanwise section shapes presented above provide considerable insight into the development of the baseline shapes for the SC^3 concept. One further study was made. The linear-theory minimum-drag shape developed by Tsien (ref. 16) was analyzed. Figure 14 shows the various shapes. These are the minimum drag camber shapes given in figure 7 of ref. 16 for the m = 0.8 case, where Tsien's m is $\beta \cot\Lambda$. The shapes include the design angle-of-attack and hence are defined at negative values of $C_L(z/x)$,

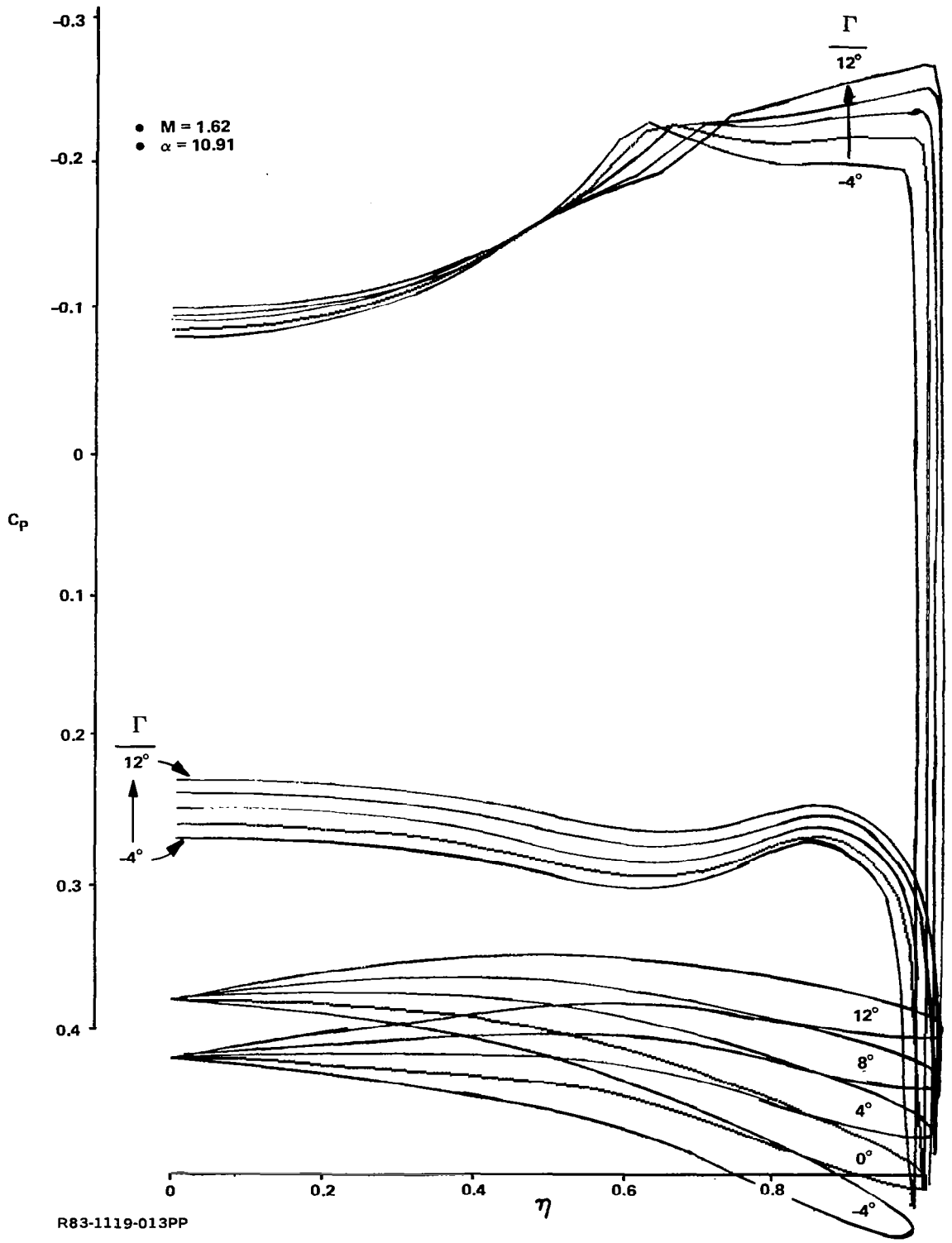

Figure 13. - Dihedral effects on a delta wing with conical camber.

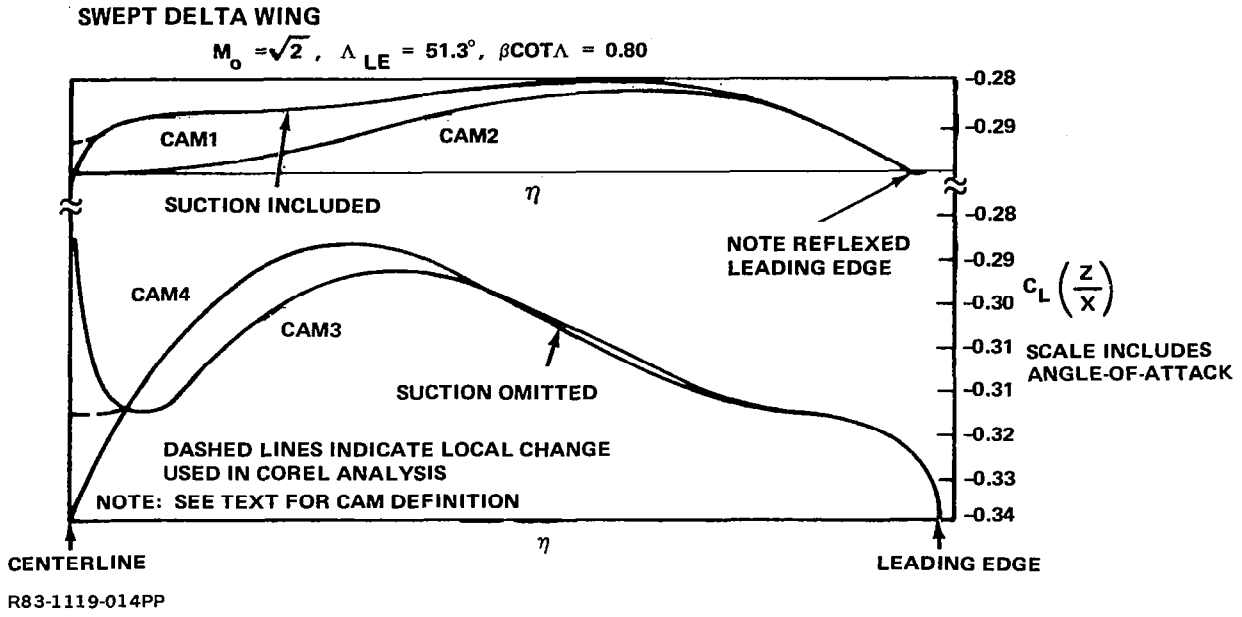

Figure 14. - Linear theory minimum drag spanwise camber shapes found by S.H. Tsien (ref. 16).

which correspond to a positive angle-of-attack. The different shapes included in the figure correspond to different assumptions regarding the leading-edge suction force. The "suction included" curves (CAM1, CAM2) assume that 100% of the theoretical leading edge suction can be obtained, and the optimization problem is solved on that basis. Notice that there is only a small amount of spanwise camber and the slope is small and, in fact, slightly reflexed at the tip. For the curves labeled "suction omitted" (CAM3, CAM4), the minimization is carried out assuming that no suction will be realized, even if the minimum drag loading would theoretically predict that a suction value should exist. In this case the camber is much more pronounced, with the camber slope being very large at the tip. For each case described above, results were obtained both with and without the singularity in camber shape at the root. The root singularity cases are designated CAM1 and CAM3. The cases without the root singularity are CAM2 and CAM4. The local singularity at the centerline was eliminated when analyzing the shapes using COREL by modifying the shapes to the dashed lines shown in figure 14. Numerical experiments with COREL indicated that the nonlinear solution was insensitive to the small and local details at the centerline. These results are consistent with the more recent "attainable

leading edge thrust" concept introduced by Carlson (ref. 8), wherein the allowance for L.E. suction leads to reduced design camber. Figure 15 shows the resulting pressure distributions obtained using COREL. The results for low lift coefficients are very similar to the flat plate solution, while at the high lift coefficient the leading edge pressure expands to a strong crossflow shock. COREL-predicted drag results presented in figure 16 demonstrate that the nonlinear inviscid theory predictions agree with the linearized theory for the low-lift-coefficient case but predict considerably higher drag for high-lift-coefficient case. These results illustrate why the linear theory shapes fail at the high lift coefficients.

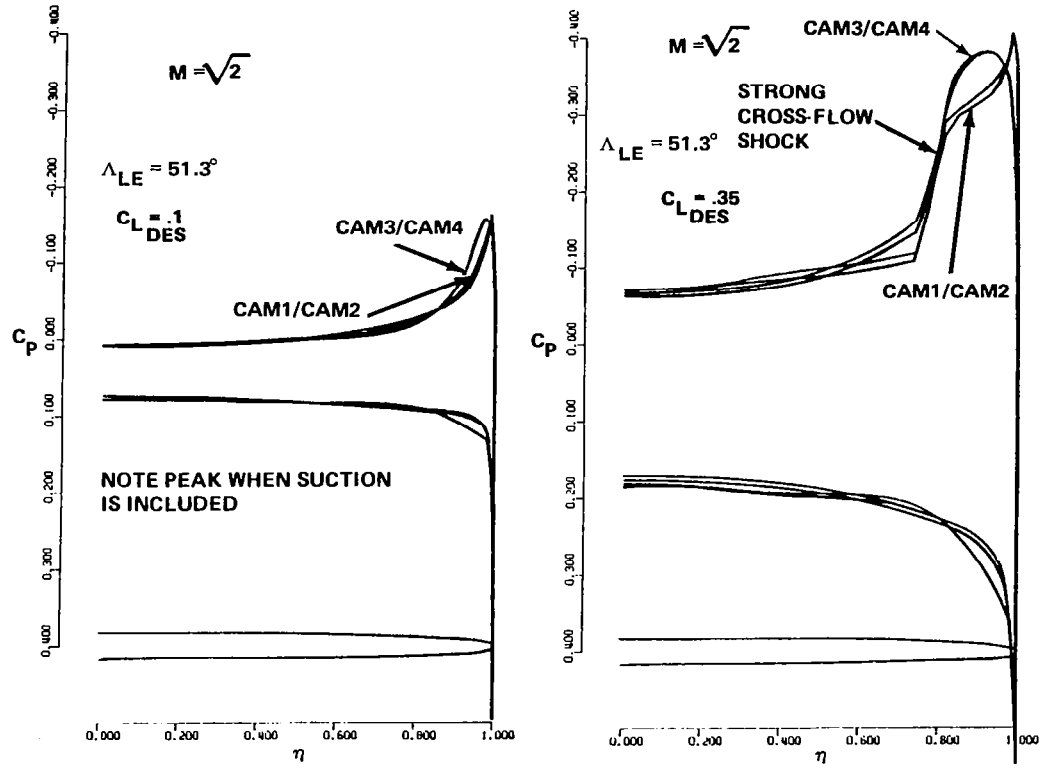

R83-1119-015PP

Figure 15. - Pressure distributions from a COREL analysis of Tsien's minimum drag shapes.

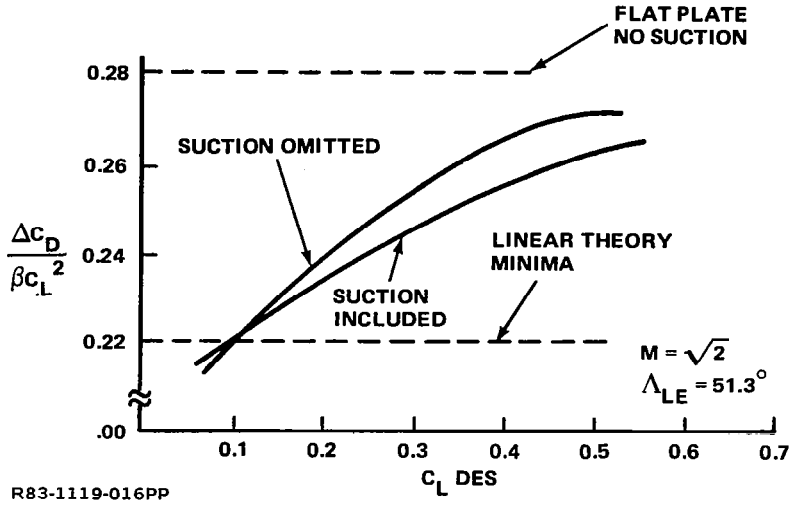

Figure 16. - COREL predicted inviscid drag-due-to-lift of Tsien's minimum drag shapes.

VALIDATION OF THE CONCEPT

The first step in developing the SC^3 concept was the implementation of an actual SC^3 design which was then to be fabricated and tested in the NASA Langley Unitary Plan Wind Tunnel. An essentially conical wing was selected in order to minimize the differences between the conical calculation method used to design the spanwise section and the wind tunnel model. This model was thus called the "conceptual wing," and is the equivalent for supersonic flow of a two-dimensional airfoil test in transonic flow. This section summarizes the work, which has been described previously in ref. 6, with the complete details and data given in ref. 24*.

A planform sweep of 57° was selected based on advanced aircraft studies (ref. 23). The design Mach number of 1.62 and design lift coefficient of 0.40 were selected by choosing the linear theory parameters of $\beta \cot \Lambda = 0.825$, and $C_L = 0.5/\beta$. This represented a decrease in design Mach number from the originally envisioned value of 1.70 based on the results given previously.

- - - - - - - - - -

*Note that Appendices C2 and C3 in ref. 24 were accidentally omitted in the published volume, and D.S. Miller of the NASA Langley Research Center should be contacted for that information.

Aerodynamic Design

The design was developed using the circular arc camber described in the next section as a starting point. When the balance housing was included in the computational model, the additional interference lift of that shape on the lower surface led to a conical, wing-balance housing design lift of about 0.46. The balance housing also led to an increase in the basic camber from 20° to 24° to account for the additional leading edge expansion due to its presence.

Figure 17 shows one of the resulting spanwise section designs which comes close to meeting the desired pressure distribution. The figure contains the spanwise shape, the pressure distribution, and the crossflow Mach number distribution. Basically, the spanwise shape is a 24° circular arc camber line with the baseline superelliptic thickness distribution added perpendicularly to the camber line, and an 8° half-cone included on the lower surface to provide room for the balance and pressure transducers. The crossflow Mach number distribution shows that a peak Mach number of about 1.4 is reached, followed by a recompression to a crossflow shock wave with a normal Mach number of about

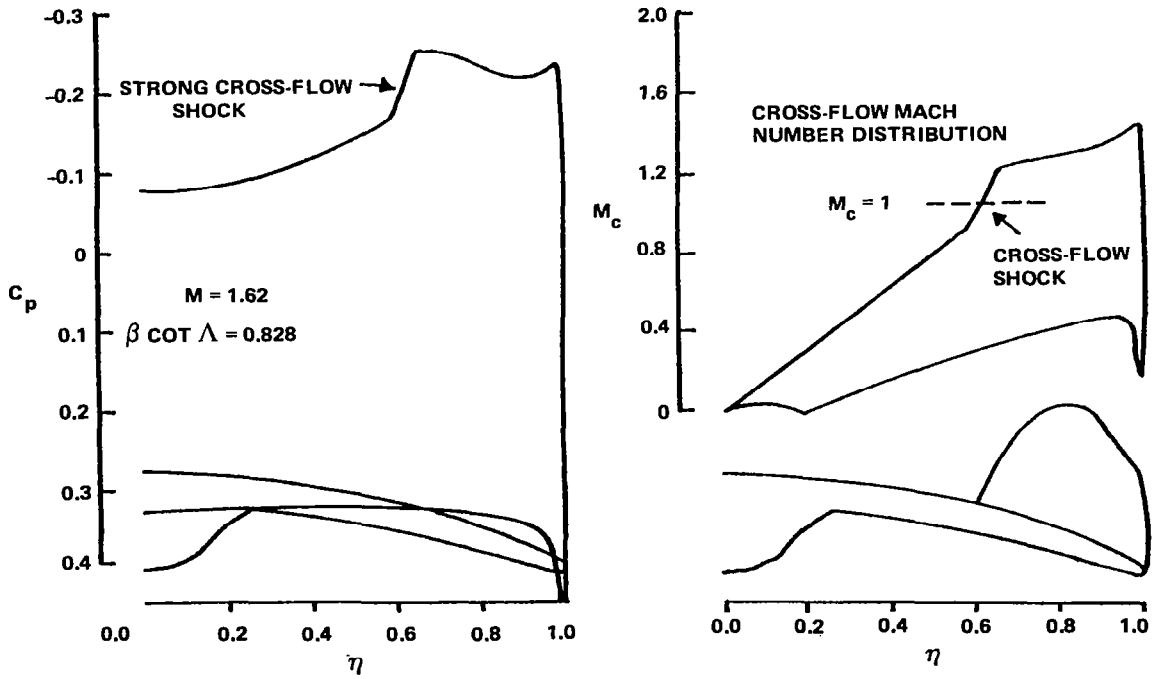

R83-1119-017PP

Figure 17. - Baseline cambered section for conceptual wing.

1.2; this is about the maximum allowable shock strength for which a turbulent boundary layer can be expected to remain attached. The pressure distribution shows that the pressure expansion continues as the shock is approached despite the decreasing speed of the crossflow. This is due to the continually increasing radial velocity component of the flow along the ray, which is not depicted in the figure.

Some further changes were made to the basic design of figure 17 to refine the leading edge expansion slightly and reduce the strength of the crossflow shock wave. Recall that, although the separate treatment of camber and thickness effects are indeed useful, superposition of the thickness and camber results is not valid for a nonlinear flow field. Therefore, the final details of the design were obtained by modifying the actual spanwise section geometry. This was done by repeated applications of the COREL code in the analysis mode to a series of local shape perturbations. The shock strength was decreased by reducing the curvature of the cross-section outboard of the shock and then increasing it inboard of the shock, as shown in figure 18. This led to a thicker section. The basic section thickness then was retained by subtracting thickness from the lower surface. As expected, lower surface pressures are not

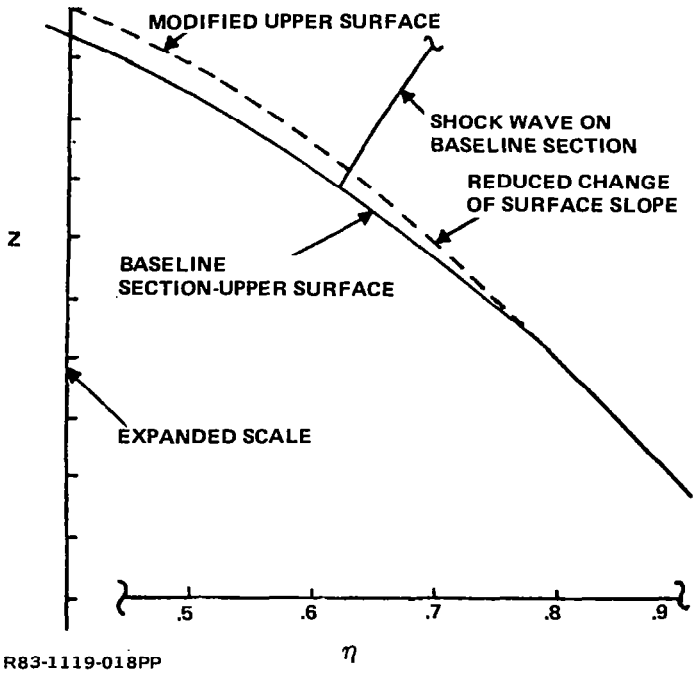

Figure 18. - Upper surface shape tailoring to control supercritical crossflow on the conceptual wing.

sensitive to small changes in the lower surface geometry. The resulting design is shown in figure 19. The upper surface tailoring was so successful that the crossflow shock wave appears to be entirely eliminated. To reiterate, this type of precise tailoring of the surface using fully nonlinear tools to perform aerodynamic design is the key to eliminating adverse viscous effects and achieving the full performance benefits which should be available for a properly designed optimum wing. The design shown in figure 19 represented a large step forward in high lift supersonic wing design and was selected for experimental verification.

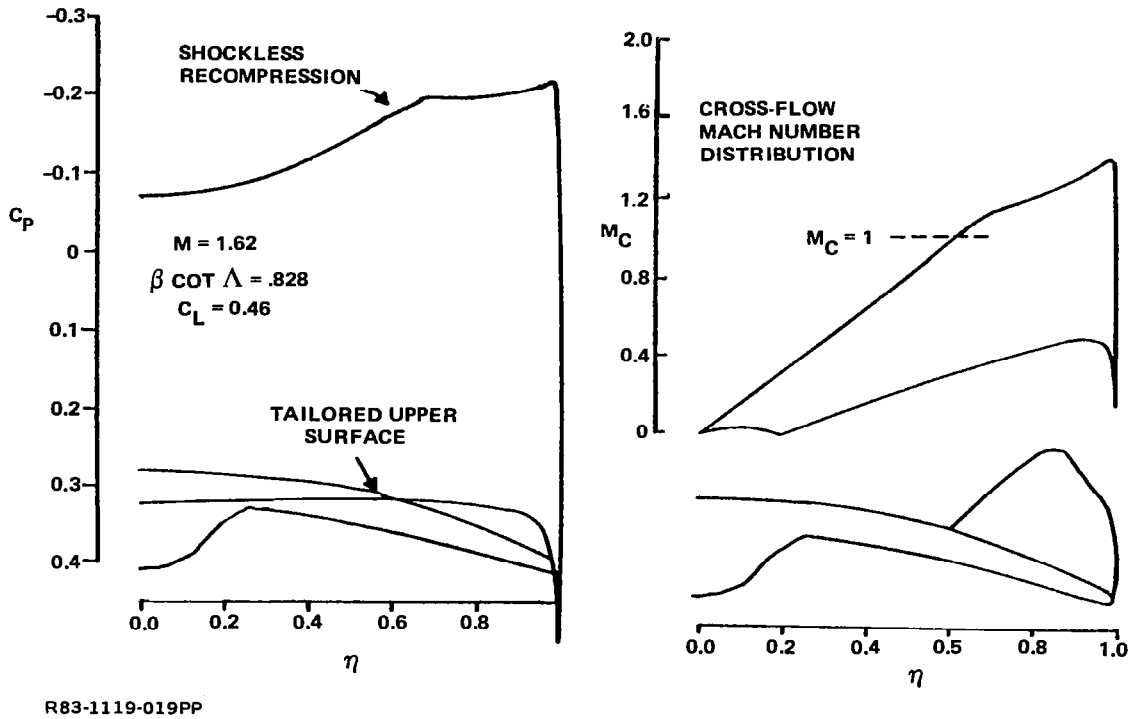

Figure 19. - Final spanwise section design for the conceptual wing.

Model Fabrication and Wind Tunnel Test

The wind tunnel test was designed to experimentally verify the controlled supercritical crossflow concept. For comparison purposes, a flat wing was also tested. Analysis indicated that the flat wing would have a strong crossflow shock wave at the design C_L. Thus, the experiment could also be used to

establish the exact nature of viscous effects and the relative drag-due-to-lift performance of the spanwise sections. Both wings could be used to assess the predictive capability of the COREL code (ref. 19) under conditions of interest for aerodynamic design, but for which no data were previously available. The models were initially conical, but made a transition to constant thickness over the aft portion.

A major concern in designing the experiment was the ability to make a model with a large leading edge. There were three reasons for this: the requirement for accuracy in fabrication, space for installing detailed pressure instrumentation, and a high leading edge radius Reynolds number. Numerical studies, such as those illustrated in figures 9 and 17 indicated that the details of the expansion would depend on accurate construction of the leading edge. An additional concern was the ability to trip the boundary layer flow near the leading edge without disturbing the local flow and, hence, the pressure measurements. Subsequent analysis of the wind tunnel results indicates that these potential difficulties did not materialize. The two wind tunnel models were constructed at the NASA Langley Research Center. The cambered wing model was designed to obtain the pressure distribution shown in figure 19. The flat wing, employing the same planform and thickness distribution as the cambered wing, was constructed to obtain the reference volumetric wave drag and pressure data containing crossflow shocks.

As described above, the cambered wing was designed in the presence of a 8° half-cone centerbody, which was placed under the wing to house the force balance and two scani-valve pressure transducers. The first 60% of the model length was pure conical with a centerline half-angle of 1.5°. Aft of this location, a smooth transition was made to a constant-thickness geometry and, for the cambered wing, a straight leading edge was maintained across the entire span of the cambered wing. The wing tip was cut back in order to reduce wing area. The resulting thick trailing edge was recessed and the balance housing half-cone was truncated at a buttline of 2.5 inches and a waterline of -2.024 inches. These cuts were smoothed by 0.5-inch radius fairings.

The theoretical results for wings with supercritical expansions were found to be sensitive to the details of the leading edge geometry. In order to verify geometric accuracy, both models were inspected prior to testing. As a

result, the leading edges of each wing were reworked while located in the NASA numerical recording measuring machine. The final leading edges were within a few thousandths of an inch of the desired shape over the entire leading edge; this corresponded to a tolerance of about 2% of the leading edge radius at the principle row of spanwise pressure instrumentation.

The models were instrumented with 79 pressure taps, of which 40 were located on the main conical flow measuring station. Four taps were located in the recessed base of the wing and two pressures were measured on the inside of the balance housing to determine the base drag on the models. An initial spanwise row of pressures was included to check the conicity of the flow field.

Figure 20 shows the cambered model installed in the tunnel. Both models were tested in the NASA Langley Supersonic Unitary Plan Wind Tunnel. Pressure, flow visualization, and force and moment data were obtained. The basic testing was conducted at an Re/ft of 2 million, transition fixed, over a range of Mach numbers from 1.60 to 2.0. Transition-free surface pressure results were obtained on the uncambered wing. Based on the pressure distribution results, oil flow photographs were taken on the flat wing at M = 1.70, α = 2, 3, 4, and 6° ($0.09 < C_L < 0.24$), and on the cambered wing at M = 1.62 and α = 10, 11, and 12° ($0.37 < C_L < 0.46$).

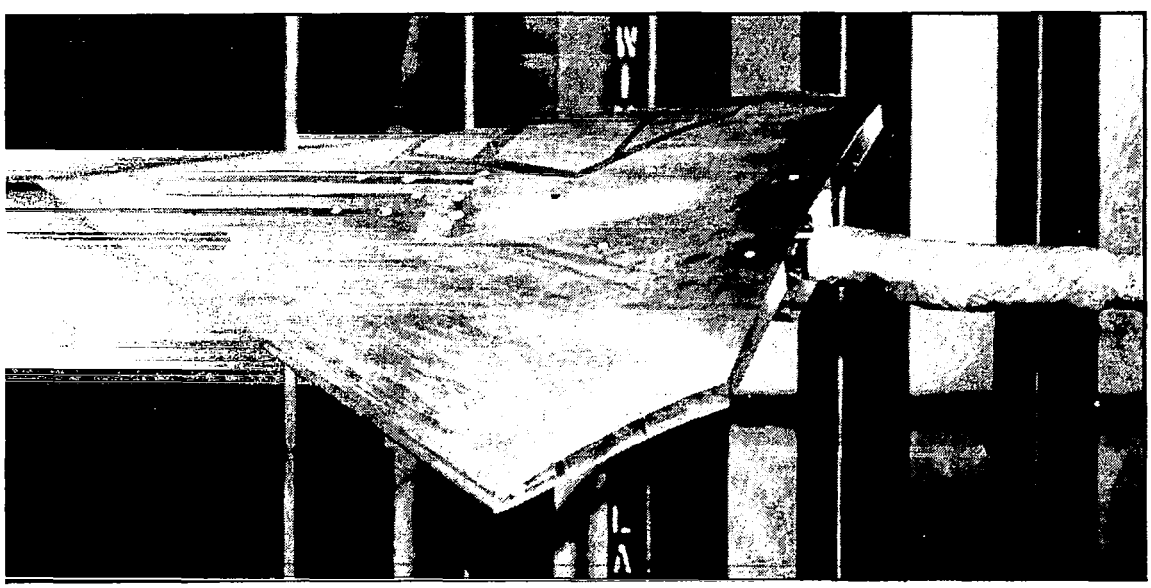

Figure 20. - Conceptual wing model installed in NASA Langley Unitary Plan Wind Tunnel

Analysis of Experimental Results

The primary results shown in figure 21 for the cambered wing are from the main conical row of pressures at M = 1.62, and demonstrate that a shockless recompression was obtained! Note that the pressure taps on the lower surface start at η = 0.26 due to the presence of the housing, which extends outboard to an 0.22.

Figure 21 provides results for angles-of-attack slightly above and below the nominal design angle-of-attack of 10°. The crossflow is supercritical at α = 8.93°, but has not quite reached the full constant plateau shape. The plateau becomes stronger as the angle-of-attack increases so that, at α = 10.91°, the pressure plateau attains a constant rooftop terminated by a gradual recompression. The wing C_L for this case was 0.415. No crossflow shock wave

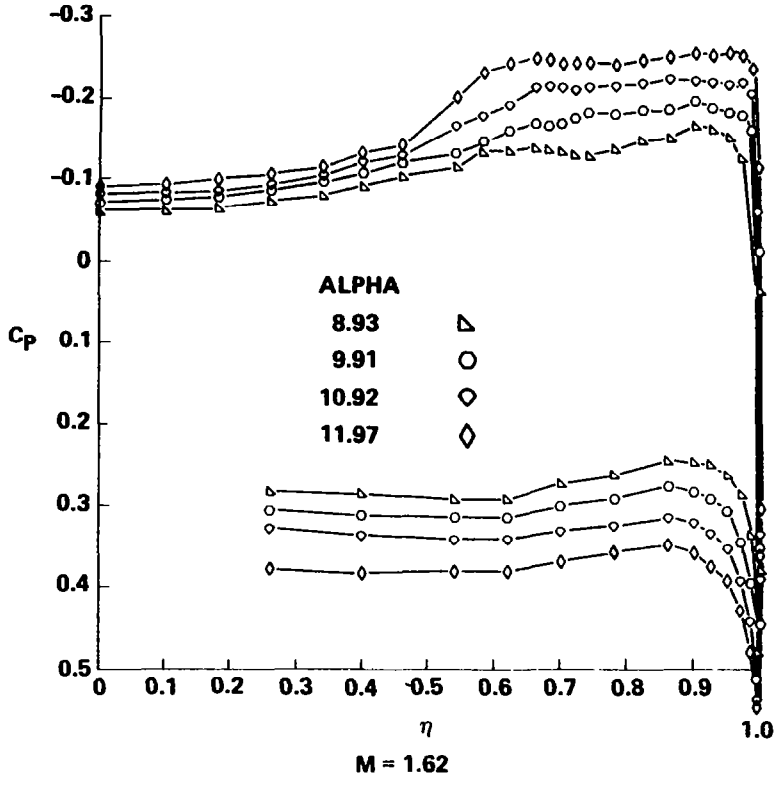

R83-1119-021PP

Figure 21. - Spanwise pressure distribution results on the conceptual wing demonstrate shockless supercritical crossflow.

is evident. At $\alpha = 11.97°$ ($C_L = 0.463$), the recompression begins to steepen into a crossflow shock wave. This analysis shows that the design pressure plateau was reached at about 1° above the design angle-of-attack.

These results proved that stable supercritical crossflow wing flow fields could be established and that the recompression can even be accomplished without a crossflow shock wave. Similar results were obtained at Mach numbers of 1.60, 1.66, and 1.70.

Figure 22 provides the corresponding results for the transition fixed testing on the flat wing. The differences between the flat and cambered wings

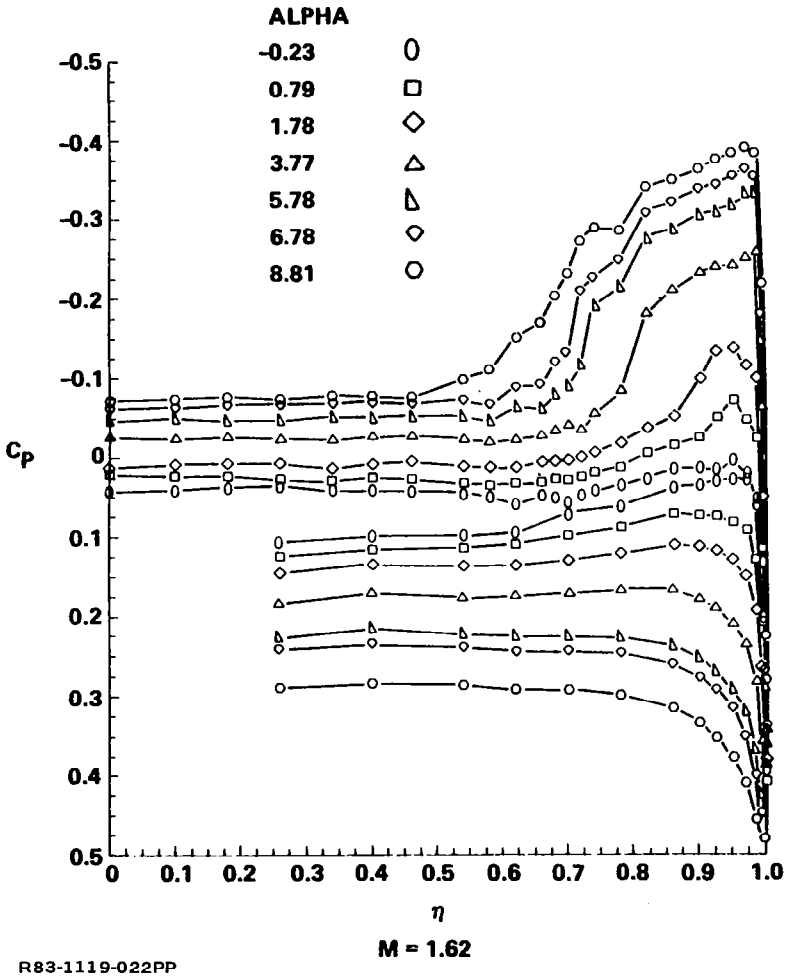

Figure 22. - Spanwise pressure distribution results on an uncambered wing demonstrate strong crossflow shock.

are immediately evident. At $\alpha = -0.23$, the wing has a positive lift due to the pressure field induced by the conical housing on the lower surface. At $\alpha = 1.78$, the flow expands about the leading edge and then recompresses in a typical subcritical crossflow recovery. At $\alpha = 3.77°$, the flow expands to a distinct supercritical pressure plateau for which the recompression to subsonic crossflow is accomplished through a shock wave; this is shown as a clean jump in pressure. The boundary layer acts to spread the pressure jump over several displacement thicknesses, but the shock wave is still very distinct since the boundary layer has been tripped prior to the shock. At this α the C_L is 0.198. At an α of 5.78, the flow shows an additional expansion and the shock wave is not as distinct; this indicates that some flow separation is beginning to occur at the shock.

Figure 23 presents some comparisons between the experimental results and the inviscid irrotational theoretical predictions obtained from COREL. The $M = 1.66$ results are selected for the comparison in figure 23A to include another set of experimental data. Overall agreement is good; however, the predicted plateau levels are slightly lower than the experimental results. The transition fixed flat wing data are compared with theory in figure 23B. The predictions are as good as could possibly be expected, and this agreement is the same for all the attached flow results on the flat wing. It is especially satisfying to see how well the crossflow shock predictions agree with the experiment.

Although the thick, nearly conical models were designed primarily to achieve design pressure distributions to demonstrate controlled supercritical crossflow, it is instructive to examine the relative drag-due-to-lift performance of the two wings. This is best illustrated using the linear drag-due-to-lift parameter $\Delta C_D/\beta C_L^2$, where C_D is the minimum drag of the flat wing. Figure 24 shows the superiority of the cambered wing. The linear-theory minimum drag and the flat plate 0%-leading-edge-suction values are also shown. The flat wing is not developing any leading-edge suction at the design point, whereas the cambered wing is attaining about 65% of the reduction in drag that linear theory predicts is available. The figure also shows that the experimental value of the cambered-wing drag-due-to-lift parameter reached its minimum value at the design point. This is in direct contrast to the usual results for wings

designed using linear theory where, even at low lift coefficients, the minimum value of the drag parameter is attained at lift coefficients somewhat higher than the design lift coefficient.

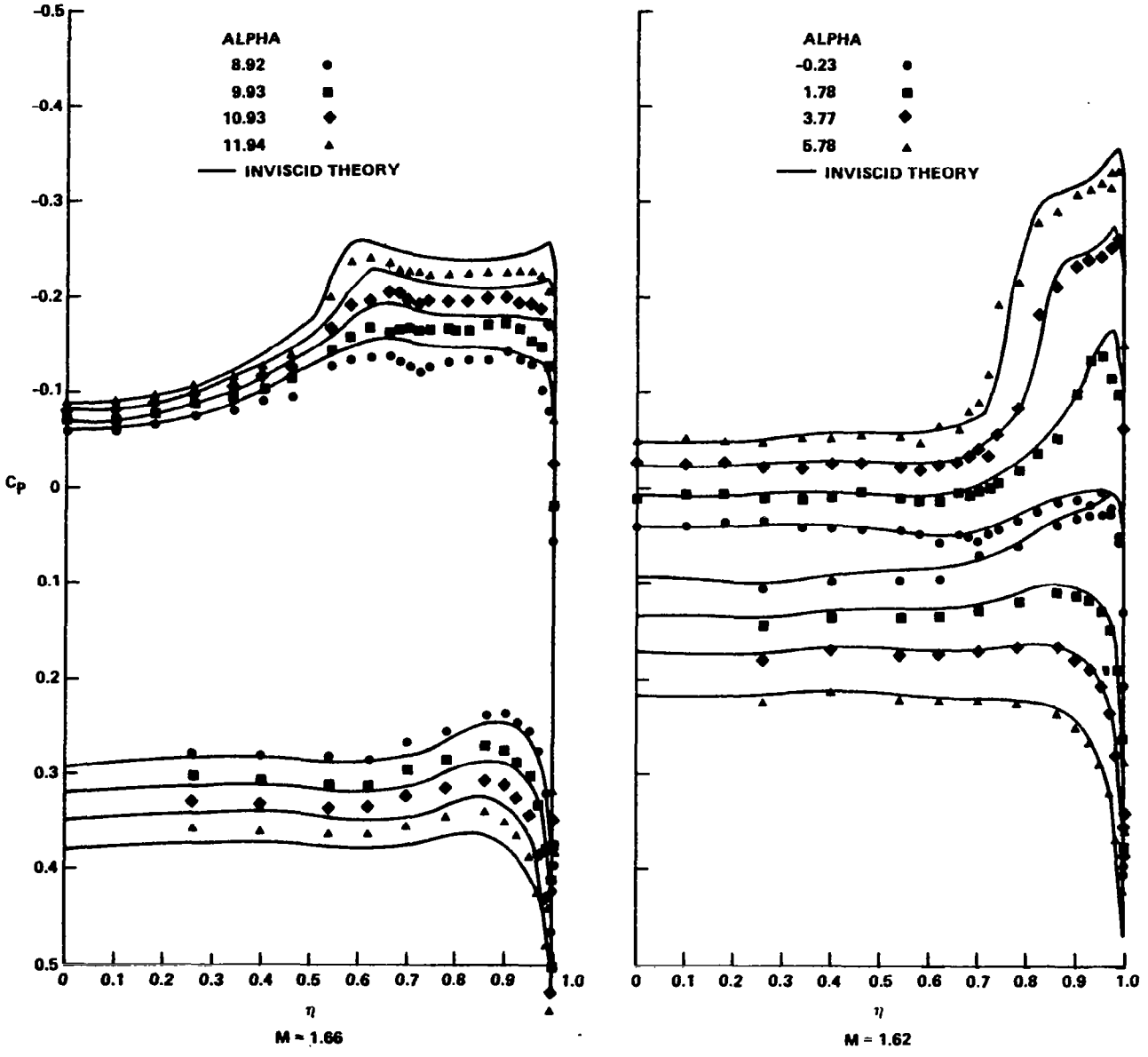

Figure 23. - Comparison between COREL predictions and experimental results.

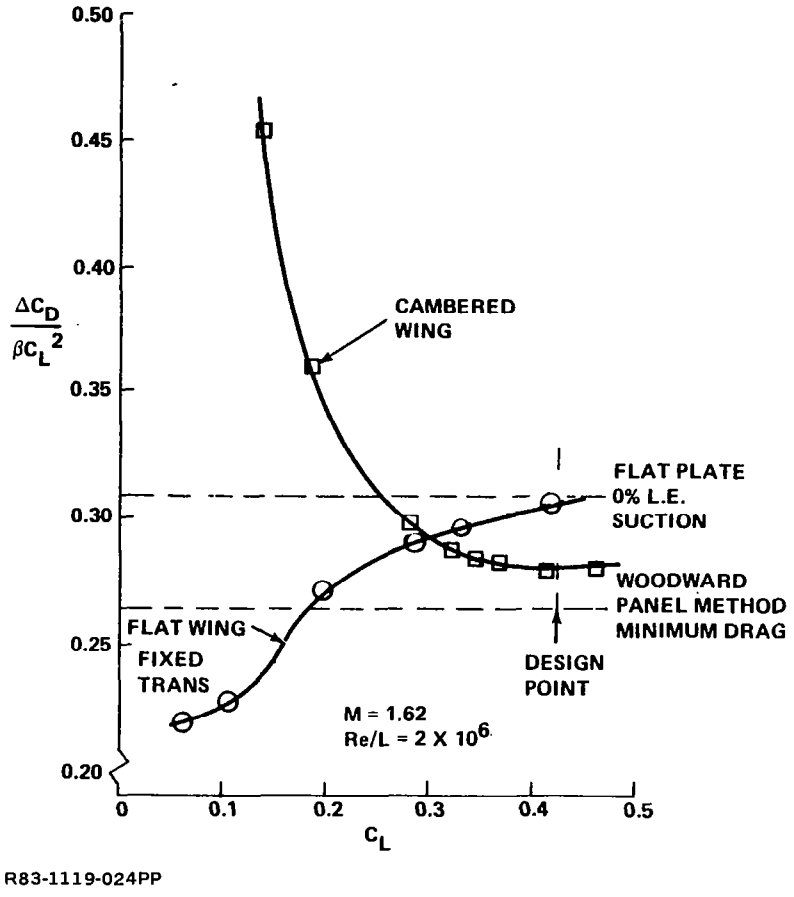

Figure 24. - Drag-due-to-lift comparison of the conceptual wing and the uncambered wing.

SC^3 IN A FIGHTER WING

With the basic SC^3 concept validated for the conceptual wing, the next step was to design and test a non-conical wing with a planform and thickness distribution representative of the anticipated advanced fighter requirements (ref. 3). With the previous numerical and experimental results providing a solid foundation, the extension to the general case of a fighter wing was initiated. A planform was selected that included a varying leading and trailing edge sweep as shown in figure 25, and an isolated wing case was selected in order to concentrate entirely on the SC^3 concept*. This wing is known as the

- - - - - - - - - -

*Body and Canard interference effects on the SC^3 concept have been evaluated experimentally on the conceptual wing; see Appendix B.

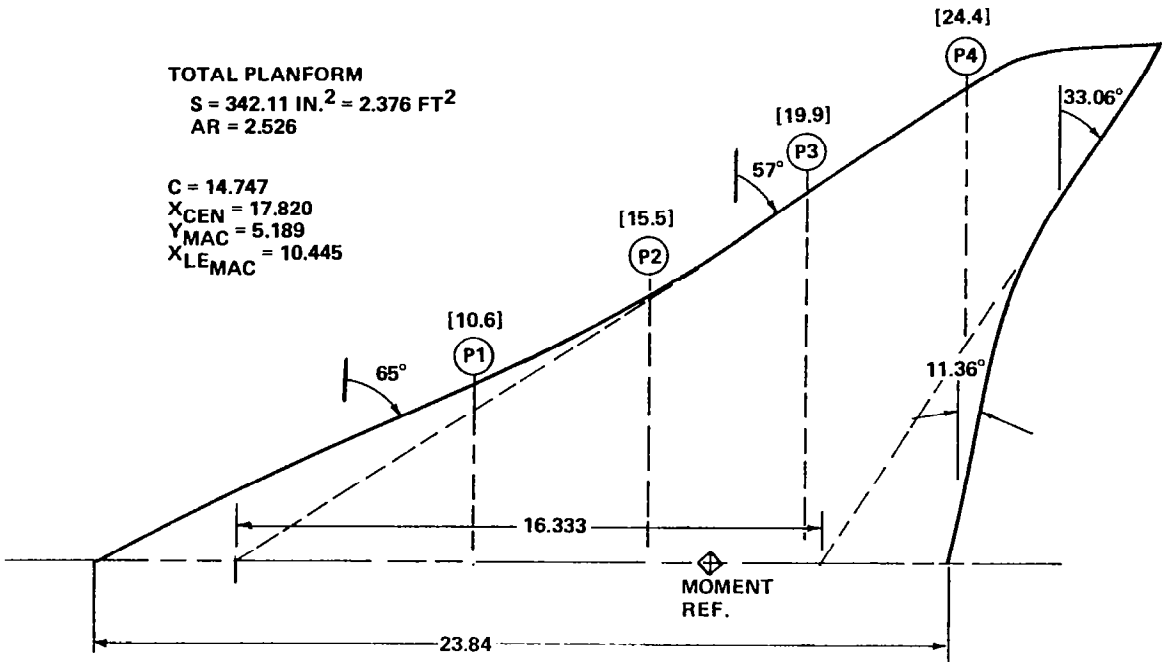

Figure 25. - Demonstration isolated wing planform.

"demonstration wing.". Aside from planform and thickness considerations, no configuration integration issues were addressed in the design process. This section describes work which has been reported in ref. 25, with the complete details and tabulated data presented in ref. 26.

Aerodynamic Design

Design conditions of M = 1.62 and C_L = 0.4 were selected as being representative of typical maneuver conditions. This lift coefficient is about twice the upper limit on design C_L for wings based on linear theory. The maximum thickness ratio was specified to be constant across the span, with a value of 4% selected as being representative of future tactical aircraft. Tailoring of the thickness distribution across the span was not considered during the design process.

In considering the thickness envelope, the leading edge radius selection was based on the requirement for a large leading edge radius to generate a significant load on the leading edge while avoiding the typical large expansion pressure peak. Results presented previously suggest that a radius typical of transonic supercritical airfoil leading edges was required. This represents a several-fold increase in leading edge radius compared to the typical NACA 6A series sections used for supersonic wings.

The modified NACA 4-digit series thickness distribution appeared to meet these requirements and was selected. The 4% value of the maximum thickness point was located at X/C = 0.40 to correspond to the 64A series airfoils, and the leading edge radius was increased relative to the basic 4-digit series by about a factor of two. This radius varied from a r/c value of about 0.001 inboard to 0.004 outboard, which is consistent with typical transonic supercritical airfoils.

The aerodynamic design problem then consisted of determining the geometry that would produce an essentially conical pressure distribution, with a constant-pressure plateau-type supercritical crossflow region on the upper surface terminated by a weak shock or possibly shockless recompression to the subcritical crossflow portion of the wing. The problem thus became one of defining a target pressure distribution and then developing the geometry that would produce it.

The target pressure distribution was developed as part of the preliminary analysis of the wing using linear theory methods. W12SC3 was used to determine the drag due to lift for various cases. W12SC3 ignores local edge forces in the total force calculation (as do both Woodward I, ref. 20, and Woodward II, ref. 21) and thus the results presented below assume 0% leading edge suction. The results are shown in figure 26 for the flat, constant-pressure, linear-theory minimum-drag wing and the constant-pressure supercritical crossflow plateau drag (linear theory SC3 panel). The magnitude and extent of the constant-pressure panel was selected based on a parametric study that determined the combination of these parameters which provided low linear theory drag results and a supercritical panel constant-pressure value which appeared attainable in the real flow. This established a nominal target pressure distribution which, based on linear theory, would lead to only a small drag

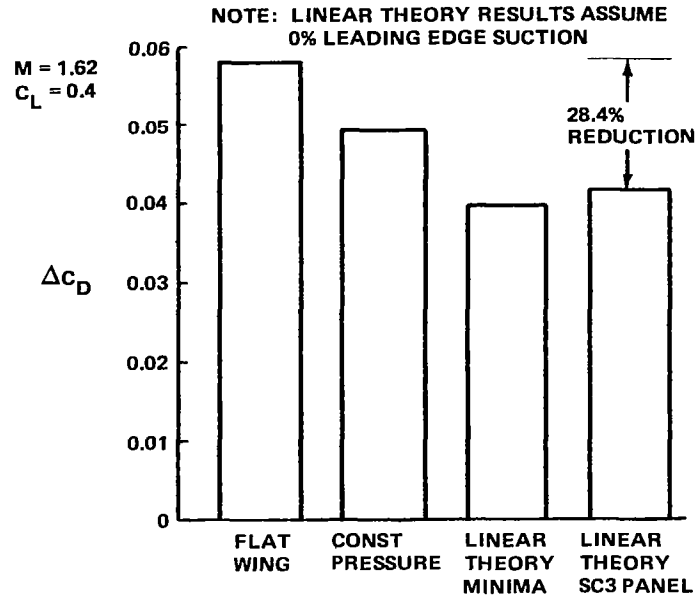

R83-1119-026PP

Figure 26. - Drag-due-to-lift goals for the demonstration wing from linear theory.

penalty compared to linear theory minimum drag.

Once the nominal target pressure distribution was established, a systematic means of developing the required wing geometry had to be devised. After some initial analysis, it became clear that an analytic model of the entire wing was required. The "analytic wing" representation was formulated into a computer program which allowed for a continuous and smooth representation of the wing between the spanwise stations at which pressure results were examined in detail. The wing was then analyzed and modified in a series of steps leading toward the target pressure distribution. The COREL and NCOREL computer codes were used in this process. In carrying out the design, changes in shape were made using the camberline. Although the camberline was specified, the actual upper and lower surface contours were required in the design process and the use of the camberline as a design parameter was actually an artificial choice made for convenience. The thickness was added vertically to the camberline. In essence, camberline changes were made to obtain desirable upper surface contours, and the lower surface shape was simply a "fallout" obtained by maintaining the specified thickness distribution.

The initial baseline camber distribution was selected based on the work described previously to be a circular arc conical camber starting at the wing centerline. For the specified design conditions, the previous work indicated that a wing tip angle of 20°-24° measured spanwise at the leading edge would be desirable, and the circular-arc conical-camber configuration comprised the initial "guess" for the design. COREL results indicated that 22° camber would be desirable, with more camber forward, where the leading edge sweep was 65°. The additional camber was added on the front portion of the wing to eliminate the adverse pressure gradient and thus be conservative with respect to boundary layer separation. Subsequent NCOREL calculations verified that the increased forward camber was conservative.

In addition to the basic camber shape described above, other shape parameters were used to attain the target pressure distribution. These included dihedral, spanwise twist, a spanwise "bump" to reduce wing upper surface curvature, and local leading edge droop. The basic design did not generate a constant-pressure plateau but rather a supercritical crossflow, with pressure decreasing continuously to the crossflow shock as shown in figure 27. Ten degrees of dihedral, which according to linear theory has no effect, is shown to change this type of pressure distribution to one with a nearly constant plateau.

In addition to dihedral, the other design shape parameters include 2° of washin in twist and an additional 5° of nose droop added locally at the leading edge to eliminate any spike in the local pressure distribution. Finally, the circular arc camber (which has a constant curvature spanwise) was modified to decrease the shock strength by reducing the curvature in the supercritical crossflow region. A spanwise "bump" was used to achieve this effect. The conceptual wing used a height of 1½% semispan, but numerical experiments indicated that a 2% change would be better for the demonstration wing. This change was added conically with the bump modification starting at the centerline, reaching a maximum at 40% semispan and terminating at 92% semispan. In the resulting wing shape, the camber is very apparent in the spanwise direction but is hardly noticeable in the streamwise direction.

The true wind-tunnel model geometry was used in the final design, including the balance housing. The winglines were blended smoothly into the balance

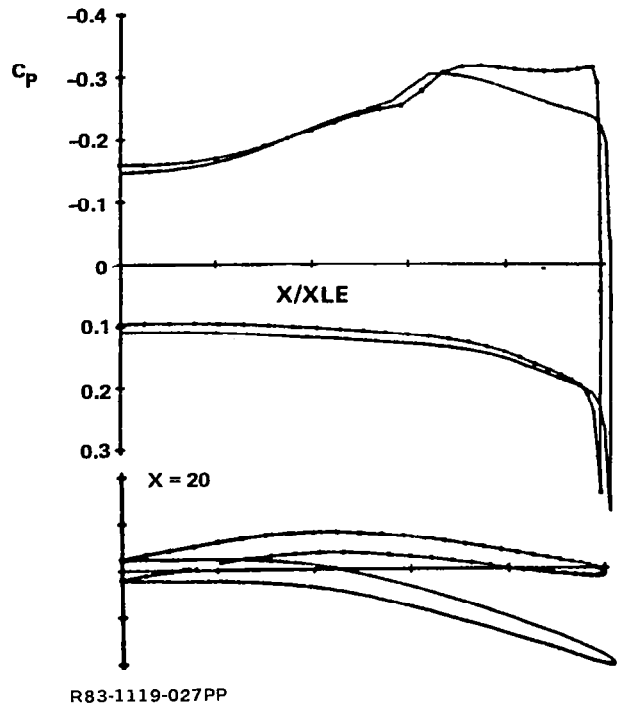

Figure 27. - Example of dihedral change on plateau pressure distribution.

housing by first fairing the wing spanwise at the centerline and then adding a circular centerbody which had a maximum diameter of 0.06 span. A constant-radius fillet was then used between the wing and balance housing. NCOREL analysis of both the basic wing and the wing including the balance housing indicated essentially no change in the pressure distribution due to the balance housing. The exact analytic details of the wing have been given, together with inspection results, in ref. 27. A comparison of the final predicted wing design pressures with the original uncambered thickness distribution is shown in figure 28. Note the large expansion peak and crossflow shock on the uncambered wing. The initial expansion at the leading edge is greatly reduced for this uncambered wing compared to a wing with the small leading edge radius of a typical NACA 64A-type airfoil. Thus, this flat wing result is already greatly improved relative to conventional supersonic wings. The cambered wing eliminates the strong crossflow shock and expansion peaks, which produces crossflow shock wave drag and could cause boundary layer separation. The design pressure distribution is shown in figure 29 where the design angle-of-attack is 12°.

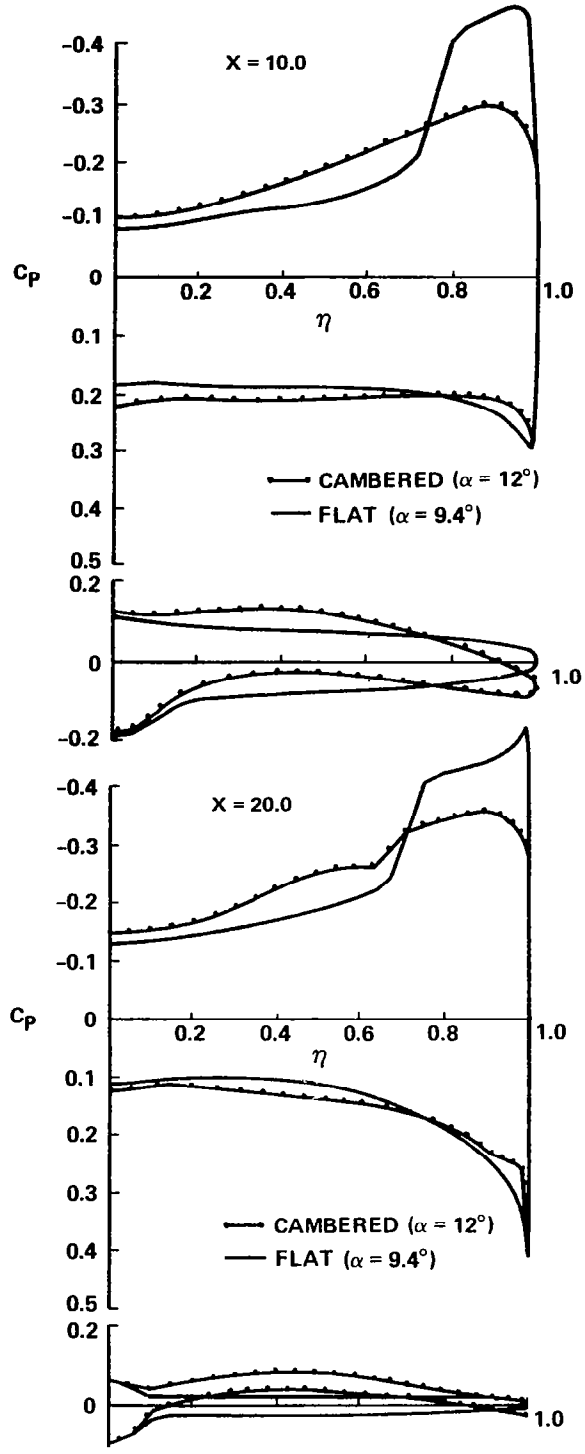

R83-1119-028PP

Figure 28. - Comparison of the flat and cambered wing shapes and predicted pressures at M = 1.62 and C_L = 0.40.

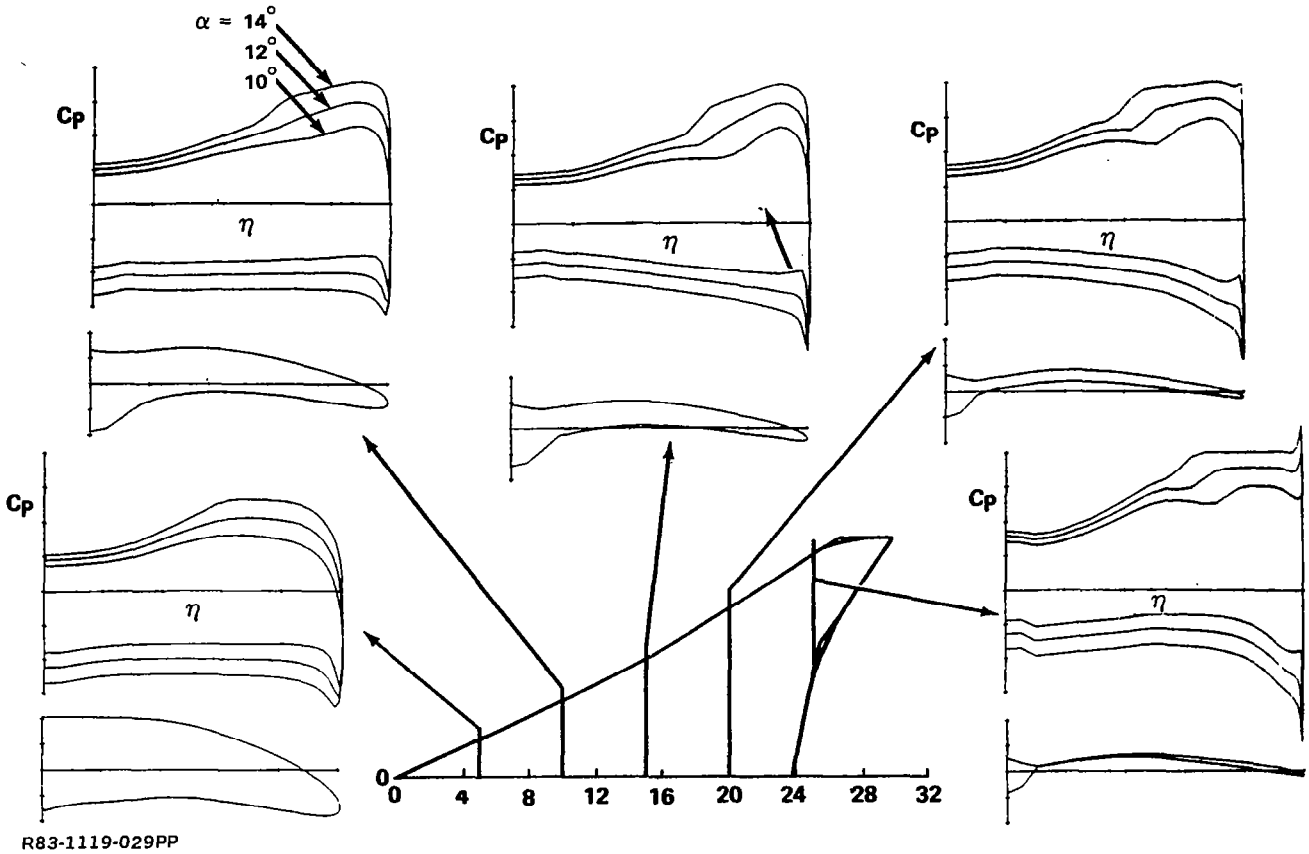

Figure 29. – Demonstration wing design pressure distribution (α = 12°), and angle-of-attack effects: M = 1.62 and α = 10°, 12°, and 14.

Once the basic leading edge shape was defined, an alternate leading edge shape was developed to remove some of the leading edge camber by changing the local leading edge additional droop from 5° down to 2° up. This permitted an experimental comparison of the shapes both at the maneuver design C_L and lower lift coefficients, where the camber penalty is of interest.

Model Fabrication and Wind Tunnel Test

After the desired design contours were obtained, a large aluminum isolated wing model was fabricated for Grumman by Micro Craft Inc. The model balance housing size was minimized by making it cover the balance alone and routing the pressure tubes directly off the wing.

The model was sized to ensure that the wing would be sufficiently large to allow for accurate fabrication, and particular care was taken to fabricate the model accurately. After being shaped on a numerically controlled milling machine, the wing was instrumented with 100 pressure taps located spanwise at the four stations indicated in figure 25. The leading edge was then hand-finished to bring the contours within 0.001 in. The technique used to achieve this accuracy was developed by Toscano at Grumman (ref. 28) and consists of comparing mylar drawings of the design contours with templates cast normal to the leading edge magnified 20x using an optical comparator. The leading edge was reworked by a skilled craftsman employing this technique repetitively using number 400 wet dry sandpaper until the desired shape was obtained. Five template control stations were used along the leading edge. After wing rework, the leading edges were generally within 0.001 inch (3% of r_{le}/C) of contour and smooth, while the main portions of the wing were within 0.005 inch of contour and generally even less. The additional leading edge, which had reduced camber, was made of steel.

The model was then tested in the NASA Langley Unitary Wind Tunnel at a Reynolds number of 2×10^6 per foot and over a range of angles-of-attack from 0° to 14°. Figure 30 shows the model installed in the tunnel. Transition strips were placed on the wing on both the upper and lower surfaces as described in ref. 27. In addition to the basic design Mach number, the test was conducted over the 1.58 to 2.00 Mach range. The initial test consisted of obtaining pressure results. Subsequent tests, with the pressure instrumentation eliminated from the aft end of the model and the wing faired to a smooth contour at the tube exits, produced force and moment and schlieren results. Finally, oil flow photographs at a selected number of conditions were taken. Essentially the same set of data was obtained for both leading edge shapes.

Analysis of Experimental Results

Selected results are presented in this section. Complete results, including tabulated data, are included in ref. 26. These results constitute the first set of wind tunnel data in which supercritical crossflows are developed with a controlled expansion and terminated by a weak crossflow shock wave for a

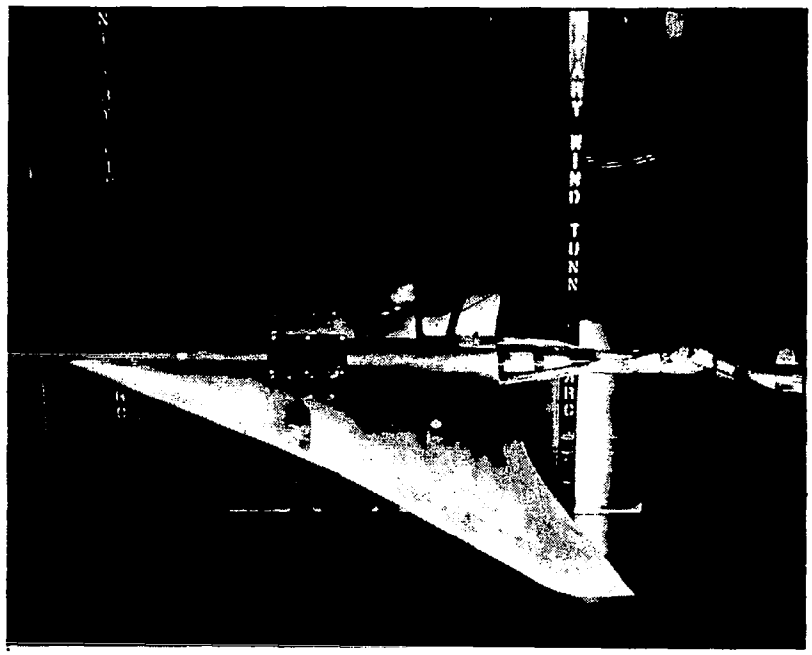

A. UPPER SURFACE

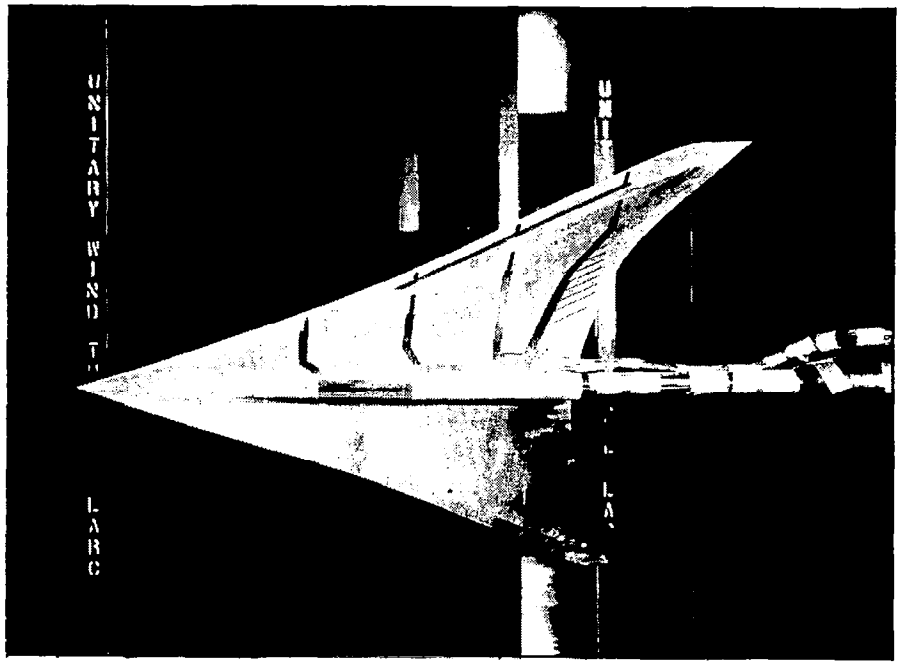

B. LOWER SURFACE

R83-1119-030PP

Figure 30. - Demonstration wing model installed in NASA Langley Unitary Plan Wind Tunnel.

planform and thickness distribution representative of advanced fighter aircraft.

Pressure Distributions. - The spanwise pressure distributions obtained at M = 1.62 over an angle-of-attack range below, at, and over the design conditions are presented in figure 31. These are the key pressure distribution results obtained during the test. The pressures show a well-controlled expansion at the first station (X = 10.6) with a mild recompression at α = 10°, and a progressively stronger recompression with increasing angle-of-attack. It appears that there may be a slight crossflow shock wave at α = 12°, and a

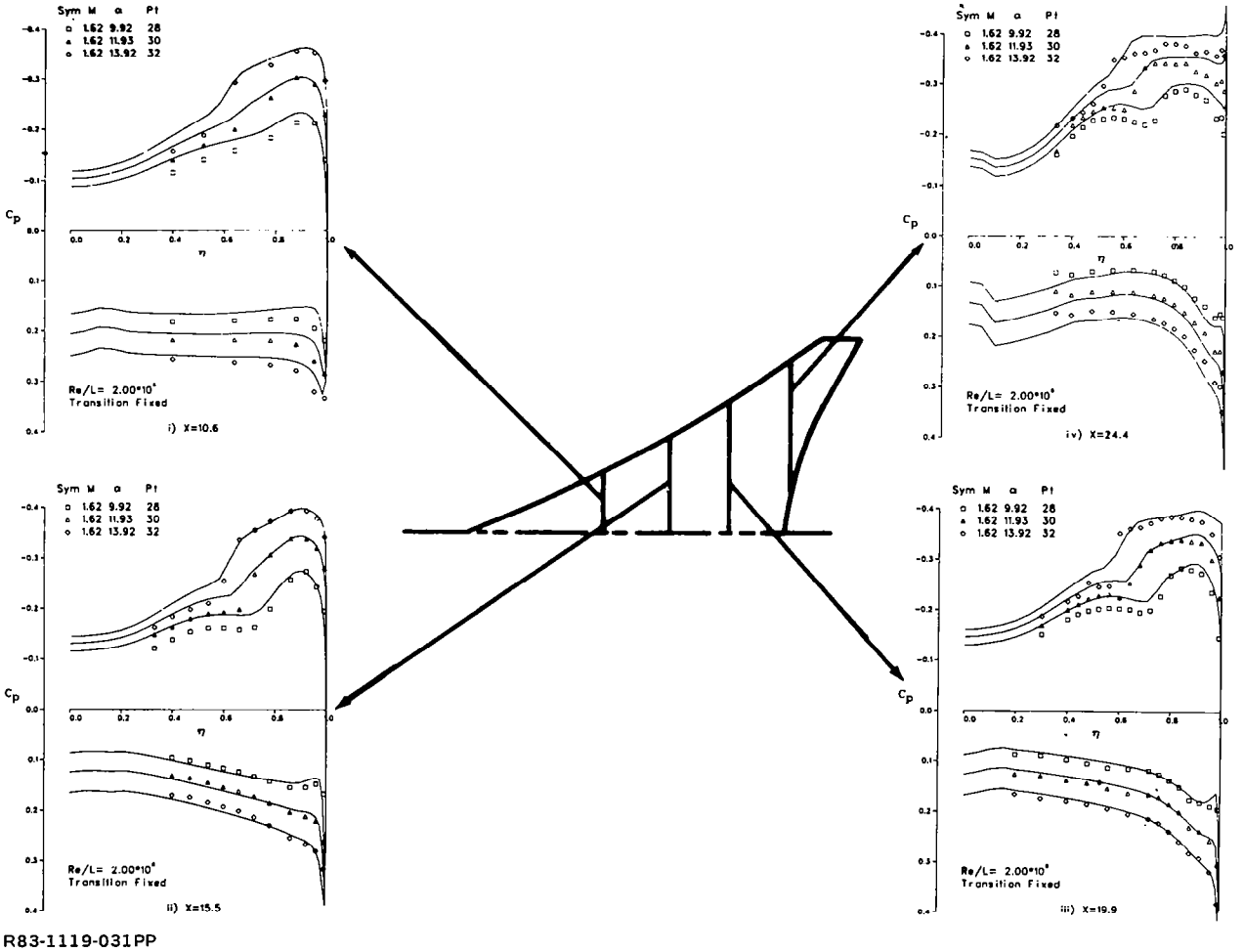

R83-1119-031PP

Figure 31. - Experimental results and NCOREL predictions, M = 1.62 and α = 10, 12, and 14 deg, baseline leading edge.

definite crossflow shock at $\alpha = 14°$. The expansion remains controlled at X = 15.5, with an immediate recompression at $\alpha = 10°$ and 12°. However, for this station, at $\alpha = 12°$, the plateau is terminated by a crossflow shock that is stronger than that predicted by the design pressure distribution (figure 29). The flow starts to develop a crossflow plateau at $\alpha = 14°$ although the pressures are not constant, and the supercritical region is terminated by a strong crossflow shock wave. At X = 19.9 the nearly constant pressure supercritical crossflow plateau is found at $\alpha = 12°$, although the plateau is again terminated by a crossflow shock that is stronger than that predicted by the design pressure distribution (figure 29). Increasing the angle-of-attack to 14° results in a very well-developed plateau and a strong crossflow shock wave. The pressure distribution obtained at X = 24.4 is essentially the same as the result at X = 19.9 for the upper surface. The lower surface pressures are decreasing significantly as the basic airfoil thickness distribution starts to close.

The NCOREL predictions made prior to the test are also included in figure 31. Generally, the experimental results are in agreement with the design pressure distribution obtained from NCOREL although some differences are evident. These include a stronger crossflow shock in the data than predicted by NCOREL, and a fairly large difference in the level of pressures inboard of the shock. These differences are currently unexplained. The predictions are, of course, obtained from an inviscid theory and M. Siclari has pointed out that the viscous effects, while expected to be small, have not been analyzed. Figure 32 provides comparisons between COREL, COREL + nonconical correction (ref. 19), NCOREL, and data for M = 1.62 and $\alpha = 12°$. In general, the COREL + nonconical correction results agree fairly well with the data considering the nature of the approximate correction. The exception is the X = 10.6 station, where the streamwise thickness is changing rapidly and the results are not well approximated by the conical solution. However, flow over the main portion of the wing is well predicted, including the position of the crossflow shock and the inboard pressures. The character of the leading edge expansion is also well predicted, but the expansion levels are under-predicted. The quantitative differences shown in figure 32 are similar to comparisons made for the other flow conditions.

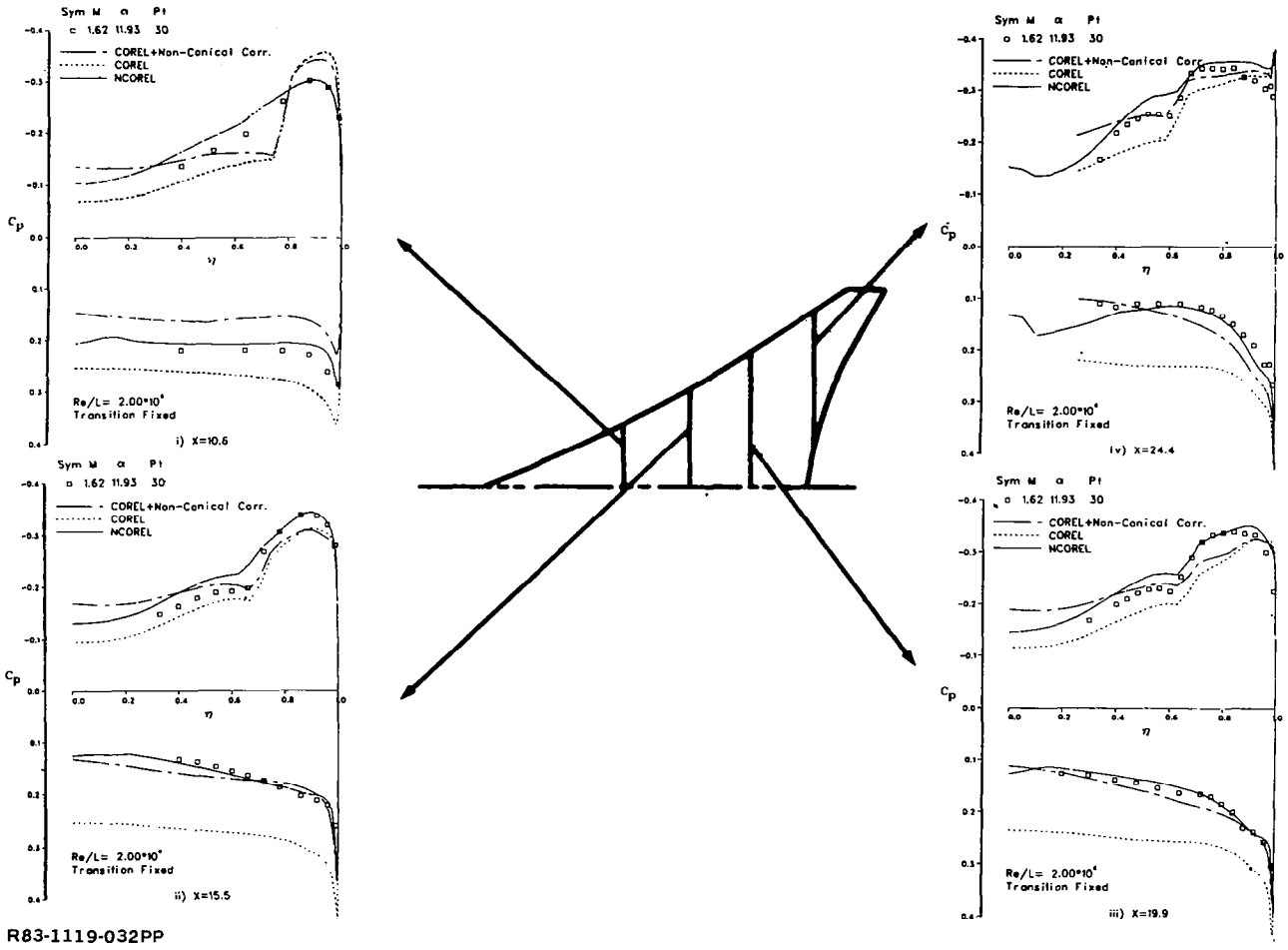

Figure 32.– Comparison of results with NCOREL, COREL, and COREL + nonconical correction, M = 1.62, α = 12 deg.

Figure 33 provides surface pressure comparisions between W12SC3, and experimental pressure data. The agreement is generally good on the lower surface, with the upper surface results in poor agreement inboard in the same manner as NCOREL. Outboard on the upper surface, linear theory does not capture the character of the leading edge expansion and nonlinear crossflow features of the flow; these are not modeled in linear theory. Nevertheless, on average, the general pressure levels are predicted fairly well.

The effect of Mach number is shown in figure 34 at α = 12° for a Mach number range of 1.58 to 1.70. Mach number effects are seen to be limited to the upper surface in the vicinity of the leading edge. This is the region of supercritical crossflow. The pressures increase noticeably with increasing

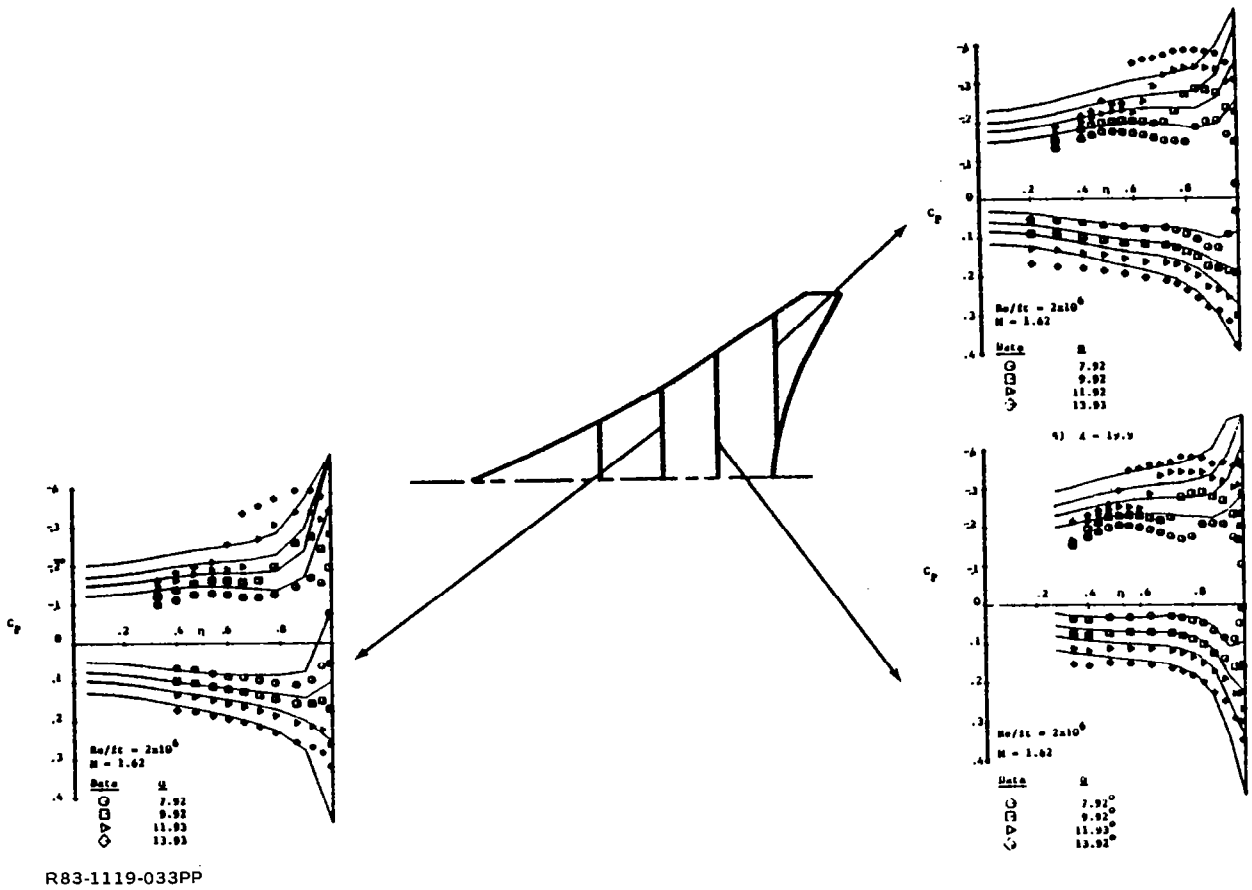

Figure 33. - Comparison of data with the Linear Theory Panel Method, W12SC3, M = 1.62, α = 8,10,12, and 14 deg.

Mach number on the upper surface outboard, and NCOREL predicts the magnitude of the change very well. This reduction in peakiness at X = 10.6 and plateau pressure at X = 24.4 is a trend that is consistent with typical results for 2-D transonic supercritical airfoils. Finally, note that the crossflow shock wave position does not change with Mach number. Again, this feature of the experimental results is correctly predicted by NCOREL.

The difference in pressure between the two leading edge shapes was found to be small and restricted to the immediate vicinity of the leading edge, as shown in figure 35.

Oil Flow Results. - Oil flow photographs are presented in figures 36 and 37 for the design Mach number of 1.62 and angle-of-attack range of 8° to 14°.

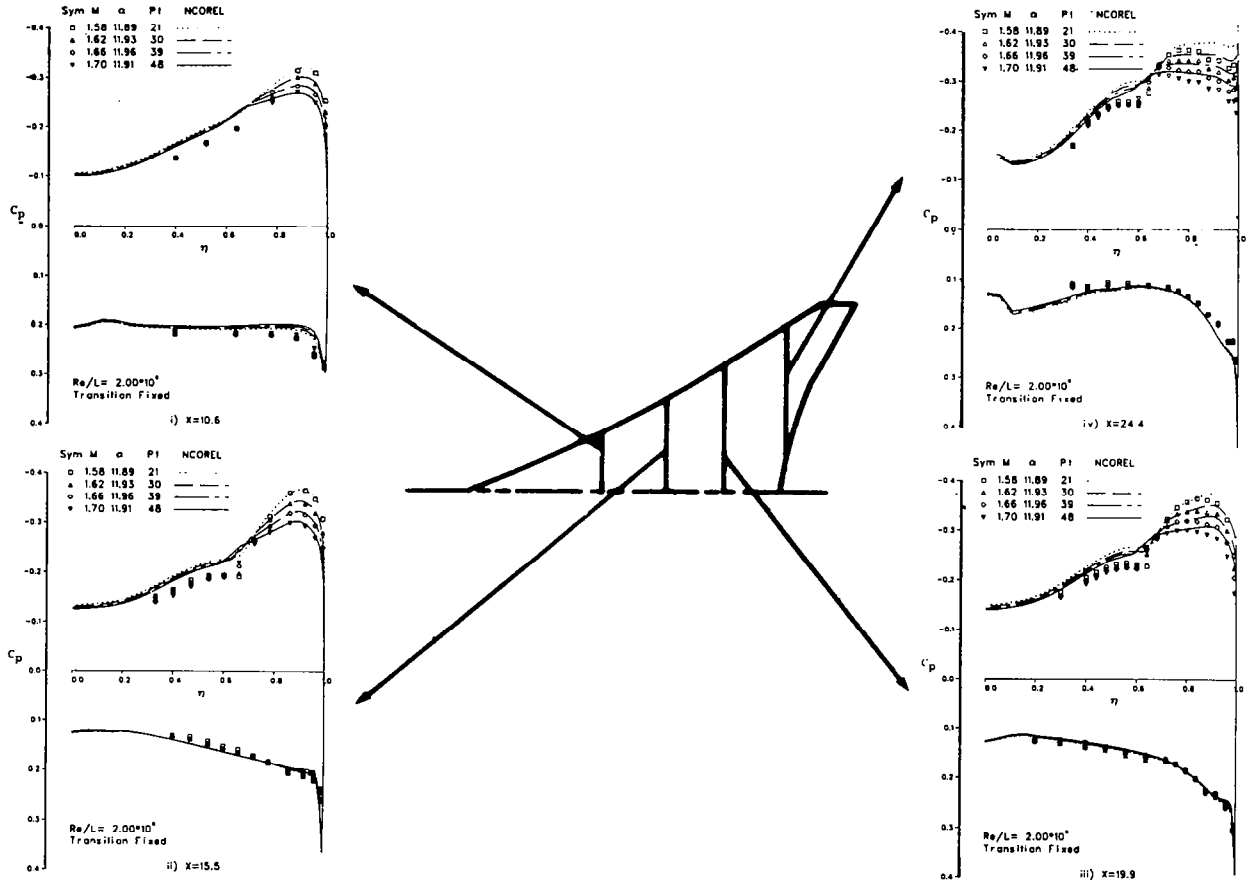

R83-1119-034PP

Figure 34. - Mach number effects, data and NCOREL, α = 12 deg, M = 1.58, 1.62, 1.66, and 1.70.

These photographs provide considerable insight into development of the flow-field. Figure 36 contains the results for α = 8° and 10°. At α = 8°, the streamlines progress smoothly over the wing with only a hint of trailing edge separation outboard. At α = 10°, the streamlines continue to progress smoothly over the leading edge while the trailing edge separation has become quite clear, although it is still limited in extent. Trailing edge separation occurs because the upper surface pressures have become low enough so that the pressure cannot adjust to the freestream level without causing separation, which leads to a significant upstream interaction. In effect, the local flow is similar to that in a compression corner. Figure 37 contains the results for α = 12° and 14°. At α = 12° (the design angle-of-attack), the leading edge flow remains

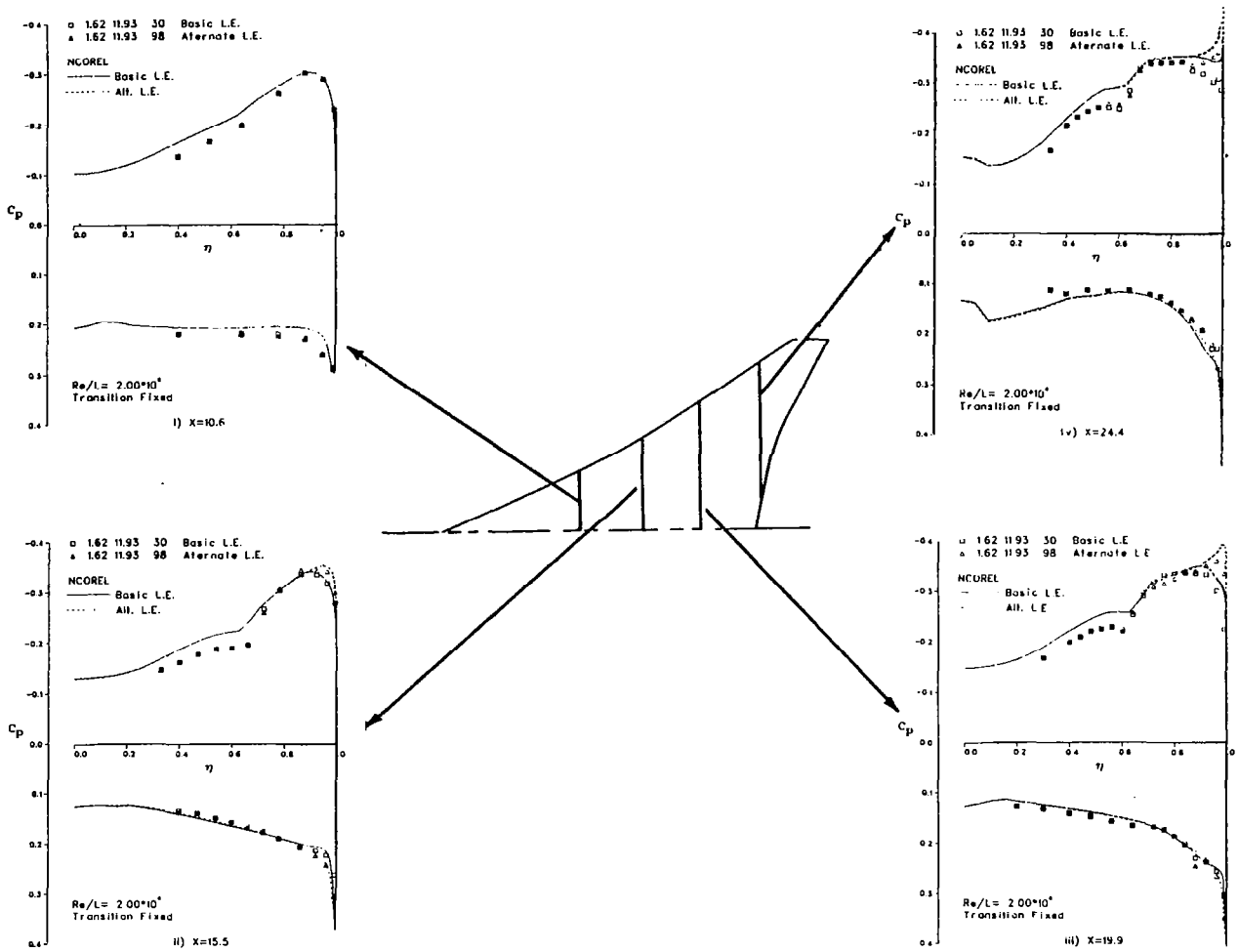

R83-1119-035PP

Figure 35. - Effect of leading edge shape on pressure distribution at M = 1.62 and α = 12 deg.

well-behaved, with smooth streamlines, and the crossflow shock can be identified by noting the turning of the oil beneath it (the corresponding pressure distribution is shown in figure 31). The size of the trailing edge separation is also increasing. At an angle-of-attack of α = 14°, the leading edge flow remains well-behaved, while the photo shows further increases in trailing edge separation and a very pronounced turning underneath the crossflow shock. Note that, in all cases, the tip appears to be well-behaved.

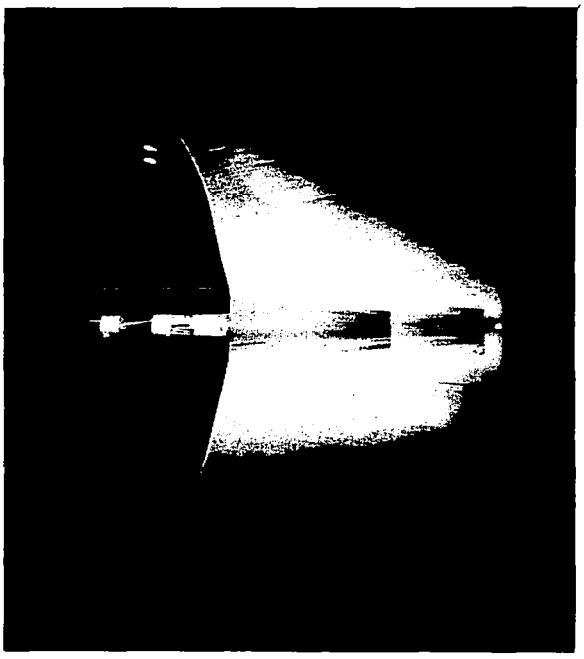

$\alpha = 8°$

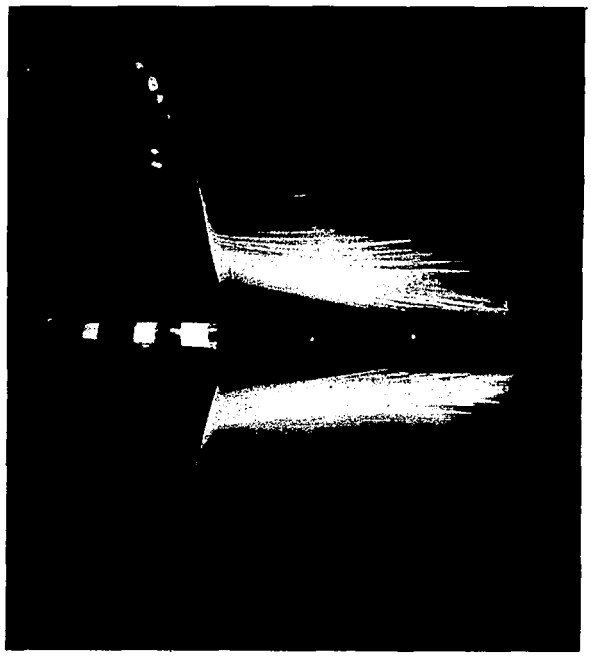

$\alpha = 10°$

R83-1119-036PP

Figure 36. - Demonstration wing oil flows at M = 1.62 and α = 8 deg and 10 deg.

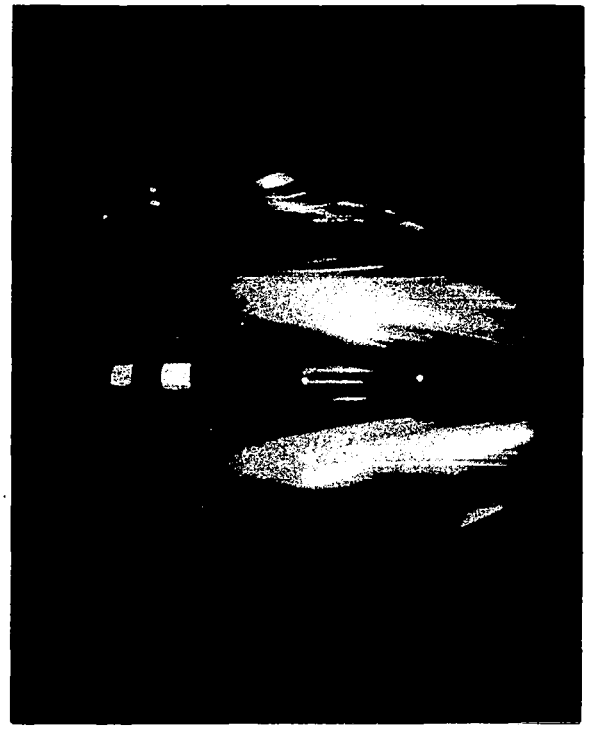

$\alpha = 12°$

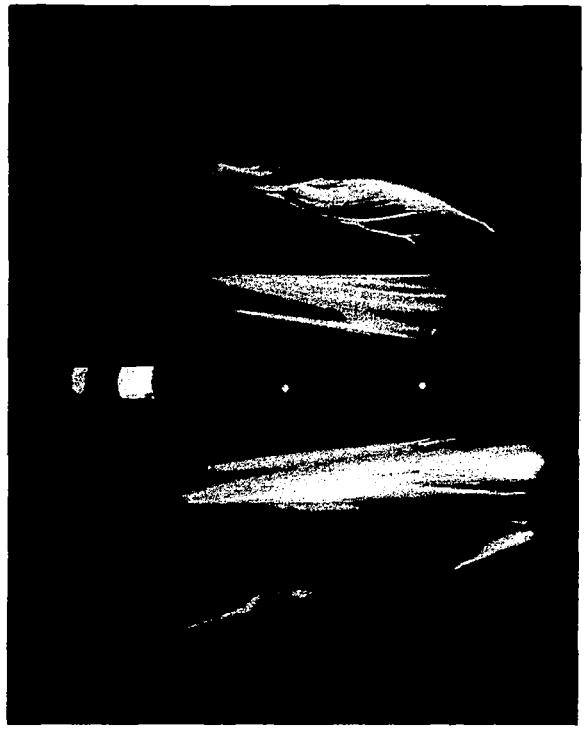

$\alpha = 14°$

R83-1119-037PP

Figure 37. - Demonstration wing oil flows at M = 1.62 and α = 12 deg and 14 deg.

The conditions under which the trailing edge separation first appears, and the extent of the separation zone, require additional analysis. Consider first the conditions for which trailing edge separation will occur; this has been done by Kulfan and Sigalla in ref. 29. They presented a criterion based on experimental results and the analogy between the supersonic trailing edge viscous interaction, and the flow in a compression corner. The analysis of the wing pressure data given in figure 38 confirms that the empirical equation is indeed valid for this set of data. Figure 38A presents the trailing edge limit pressures for attached flow from ref. 29 for the Mach number and trailing edge

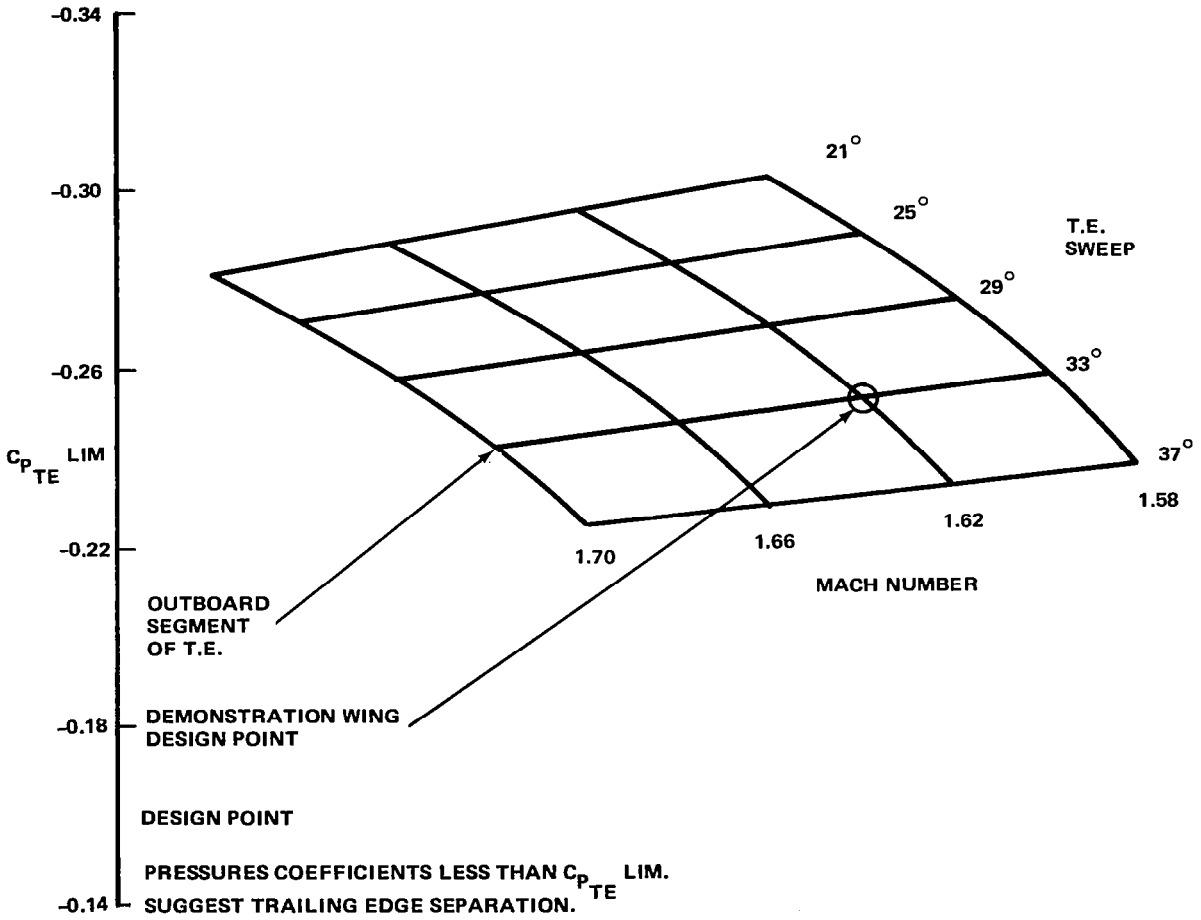

A. CRITICAL TRAILING EDGE PRESSURE ESTIMATES USING KULFAN & SIGALLA (REF. 30)

R83-1119-038(1)PP

Figure 38. - Pressure coefficient levels and trailing edge separation. (Sheet 1 of 2)

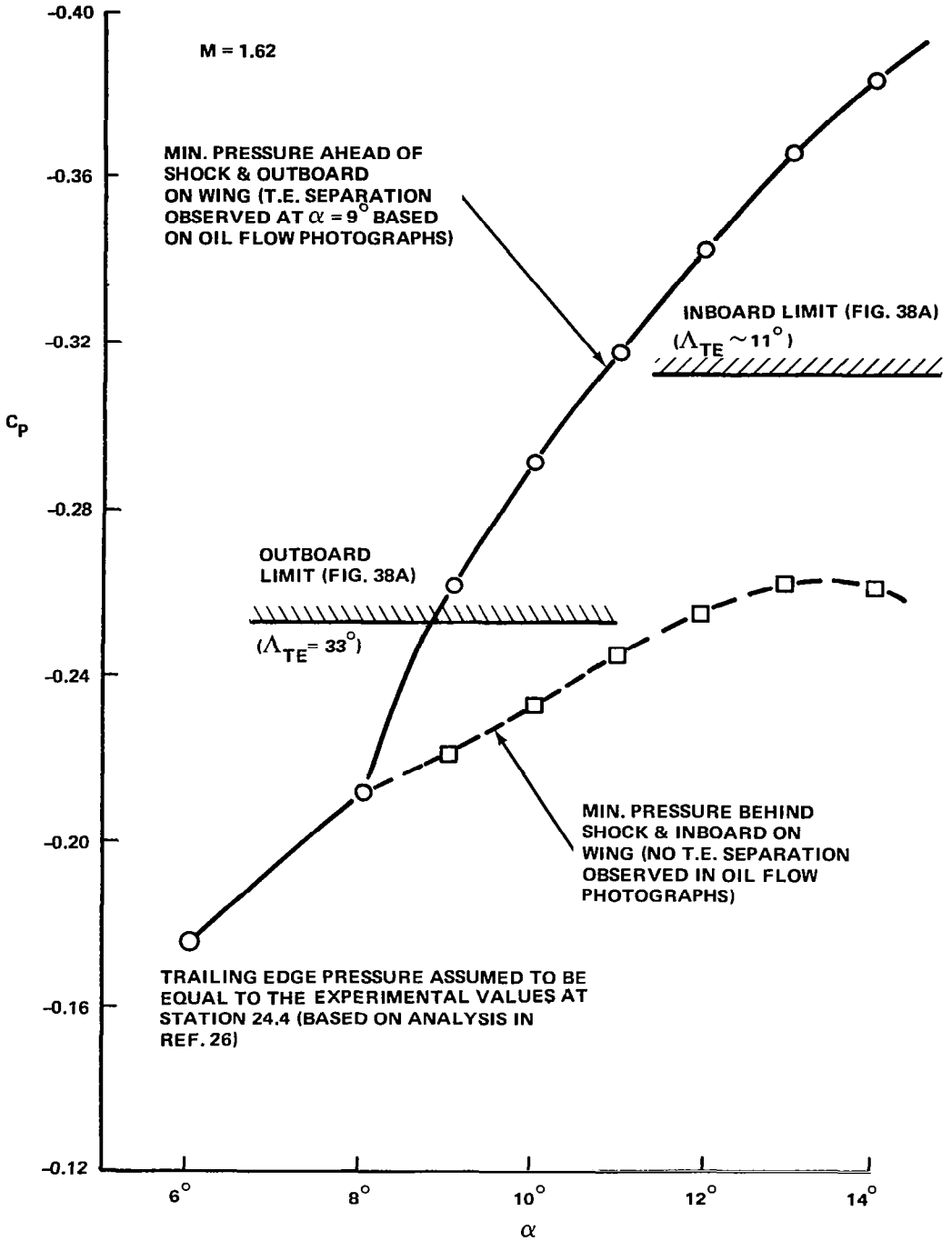

B. TRAILING EDGE PRESSURE CHANGE WITH ANGLE-OF-ATTACK ON THE DEMONSTRATION WING.

R83-1119-038(2)PP

Figure 38. - Pressure coefficient levels and trailing edge separation. (Sheet 2 of 2)

sweep combinations of interest for typical SC^3 conditions. Figure 38B compares the predicted separation pressures with the experimental results. The oil flow photograph determined angle-of-attack for separation and the corresponding pressure agrees with the empirical prediction. The appearance of separation is not strongly dependent on Reynold's number. However, the extent of the upstream influence of the trailing edge separation does depend on Reynold's number. This problem has been studied by Settles, et al in ref. 30. Using a Reynold's number scaling relation developed by Settles, it was found that the extent of upstream influence associated with trailing edge separation might be reduced by as much as a factor of four at flight Reynold's numbers for a specified lift condition.

Force and Moment Results. - Figure 39 shows the C_L and C_m results at M = 1.62 for the two leading edge shapes tested. The baseline leading edge is used in the force and moment analysis. The C_L - α and C_L - C_m curves are linear up to about 9° or 10° angle-of-attack. Above this angle-of-attack, the lift curve slope decreases slightly and the slope of the moment curves decreases with C_L. The straight-line extrapolations of the low angle-of-attack results are included on the figure to allow a quantitative measure of the departure from the linear lift and moment curves. The loss in lift and moment coincides with the trailing edge separation found in the oil flow photographs.

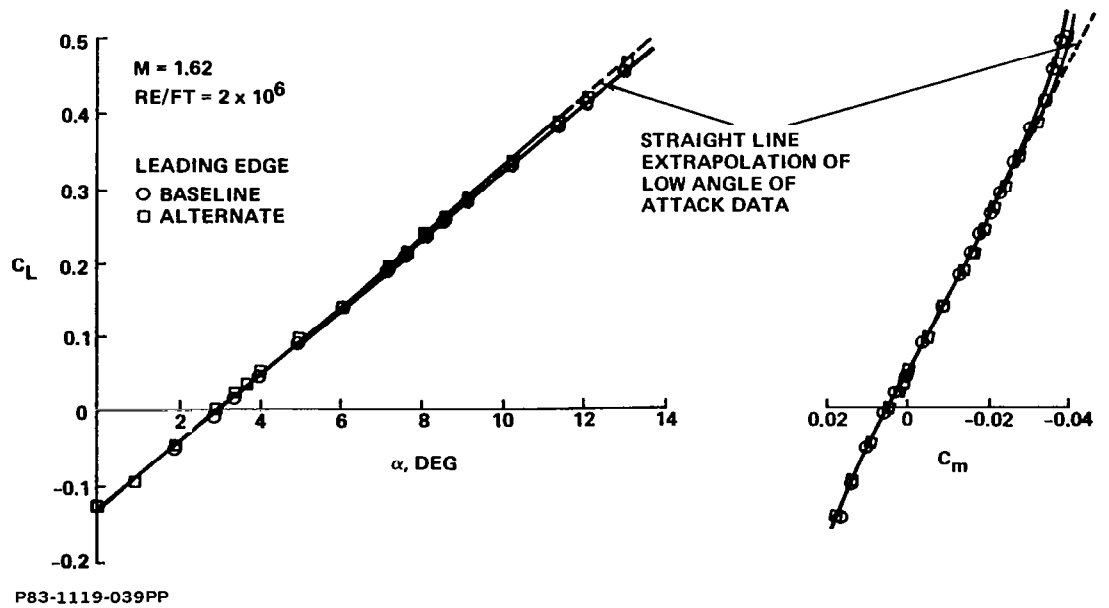

Figure 39. - Lift and moment results at M - 1.62.

Figure 40 presents the drag polar for the wing with the baseline leading edge. At the design lift coefficient, the alternate leading edge had the same drag. The figure also includes drag polars corresponding to the linear theory optimum envelope polar and the equivalent flat wing drag polar. These polars are based on an estimated $C_{D,o}$ of 0.0122. The NCOREL drag prediction at the design point for the wing is also shown. The excellent agreement is crucial to establishing the consistency between the numerical and experimental pieces of the SC^3 concept development program. The wing demonstrated a 21% drag-due-to-lift decrease compared to the equivalent flat wing, and at a lift coefficient approximately twice that which can be used in current wing design methodology.

The difference between the baseline and alternate leading edge drag-due-to-lift performance emerges at the lower lift coefficients, where the alternate leading edge has less camber and therefore less camber drag. Figure 41 illustrates these differences in terms of $\Delta C_D/\beta C_L^2$. The minimum value of the drag-due-to-lift parameter occurs at C_L = 0.25 for the baseline leading edge, and at

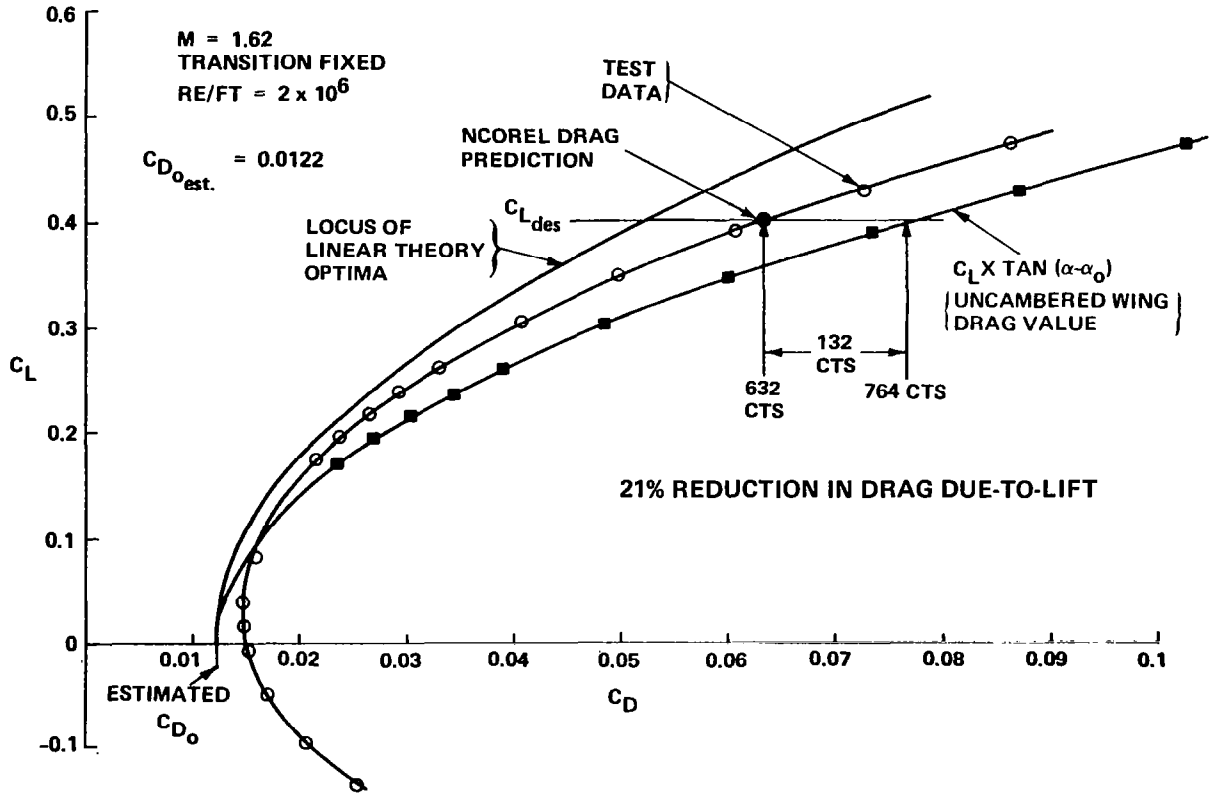

P83-1119-040PP

Figure 40. - Drag performance of demonstration wing.

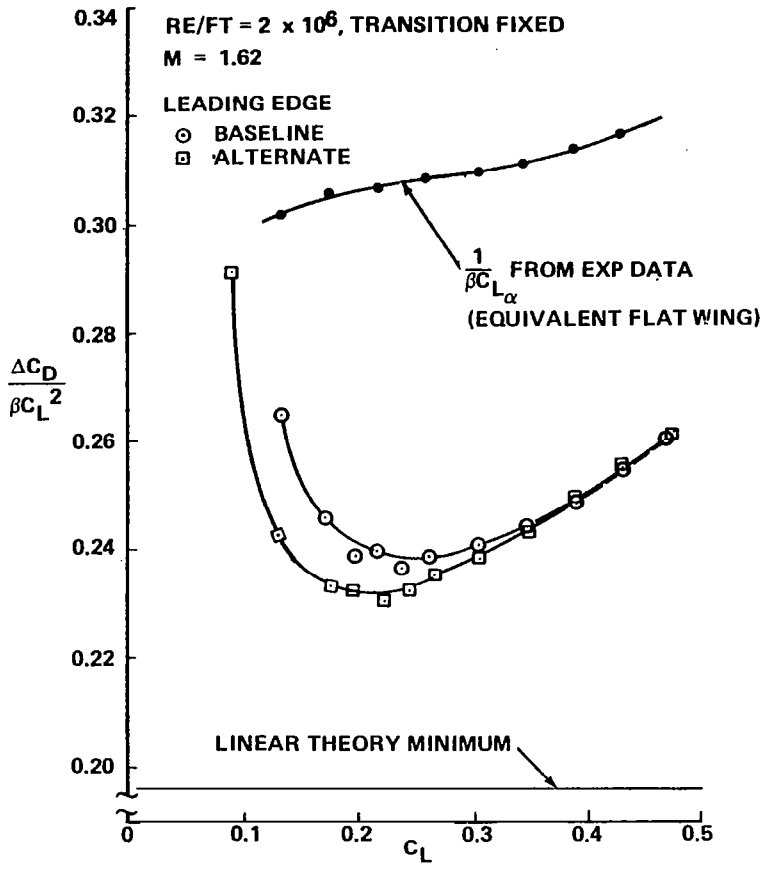

Figure 41. - Drag due-to-lift performance, baseline and alternate L.E. results at M = 1.62.

C_L = 0.22 for the alternate leading edge. The alternate leading edge, which had less camber, also has a lower absolute value of drag-due-to-lift at lower lift coefficients. This figure includes the linear theory minimum and the experimental equivalent flat plate values for comparison. Similar results were obtained at Mach numbers from 1.58 through 1.70.

One aspect of the wing and experimentally observed flowfield requires further analysis before discussing the agreement with theoretical drag predictions in detail. This feature was not considered in designing the wing, and estimates described below indicate that it would add an additional 13 counts to the original goal drag. This feature is the appearance of trailing edge separation.

Trailing edge separation leads to a normal force loss due to the upstream effects of the trailing edge interaction. The magnitude of the loss is estimated at M = 1.62 and α = 14° by using the oil flow photos to determine the separation size. Based on those photos, it was assumed that the affected region consisted of 7% of the reference area. The full plateau pressure of C_p = -0.37 was assumed at the separation line while the freestream pressure was assumed at the trailing edge, with a linear variation between these locations. Experiments for compression corners show that the pressure interaction starts ahead of separation, rises more rapidly than a linear variation, and does not reach the full pressure rise at the corner. The linear variation assumed here probably provides a reasonable representation of the average pressure. Based on this assumption, losses of 0.013 in lift coefficient and 0.011 in moment coefficient can be estimated. These values are almost precisely equal to the variation from the linear lift and moment curves found in the data. Thus, the departure of lift and moment from linearity can be explained almost entirely by the trailing edge separation. The loss of normal force also affects the drag. The drag increment is estimated as follows. At α = 12°, it is assumed that the loss in C_N varies linearly between 8° and 14°. The local upper surface slope relative to the freestream is about 10° at α = 12°, and the C_L and C_D are corrected by adding the loss in C_N back into C_L and C_D. The drag is then corrected back to C_L = 0.4 by assuming that the drag-due-to-lift polar shape is based on the zero suction shape. The additional drag due to trailing edge separation is found to be 13 counts.

Comparisons Between Experimental and Predicted Drag. - Theoretical drag predictions were made with NCOREL for the baseline leading edge at the M = 1.62. The results are shown in figure 42. The NCOREL geometry model included the balance housing in the calculation. Skin friction estimates were added to the NCOREL predictions shown in figure 42. In considering the NCOREL results, it is important to realize the NCOREL does not currently compute the flow over the wing area aft of the tip leading edge. This represents about 6% of the planform area.

A closer examination of the comparisons near the design lift coefficient is presented in figure 43. Some adjustments to the NCOREL results have been made therein. By estimating the omitted incremental lift and drag, the final

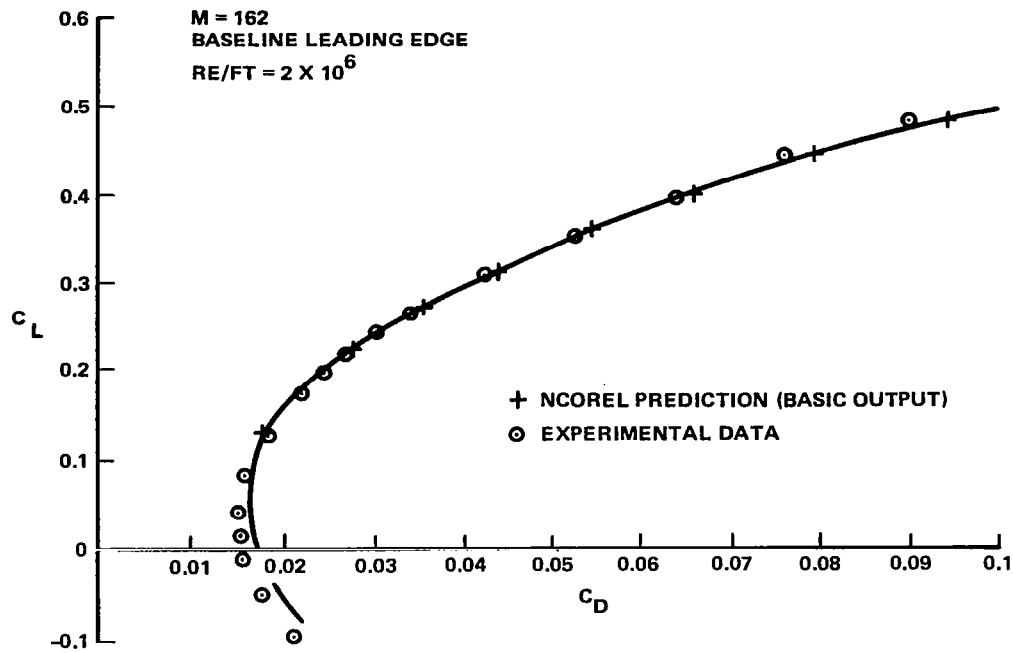

R83-1119-042PP

Figure 42. - Comparison of theory and data for the baseline leading edge drag polar.

corrected NCOREL predictions are seen to agree extremely well with the data. Recall, however, that the NCOREL predictions are inviscid, and do not include the trailing edge separation drag (estimated to be about 13 counts). This figure shows that the NCOREL drag predictions can be used to evaluate supersonic wing design performance, including nonlinear inviscid effects, an important result for future supersonic maneuver wing design work.

In summary, the test results indicate that, for the first time a supercritical crossflow-type pressure plateau has been obtained for an isolated wing planform and thickness distribution representative of those currently envisioned for advanced supersonic fighters. The pressure distributions obtained experimentally showed generally good agreement with the design pressure distribution, although the crossflow shock wave was somewhat stronger than expected. At a lift coefficient of about twice that at which linear theory wing camber designs have been shown to be effective, the wing experimentally demonstrated at 21% drag-due-to-lift reduction compared to an equivalent uncambered wing. The wing design described in this section thus represents a significant advance in supersonic wing design.

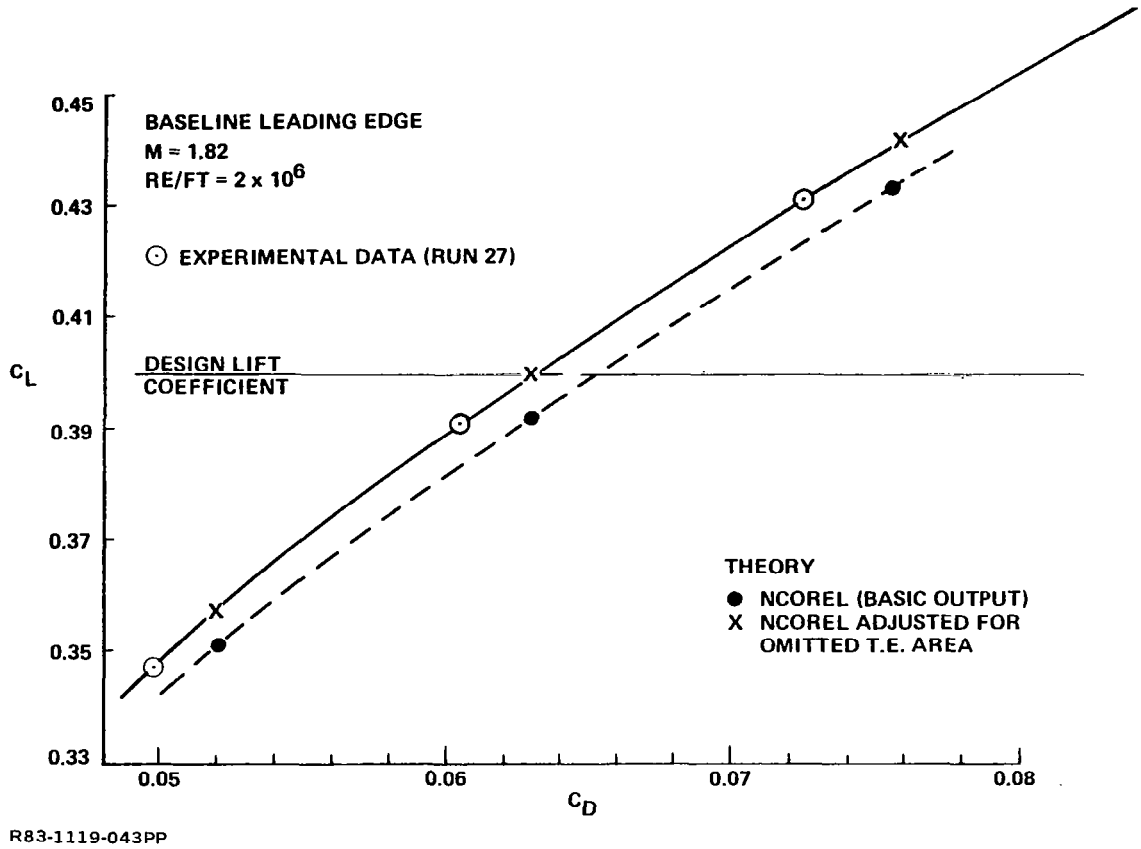

Figure 43. - Comparison between theory and data near design point on drag polar.

SC^3 WING DESIGN PROCEDURES

Based on the experience gained in designing, testing, and analyzing the results for the conceptual and isolated demonstration wings, a recommended procedure for designing SC^3 concept wings can be given.

Recall that the SC^3 concept is essentially an idea for a pressure distribution, as shown in figure 5. In order to define a specific target pressure distribution, the design pressure can be characterized by the plateau pressure level, $\Delta C_{p\ SC3}$, and extent, η_{DR}, as shown in the following sketch.

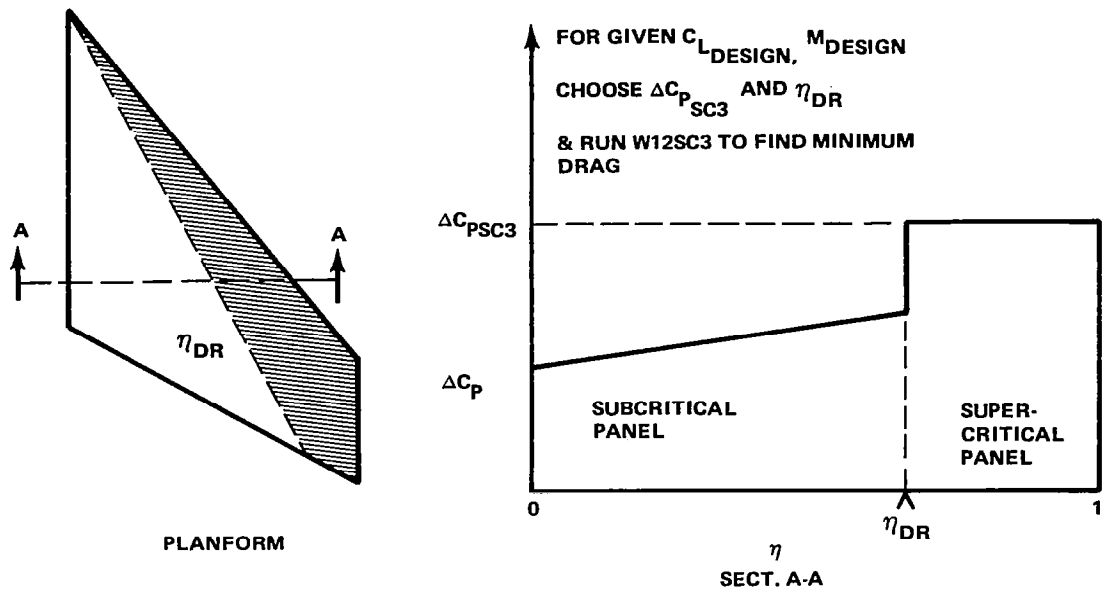

Two approaches can be taken in establishing these values for a particular design case. In the first approach, W12SC3 is used to define a linear theory basis for the target pressure distribution by making a parametric study of the sensitivity of linear theory minimum drag for various values of $\Delta C_{p\ SC3}$ and η_{DR}. In that study, the size of the supercritical panel, η_{DR}, and the pressure level, $\Delta C_{p\ SC3}$, are specified. The mixed-design option of W12SC3 is then used to determine the linear theory minimum drag of the wing, the optimum pressure distribution on the subcritical panel, and the corresponding camber slope distribution over the entire surface. An example of this type of parametric study is given in ref. 19.

The second approach is less formal, but addresses the issues of limits imposed by viscous effects and acceptable geometries. In this approach, a series of COREL or NCOREL calculations is made using a geometry based on the demonstration wing design obtained in the present study. Using these results, a value of $\Delta C_{p\ SC3}$ should be found such that the Mach number normal to η_{DR} does not exceed about 1.2. These results will also help establish whether a realistic choice of C_L has been made. Note that an incompatibility between the specified $\Delta C_{p\ SC3}$, η_{DR} pair and the design C_L could arise in using the linear theory approach. The incompatibility arises if the design C_L is large relative to the specified $\Delta C_{p\ SC3}$, producing ΔC_p's in the subcritical region larger than the supercritical panel $\Delta C_{p\ SC3}$ value.

In most applications, the target pressures will be obtained using a combination of these approaches, as well as several design iterations. At each step the $\Delta C_{p\ SC3}$, η_{DR} values should be checked to ascertain that they remain in the vicinity of the linear theory minimum values, while also verifying that any crossflow shocks are weak enough so that the boundary layer will not separate.

The demonstration wing target pressure was defined using this procedure to be $\Delta C_{p\ SC3} = 0.50$, and $\eta_{DR} = 0.65$. The final design shape determined by repetitive analysis produced a target pressure distribution which essentially attained these values.

The first step in determining the wing geometry required to attain the design target pressures is the establishment of an analytic wing. An analytic wing means that a computer program has been established such that the wing surface coordinates are available at any arbitrary location on the planform. Tabulated data could be used within the program, but the rules for interpolation must be automated. This requirement arises for a variety of reasons. The most important one is that the nonlinear inviscid methods which achieve numerical accuracy and efficiency require accurate and, in some areas, closely spaced data. For example, the leading edge should be defined such that several surface coordinates of the section are available within the leading edge radius region. By developing the wing section contours as part of an overall lofting plan, greater insight into the shape requirements can be obtained. In addition, the mechanics of the design, analysis, fabrication, and inspection of the model will require that contour data be readily available. Examples include spanwise section data for COREL, spherical-cut data for NCOREL, streamwise data for many NC machine tape programs, and section cuts normal to the leading edge for making inspection templates. Without an analytic wing, the labor requirements make an SC^3 (or any) wing design using nonlinear methods impractical.

Given an analytic wing framework, the design contours of an SC^3 type wing should be established as follows:

1. Define a thickness distribution with a reasonably large leading edge radius in order to support the controlled expansion and relatively highly loaded leading edge. Values similar to the transonic supercritical airfoils should be used. Typical values would exceed the NACA four-digit values by 50%.

2. Select a circular arc camber distribution as the baseline camber. Add pure dihedral and a spanwise "cubic" bump of the form described previously in order to obtain the desired plateau pressure shape and weak crossflow shock.
3. Make local modifications, as required, to refine the target pressure distribution. Examples include increased camber forward on the wing, local deflections near the leading edge, and the use of twist to provide an additional degree of control for the pressure distribution.

The above steps are at present carried out in a series of computational analyses of the prescribed geometry. Initially, COREL proves useful in establishing the magnitude of the design variables. NCOREL can then be used to complete the design and make any required adjustments. Drag predictions from the NCOREL method proved to be reasonably accurate for the demonstration fighter wing, and are accurate enough to evaluate the design's drag performance.

This methodology could be refined by developing some type of inverse procedure such that the target pressure distribution is specified and the required geometry is obtained automatically as the output of a single computer submission. Elements of optimization theory, such as "smart aerodynamic optimization" (ref. 31), could then be used to expand the SC^3 concept and determine the SC^3 pressure distribution required to obtain the minimum drag for the nonlinear inviscid flowfield.

SC^3 IMPLICATIONS FOR PLANFORM SELECTION AND PERFORMANCE BENEFITS

The theoretical and experimental results can be used to select planforms that are particularly suited to the SC^3 concept. Experimental results have shown that the concept can be used for values of $\beta \cot \Lambda = 0.79$ with no indication of breakdown, and a $\beta \cot \Lambda$ of 0.070 was suggested earlier as a possible lower limit for SC^3. Thus the combination of Mach number and sweep angles available for SC^3 can be expected to range from a $\beta \cot \Lambda \simeq 0.70$ to $\beta \cot \Lambda \simeq 0.90$. The trailing edge sweep angle should be large to obtain the maximum benefits predicted from the arrow wing example of figure 8. However, the experimental results show that trailing edge separation becomes more severe

as the sweep angle increases. Thus viscous considerations lead to a requirement for low trailing edge sweep. These conflicting trailing edge sweep requirements can be resolved by recalling the previous analysis which indicated that the viscous losses are anticipated to be small at flight Reynolds numbers, and thus the inviscid trends should be used for selecting trailing edge sweep angle when performing design tradeoffs.

The impact of the improved performance available to aircraft using the SC^3 concept can also be projected in order to relate the aerodynamic advances to either improved maneuvering performance or reductions in aircraft size required to meet specified maneuver requirements.

The sustained-g-capability changes due to improved wing performance can be evaluated by forming the ratio of the load factors, n_z's, for aircraft in which the only differences are in the wing contours. Assuming that the drag polar can be represented by the simplified form

$$C_D = C_{Do} + KC_L^2,$$

the ratio of the sustained load factors is simply

$$\frac{n_{z2}}{n_{z1}} = \sqrt{\frac{K_1}{K_2}}.$$

For the 60° sweep arrow wing with a notch ratio of 0.4, the ratio of sustained g performance is shown in figure 44. This figure can be used to estimate the actual increases in performance available using the SC^3 concept. At M = 1.5, it shows that a 25% increase in sustained g level could be attained if even 75% of the potential gain is realized. This is a substantial improvement, and even further increases appear to be achievable based on the results shown. While quantitative, these results do not provide insight into the benefits in the standard manner. The standard measure of assessing the impact of the SC^3 concept on an aircraft design would be to determine its impact on takeoff gross weight for a given mission and maneuver requirement. This comparison of conventional and SC^3 wing technologies has been made for the representative fighter configuration shown in figure 45.

The fighter configuration of figure 45 was sized using the standard Grumman preliminary design methodology. The maneuver design point was speci-

fied to be $n_z = 3$ at M = 1.4 and h = 48K ft. This represents a plausible requirement for an advanced fighter and a flight condition with the same q as the typical design point for specifying transonic maneuvering: M = 0.9, h = 30Kft. The basic mission requirements (subsonic and supersonic radius, loiter, and acceleration) were maintained at levels typical of current Air Force mission requirements for next-generation fighters.

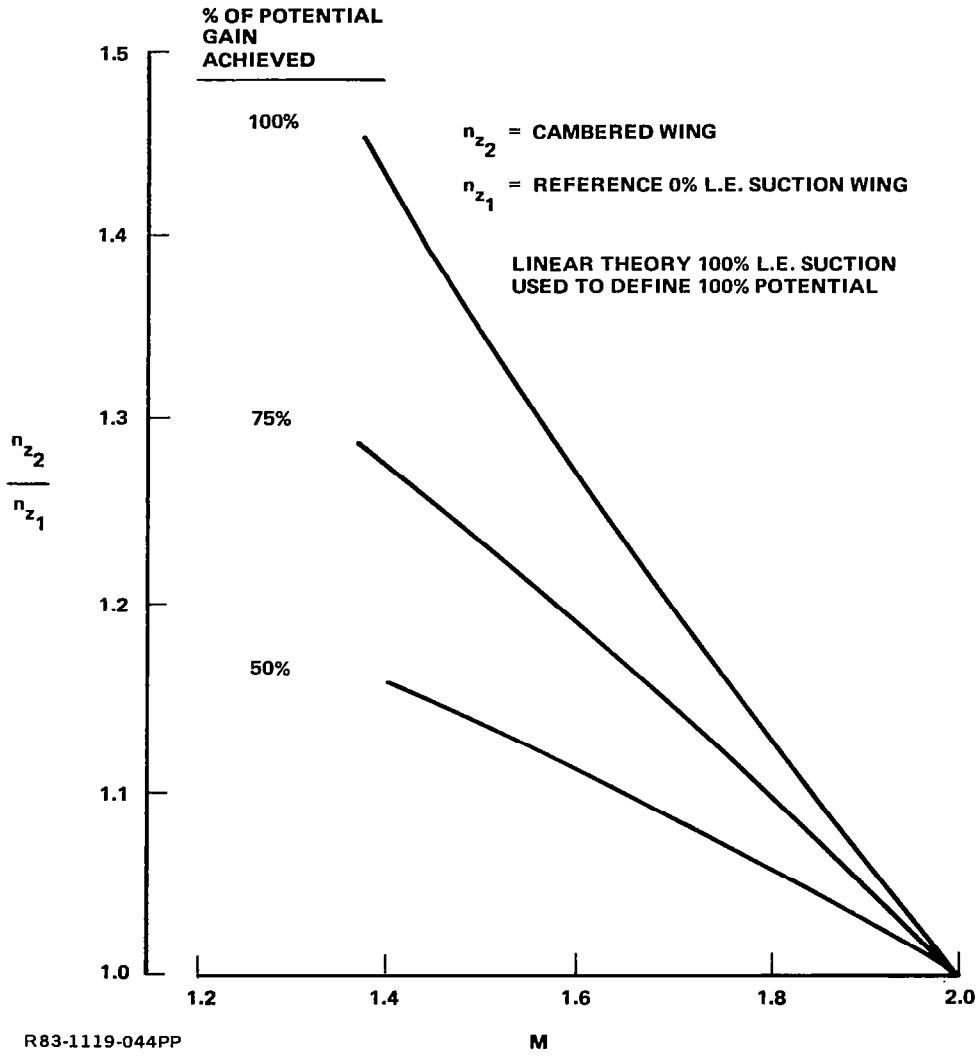

Figure 44. - Sustained g improvements due to SC^3 for an arrow wing with 60° sweep and 0.4 notch ratio.

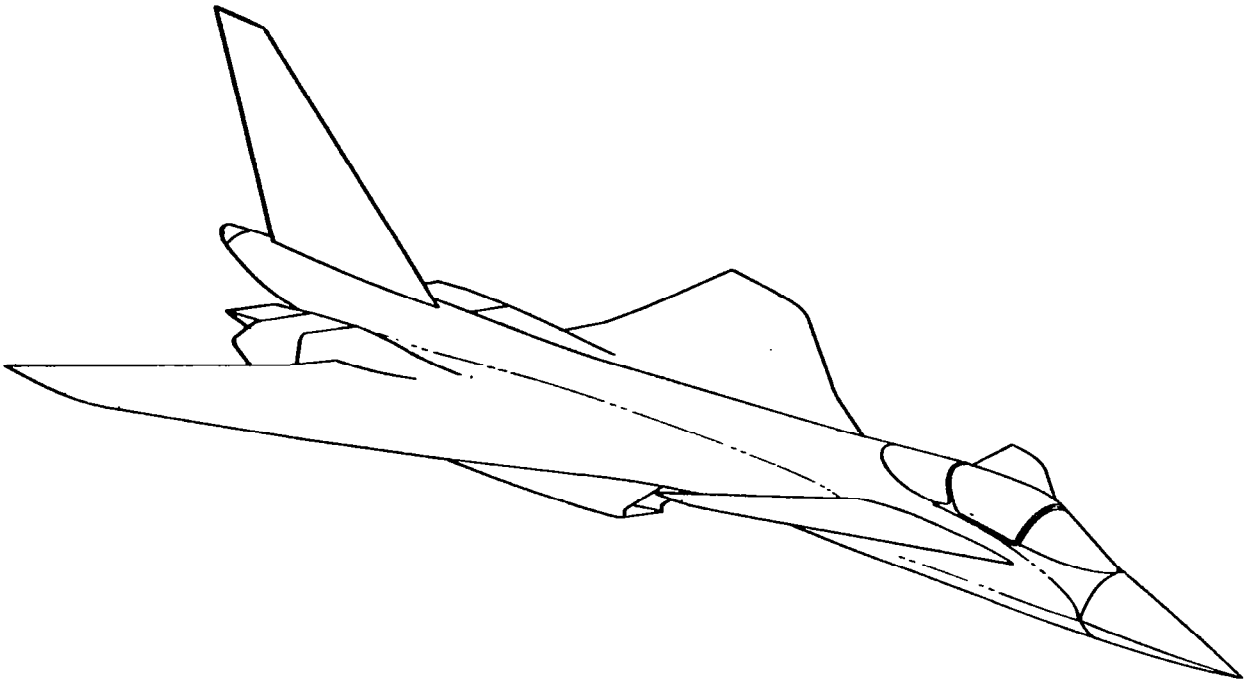

R83-1119-045PP

Figure 45. - Typical advanced fighter-type configuration used to find technology effect on aircraft size.

A carpet plot which shows the difference between the two maneuver wing technologies is presented in figure 46. Note that the aircraft sizing procedure used here optimizes the aircraft T/W and W/S for each wing technology. The two different resulting designs are compared in the following table:

	CONVENTIONAL WING	SC^3 WING
TOGW lb	42,609	38,229
S, ft^2 wing	706	518
W/S	60.3	73.8
T/W	1.26	1.12
C_{LMDP}	0.42	0.51

For the selected maneuver condition, the advanced SC^3 wing technology leads to a TOGW that is more than 10% lighter than the conventional wing aircraft. The conventional wing solution has both a much larger wing and

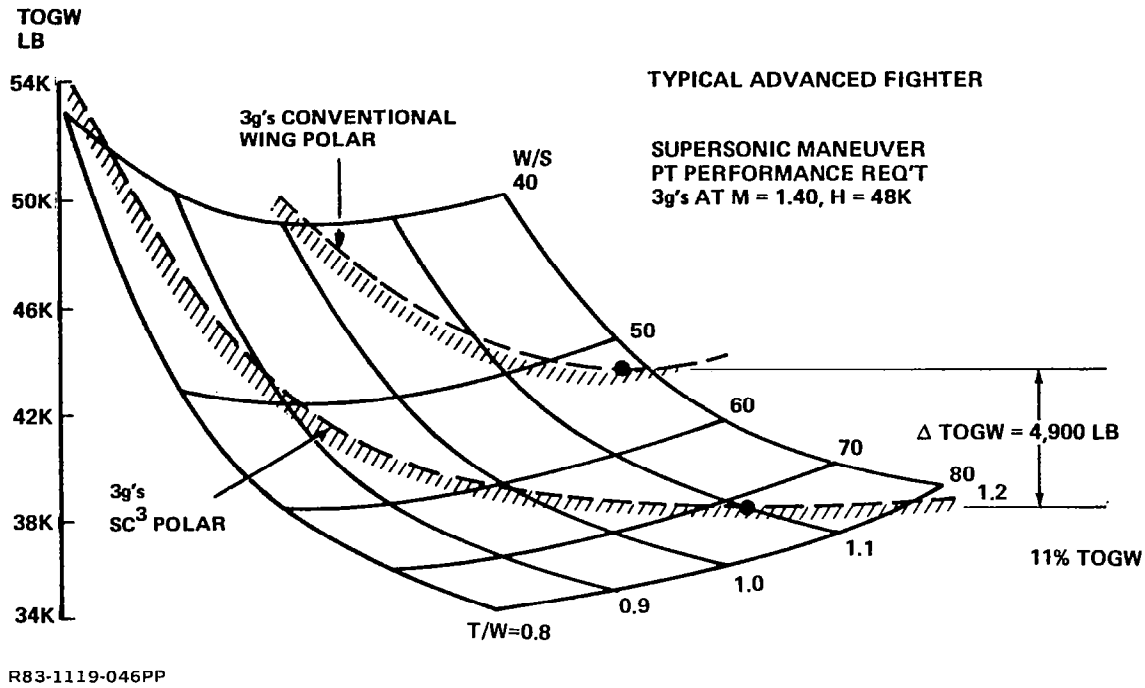

Figure 46. SC^3 wing technology impact on aircraft size.

higher thrust level. Note also that the maneuver lift coefficient for the SC^3 wing is almost exactly equal to the nominal value of $0.5/\beta$ given in figure 1.

CONCLUSIONS

The SC^3 wing concept, and its related numerical and experimental development program, constitute an important advance in supersonic wing design. In general, the approach and its methodology demonstrate how the advances made using transonic supercritical aerodynamics concepts can be incorporated in supersonic wing design. Significant specific results obtained in this development program include:

- A conceptual wing design (conical) in which controlled supercritical crossflow and shockless recompression was achieved experimentally
- An isolated fighter wing has been designed, fabricated, and tested in which an SC^3-type pressure distribution has been obtained. This wing demonstrated a 21% drag-due-to-lift reduction compared to an equivalent

flat wing representative of current technology at a lift coefficient approximately twice the limit of applicability of linear theory methods

- The ability to treat round leading edge wings explicitly was demonstrated with numerical/experimental results
- A foundation for further work has been established which consists of the results of three wind tunnel entries, a design procedure for SC^3 wings, and several new computer codes.

Grumman Aerospace Corporation
Bethpage, New York 11714
September 9, 1983

APPENDIX A
ACHIEVING AN SC^3 WING - CALCULATION METHODOLOGY

The implementation of the SC^3 concept requires the calculation of the nonlinear inviscid flowfield, including the supercritical crossflow, and any crossflow shock waves. In addition, the detailed design is associated in large part with establishing an attached flow controlled expansion at the leading edge, and thus the calculation procedure should include an exact treatment of the boundary conditions, especially in the vicinity of the leading edge. The substantial advances in transonic computational aerodynamics were adapted to the supersonic flow case at Grumman to acquire the necessary capability. By recalling that the full potential equation for conical flow is, in fact, computationally two-dimensional and of mixed type locally (depending on the crossflow velocity), the nearly perfect correspondence to the two-dimensional full potential equation was identified. The computational method based on the ideas used in the transonic methodology (ref. A-1) was developed by Grossman (ref. A-2) and the resulting computer program became known as COREL, for conical relaxation. The adaptation of COREL to aerodynamic applications is described in a companion report (ref. A-3). The potential flow assumption was found by comparison with data to be entirely adequate for the relatively slender shapes associated with aircraft capable of cruising at moderate supersonic speeds (M = 1.4 to 2.4) and for which Mach numbers normal to the shock waves were less than about 1.3.

Although the conical geometry restriction is not so severe as might be expected, the numerical method developed for obtaining the crossflow velocity in conical flow provides the basis for a method that treats the complete nonconical equations by using the crossflow coordinate system at each successive step from the apex. This work was carried out in the Grumman R&D Center by Siclari and Grossman (ref. A-4 - A-6). The resulting computer program is known as NCOREL (non-conical relaxation) and is described in ref. A-7. In both COREL and NCOREL the nonconservative form of the potential-flow difference equation is used, and a single Joukowsky mapping is used to convert the arbitrary spanwise section to a shape that is approximately circular. This is found to be entirely adequate, even though the surface is not on a constant-

coordinate line. Typically, the calculations are carried out with a 60 x 60 grid. Reference A-3 contains more information on the effect of grid density and the number of iterations on the calculated results.

The computational methodology described above provided an important advance in the ability to compute the nonlinear inviscid solution over wings of interest for fighter applications. Quite early in the present effort numerical results demonstrated that the nonlinear effects on the pressure distribution are quite important, even at low lift coefficients. The capabilities of the NCOREL code were being refined simultaneously with the SC^3 concept development work, and hence its use was of a limited nature in the SC^3 work.

Despite the emphasis on nonlinear effects, the linear theory methods were also used extensively in the work. They still provide valuable information and can be used to establish a framework for evaluating the wing performance. A linear theory panel code developed at Grumman as a combination of the features of the Woodward I (ref. A-8) and Woodward II (ref. A-9) methods, together with a number of other enhancements, was used to obtain the various linear theory results. The version adapted for the SC^3 work, called W12SC3, is described in ref. A-3. Features of this code include mixed design-optimization and mixed design-analysis options wherein the pressures are specified over a portion of the surface and the pressures or minimum drag cambers are found over the rest of the surface (ref. A-10). A refined version of the Carlson correction (ref. A-11) is also employed in W12SC3. Typically, about 320 panels are used in most calculations. Although the method can handle from 500 to 1000 panels, the direct inverse solution method loses accuracy and becomes expensive for large numbers of panels.

The detail design of the wings for the SC^3 concept required the repetitive application of a nonlinear-flow analysis tool. No automated design methodology is presently available. Two basic types of design methodology would be useful: a drag minimization method for nonlinear inviscid flow and an inverse method. A step toward obtaining an inverse capability was made by using the analysis codes iteratively in an automated procedure which was demonstrated using COREL by Davis (ref. A-12). Design procedures such as these will have to be developed for the nonlinear wing design to be carried out on a routine basis.

The methodology discussion has been restricted to inviscid flows. However, the adverse effects of viscosity constitute one of the important considerations in the wing design. Apparently, the boundary layer does not affect the inviscid results in supersonic flow to the extent that it does in transonic flow. This is because the trailing edge interaction in supersonic flow is not crucial (assuming a supersonic trailing edge) compared to the transonic flow situation in which the circulation strength is entirely controlled by the viscous interaction at the trailing edge. In supersonic wing design, the boundary layer is important in determining how much load can be placed in the leading edge region. If the boundary layer separates, it leads to a "relieving" of the pressure gradient which amounts to a loss of effective leading edge suction. Thus, a boundary layer prediction method would be used primarily to determine separation boundaries. Due to the reduced importance of the trailing edge interaction and the extremely thin viscous layer in the leading edge region, the use of a displacement surface-type viscous interaction does not have the same importance in supersonic wing design that it has in many transonic flow applications. However, some differences between the inviscid predictions and experimental pressures were observed. Since the demonstration wing should provide "3-D relief" compared to the conceptual wing (for which the comparisons between theory and data were excellent), "classical" 3-D thinking would suggest that viscous effects are not responsible for the observed differences. Although not yet possible, the reliable prediction of fully three-dimensional viscous effects and separation for these types of wings would prove valuable and provide a challenge for the computational fluid dynamicist.

References

A-1 Jameson, A., "Iterative Solution of Transonic Flow Over Airfoils and Wings, Including Flows at Mach 2," Comm. Pure and Appl. Math., Vol. 27, 1974.

A-2 Grossman, B., "A Numerical Procedure for the Computation of Supersonic Conical Flows," AIAA J., Vol. 17, No. 8, August 1979, pp. 828-837.

A-3 Mason, W.H. and Rosen, B.S., "The COREL and W12SC3 Computer Programs for Supersonic Wing Design and Analysis," NASA CR-3676, 1983.

A-4 Grossman, B. and Siclari, M.J., "The Nonlinear Supersonic Potential Flow Over Delta Wings," AIAA Paper No. 80-0269, January 1980.

A-5 Siclari, M.J. and Grossman, B., "Analysis and Design of Supersonic Aircraft Based on Inviscid Nonlinear Eulerian Equations," Part II, Nonlinear Potential Flow Solutions with Shock Capturing, AFWAL TR-80-3110, October 1980.

A-6 Siclari, M.J., "Supersonic Nonlinear Potential Flows with Subsonic Regions and Implicit Isentropic Shock Fitting," AIAA Paper No. 81-1201, Palo Alto, CA, June 1981.

A-7 Siclari, M.J., "The NCOREL Computer Program for 3-D Nonlinear Supersonic Potential Flow Computations," NASA CR-3694, 1983.

A-8 Woodward, F.A., Tinoco, E.N., and Larsen, J.W., "Analysis and Design of Supersonic Wing-Body Combinations, Including Flow Properties in the Near Field," Part I - Theory and Applications, NASA CR-73106, 1967.

A-9 Woodward, F.A., "An Improved Method for the Aerodynamic Analysis of Wing-Body-Tail Configurations in Subsonic and Supersonic Flow," NASA CR-2228, Parts I and II, 1973.

A-10 Cenko, A., "Advances in Supersonic Configuration Design Methods," Journal of Aircraft, Vol. 17, No. 2, February 1980, pp. 119-126.

A-11 Carlson, H.W., "A Modification to Linearized Theory for Predictions of Pressure Loadings on Lifting Surfaces at High Supersonic Mach Numbers and Large Angles of Attack," NASA TP-1406, February 1979.

A-12 Davis, W.H., Jr., "Technique for Developing Design Tools From Analysis Methods of Computational Aerodynamics," AIAA J., Vol. 18, No. 9, September 1980, pp. 1080-1087.

APPENDIX B

BODY AND CANARD EFFECTS ON SUPERCRITICAL CROSSFLOW DEVELOPMENT

The SC^3 concept was initially validated on an isolated and essentially conical wing. The possible sensitivities of the supercritical crossflow development to interferences created by the addition of a body and canard were investigated by modifying the conceptual conical wing wind tunnel model to include these components and by conducting another wind tunnel test. The test documentation and an analysis of the data is contained in ref. B-1 and is summarized in this appendix.

The model planform with the body and canard is shown in figure B-1. The rather extreme body shape can be better appreciated by examining the photographs shown in figure B-2. Both the cambered and uncambered wings were modified and tested at the original design Mach number of 1.62. The cambered wing was tested with two different nose shapes, and the canard was mounted on the basic forebody at incidence values of 0°, -5°, and -10°; the flat wing was tested with only the basic forebody and the canard (at the three different incidences).

The body and canard effects on the pressure distribution are shown in figure B-3 for the main spanwise row of pressure orifices. The body presence does make a significant change in the pressure level; however, the basic crossflow development was not changed. Similarly, the canard wake makes a small but distinct change to the pressure distribution. Based on these results, it was concluded that the SC^3 concept is not particularly sensitive to interference effects generated by other aircraft components.

In addition, the drag-due-to-lift performance of the wing was not changed significantly by the addition of the body and canard. Figure B-4 compares the three different configurations. The addition of the body leads to slightly worse performance for the cambered wing, and the addition of the canard restores the performance to the wing alone value for the cambered wing. The effects were more adverse for the flat wing. The conclusion from the force and moment results agree with those based on the pressure results. Therefore, the SC^3 concept does not appear to be sensitive to typical interference effects due to the body and canard, although each interaction effect is evident in the

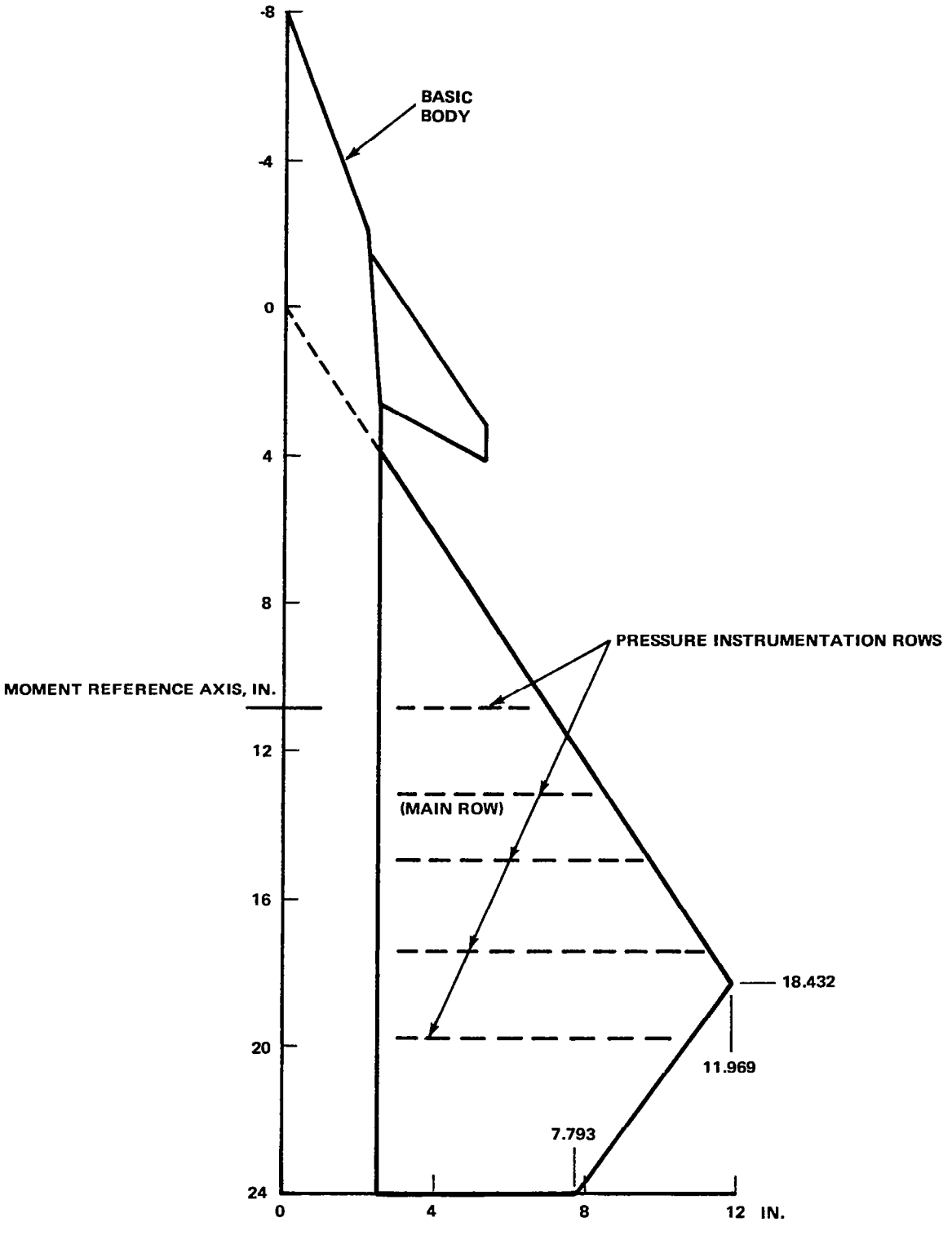

R83-1119-048PP

Figure B-1. Wing-body-canard wing tunnel model layout.

A. VIEW SHOWING CANARD ELEVATION ABOVE WING

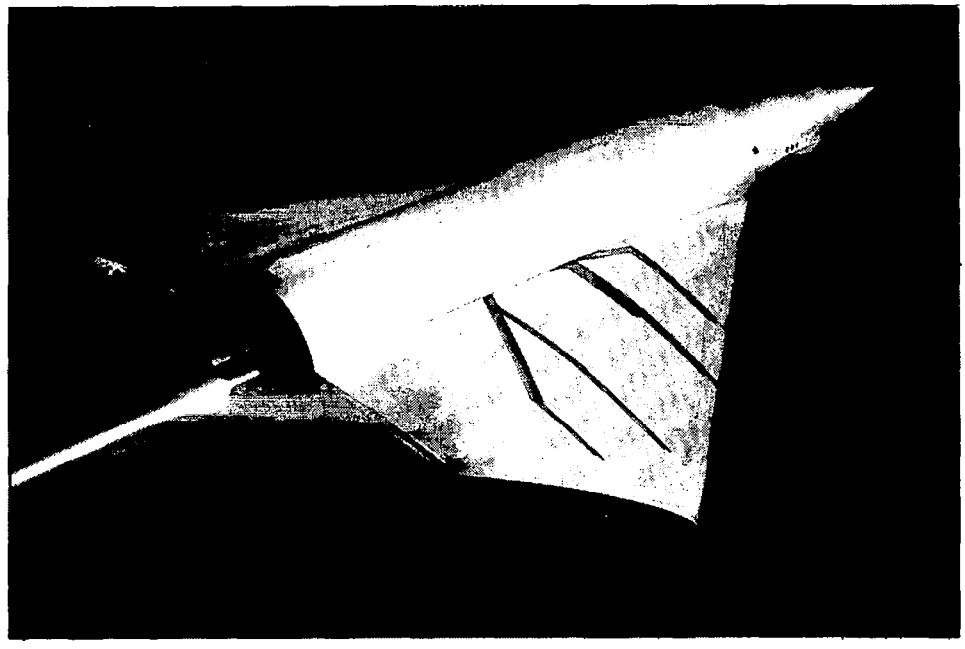

B. VIEW SHOWING THICK TRAILING EDGE DETAILS

R83-1119-049PP

Figure B-2. - Photographs of the cambered wing with body and canard.

experimental results and should be included in the SC^3 wing design process when applicable.

Reference

B-1 Mason, W.H., "Experimental Pressure Distributions and Aerodynamic Characteristics of Flat and Cambered Conceptual Wing-Body and Wing-Body-Canard Models at M = 1.62," Grumman Aerodynamics Report No. 393-81-1, October 1981.

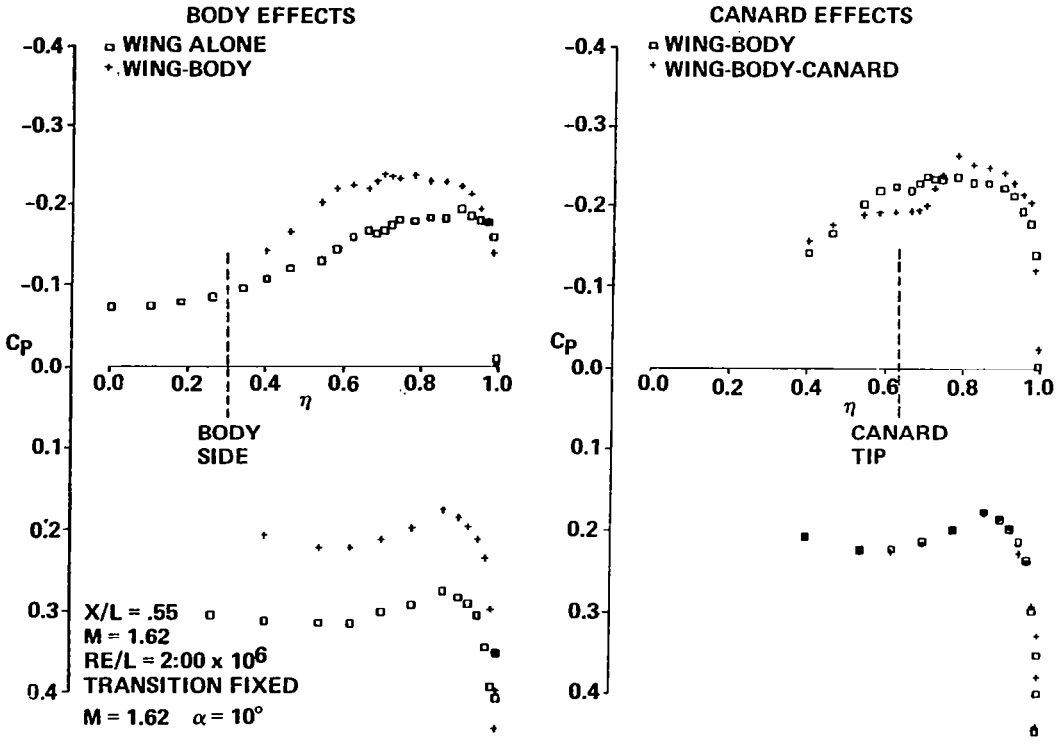

Figure B-3. - Interference effects of body and canard on spanwise pressures for the conceptual wing.

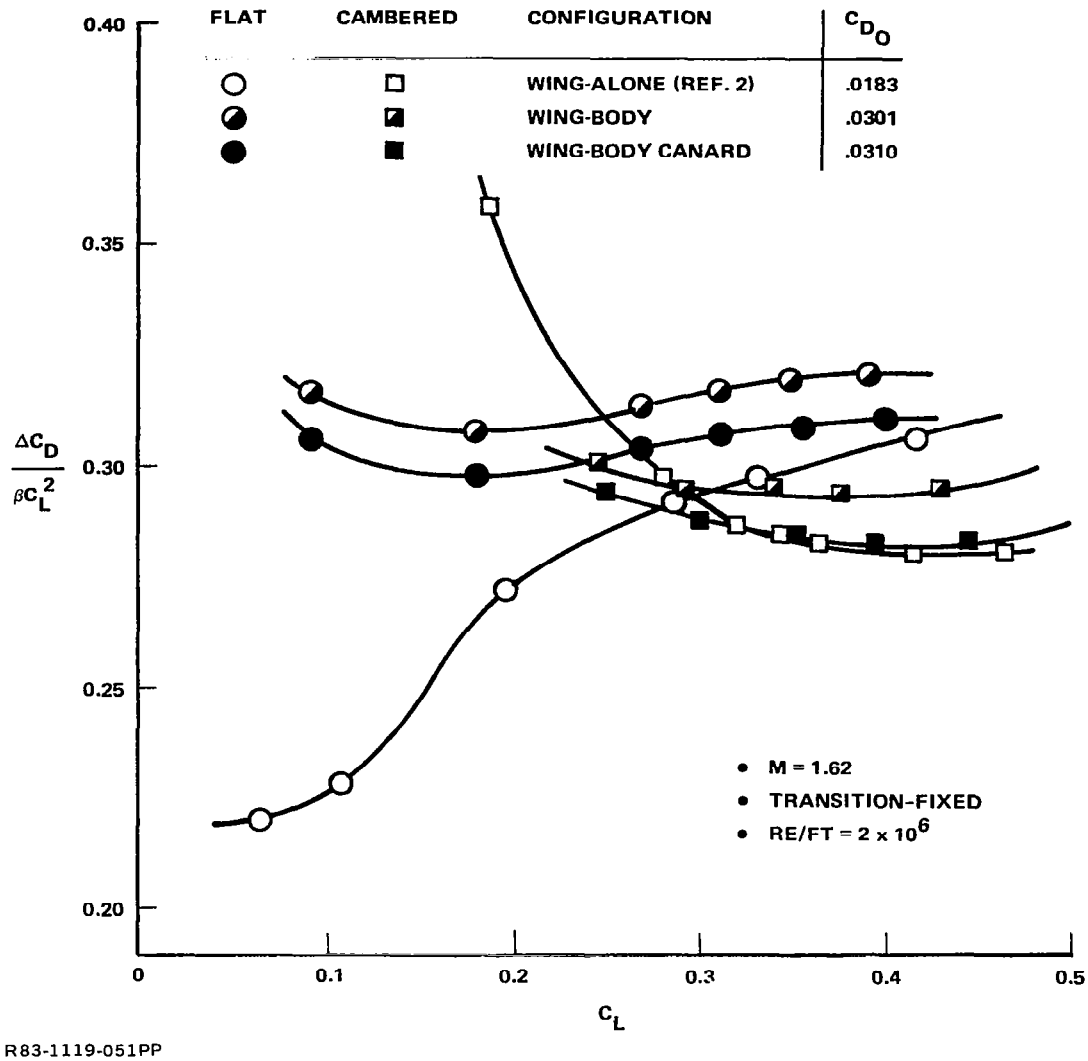

Figure B-4. - Drag-due-to-lift performance of the wing alone, wing-body, and wing-body-canard configurations.

REFERENCES

1. "Design Conference Proceedings - Technology for Supersonic Cruise Military Aircraft," Volume I. AFFDL-TR-77-85, Vol. I, U.S. Air Force, 1976.
2. "Tactical Aircraft Research and Technology," Volume I. NASA CP-2162, 1980.
3. Bavitz, P.C., et al, "Configuration Development of Advanced Fighters," AFWAL-TR-80-3142, November 1980.
4. Miller, D.S., Carlson, H.W., and Middleton, W.D., "A Linearized Theory Method of Constrained Optimization for Supersonic Cruise Wing Design," Proc. of the SCAR Conf., NASA CP-001, November 1976.
5. Brown, C., McLean, F., and Klunker, E., "Theoretical and Experimental Studies of Cambered and Twisted Wings Optimized for Flight at Supersonic Speeds", Proc. of the 2nd International Congress of Aero. Sci., Adv. in Aero. Sci. Vol. 3, ed. T. von Karman, et al, Pergamon Press, Oxford, 1962.
6. Mason, W.H. and Miller, D.S., "Controlled Supercritical Crossflow on Supersonic Wings - An Experimental Validation," AIAA Paper No. 80-1421, July 1980.
7. Mason, W.H and DaForno, G., "Opportunities for Supersonic Performance Gains Through Non-Linear Aerodynamics," AIAA Paper No. 79-1527, July 1979.
8. Carlson, H.W. and Mack, R.J., "Estimation of Wing Nonlinear Aerodynamic Characteristics at Supersonic Speeds," NASA TP-1718, November 1980.
9. Carlson, H.W. and Miller, D.S., "The Influence of Leading Edge Thrust on Twisted and Cambered Wing Design for Supersonic Cruise," AIAA Paper No. 81-1656, June 1981.
10. Hall, C.F., "Lift, Drag, and Pitching Moment of Low Aspect Ratio Wings at Subsonic and Supersonic Speeds," NACA RM A53A30, 1953.
11. Boyd, J.W., Migotsky, E., and Wetzel, B.E., "A Study of Conical Camber for Triangular and Sweptback Wings," NACA RM A55G19, November 1955.
12. Jones, R.T., "Estimated Lift-Drag Ratios at Supersonic Speeds," NACA TN 1350, 1947.
13. Phelps, E.R. and Boyd, J.W., "A Wind-Tunnel Investigation of the Effects of Conical Camber for an Airplane Configuration Having a Triangular Wing of Aspect Ratio 2.2," NACA RM A57A10, April 1957.

14. Niedling, L.G., "The F-15 Wing Development Program," AIAA 80-3044, in The Evolution of Aircraft Wing Design, March 1980.
15. Squire, L.C., "Experimental Work on the Aerodynamics of Integrated Slender Wings for Supersonic Flight," Progress in Aerospace Sciences, Vol. 20, pp. 1-96, 1981.
16. Tsien, S.H., "The Supersonic Conical Wing of Minimum Drag," JAS, Vol. 22, No. 12, pp. 805-017, December 1955.
17. Grossman, B., "A Numerical Procedure for the Computation of Supersonic Conical Flows," AIAA J., Vol. 17, No. 8, August 1979, pp. 828-837.
18. Jameson, A., "Iterative Solution of Transonic Flow Over Airfoils and Wings, Including Flows at Mach 2," Comm. Pure and Appl. Math., Vol. 27, 1974.
19. Mason, W.H. and Rosen, B.S., "The COREL and W12SC3 Computer Programs for Supersonic Wing Design and Analysis," NASA CR-3676, 1983.
20. Woodward, F.A., Tinoco, E.N., and Larsen, J.W., "Analysis and Design of Supersonic Wing-Body Combinations, Including Flow Properties in the Near Field," Part I - Theory and Applications, NASA CR-73106, 1967.
21. Woodward, F.A., "An Improved Method for the Aerodynamic Analysis of Wing-Body-Tail Configurations in Subsonic and Supersonic Flow," NASA CR-2228, Parts I and II, 1973.
22. Mack, R.J., "Effects of Leading-Edge Sweep Angle and Design Lift Coefficient on Performance of a Modified Arrow Wing at a Design Mach Number of 2.6," NASA TN D-7753, December 1974.
23. Meyer, R.C. and Fields, W.P., "Configuration Development of a Supersonic Cruise Strike-Fighter," AIAA Paper No. 78-148, January 1978.
24. Miller, D.S., Landrum, D.J., Townsend, J.C., and Mason, W.H., "Pressure and Force Data for a Flat Wing and a Warped Conical Wing Having a Shockless Recompression at Mach 1.62," NASA TP-1759, April 1981.
25. Mason, W.H., Miller, D.S., Pittman, J.L., and Siclari, M.J., "A Supersonic Maneuver Wing Designed for Nonlinear Attached Flow," AIAA Paper No. 83-0425, January 1983.
26. Mason, W.H., "Experimental Pressure Distributions and Aerodynamic Characteristics of a Demonstration Wing for a Wing Concept for Supersonic Maneuvering," Grumman Aerodynamics Report 393-82-01, July 1982.

27. Mason, W.H., "Fabrication, Inspection, and Acceptance Report on an Isolated Wing for Supersonic Maneuvering," Grumman Aerodynamics Report No. 393-81-3, November 1981.

28. Toscano, G., "Refinement of Maximum Achievable Tolerance Obtained from Best NC Machining," Presented at the AGARD "Convener's Meeting On Cryogenic Test Technology," September 23-25, 1980 (NASA Langley Research Center, Wayne McKinney - Chairman).

29. Kulfan, R.M. and Sigalla, A., "Real Flow Limitations in Supersonic Airplane Design," AIAA Paper No. 78-147, January 1978.

30. Settles, G.S., Perkins, J.J., and Bogdonoff, S.M., "Upstream Influence Scaling of 2D & 3D Shock/Turbulent Boundary Layer Interactions at Compression Corners," AIAA Paper No. 81-0334, January 1981.

31. Aidala, P.V., Davis, W.H. Jr., and Mason, W.H., "Smart Aerodynamic Optimization," AIAA Paper No. 83-1863, Danvers, MA, July 1983.

1. Report No.	2. Government Accession No.	3. Recipient's Catalog No.
NASA CR-3763		

4. Title and Subtitle	5. Report Date
A WING CONCEPT FOR SUPERSONIC MANEUVERING	December 1983
	6. Performing Organization Code

7. Author(s)	8. Performing Organization Report No.
William H. Mason	
	10. Work Unit No.

9. Performing Organization Name and Address	11. Contract or Grant No.
Grumman Aerospace Corporation Bethpage, New York 11714	NAS1-15357
	13. Type of Report and Period Covered
12. Sponsoring Agency Name and Address National Aeronautics and Space Administration Washington, D.C. 20546	Contractor Report
	14. Sponsoring Agency Code

15. Supplementary Notes

Langley Technical Monitor: David S. Miller
Final Report

16. Abstract

A theoretical and experimental program in which a wing concept for supersonic maneuvering was developed and then demonstrated experimentally in a series of wind tunnel tests is described in this report. For the typical advanced fighter wing, the problem of obtaining efficient lift at supersonic maneuvering C_L's occurs due to development of a strong crossflow shock, and boundary layer separation. A natural means of achieving efficient supersonic maneuvering is based on controlling the non-linear inviscid crossflow on the wing in a manner analogous to the supercritical aerodynamic methods developed for transonic speeds. The application of supercritical aerodynamics to supersonic speeds is carried out using Supercritical Conical Camber (SC^3). This report provides an aerodynamic analysis of the effort, with emphasis on wing design using non-linear aerodynamics. The substantial experimental data base is described in three separate wind tunnel reports, while two of the computer programs used in the work are also described in a separate report. Based on the development program it appears that a controlled supercritical crossflow can be obtained reliabily on fighter-type wing planforms, with an associated drag due to lift reduction of about 20% projected using this concept.

17. Key Words (Suggested by Author(s))	18. Distribution Statement
Aerodynamics Supersonic Flow Conical Flow	Unclassified - Unlimited Subject Category 02

19. Security Classif. (of this report)	20. Security Classif. (of this page)	21. No. of Pages	22. Price
Unclassified	Unclassified	82	A05

For sale by the National Technical Information Service, Springfield, Virginia 22161

NASA-Langley, 1983